

Modelling FX Smile - From Stochastic Volatility to Skewness

Lin Luo

Centre for Quantitative Finance
The Business School
Imperial College of Science, Technology and Medicine

In partial fulfilment of the requirements for the degree of
Doctor of Philosophy

July, 2007

Abstract

The increase of economic integration and an ease of communication has significantly improved the liquidity and depth of the Over-the-Counter foreign exchange (FX) option market. As a result, a better understanding and modelling of exchange rate dynamics is required for financial academics, practitioners, and also policy makers.

In this thesis, we firstly examine the dynamics of the exchange rate via the conditional distribution implied from option prices. We identify three sources of uncertainty that need to be modelled: the stochastic exchange rate process, which gives the random risk-neutral mean; the stochastic volatility, as reflected in both historical time series and implied distribution; and the stochastic skewness, which can be observed either from the implied higher moments or from its proxy measure – risk reversal. An error correction model (ECM) of these higher moments is thus proposed to exploit excess returns in the FX underlying market.

Following the instrumental approach, we endeavour to devise a tractable model that addresses all three sources of uncertainty and reproduce the current market implied volatility smile. Our review of the local volatility model, stochastic volatility model and jump models indicates that an individual model, although having some advantage in capturing the FX smile features, is insufficient to account for the asymptotic behaviour of the entire smile surface. The combined models, which use more than one mechanism to produce the FX smile, are interesting yet lack of tractability. The model of Carr & Wu [2005] uses two Levy processes to model the up and down jump to capture stochastic skewness, however is restricted to price European options. The model developed by Albanese and Mijatovic [2006] addresses all three sources of stochasticity with tractability. Within an innovative framework based on spectral theory and functional analysis, a model combining local volatility and Variance Gamma jumps with regime-switching controlled by a stochastic volatility process, is defined on a continuous time lattice, thus it is both rich enough to calibrate to the smile surface, and flexible enough to price both European and exotic options.

Finally, we successfully develop the methodology to price the FX barrier options within this lattice framework. A crucial component of this development is the novel adoption of an algorithm to calculate the exponential for nonnormal matrix.

Acknowledgement

I would like to thank my supervisor, Professor Nigel Meade, for his guidance, encouragement through the journey of research and thesis writing. I would also like to thank Professor Nicos Christofides for both the valuable suggestions, and the help in the sponsorship.

Great thanks goes to the Syngenta Group Treasury Service Limited, for the financial support, and the practical contribution from the Risk Management team. In particular my previous manager Adrian Williams, current manager Jeremy Horne, and colleague Russell Peddie, thank you for all the generous thoughtfulness through the years, and practical inspiration in financial markets.

I would like to thank all my previous teachers and friends, who have helped me to make my way to this stage. My special thanks go to Harry Lo, for the continuous patience, inspiration and invaluable help in broadening my knowledge in both model development and market understanding.

Last but not least, I am deeply indebted to my loving parents, who are always there to encourage and support me during my years of studies. You have not only opened up countless opportunities for me, but also brought me up to face various challenges. This work cannot be finished without your unconditional love. My thesis is dedicated to you.

Contents

1	Introduction	9
2	Implied Risk-neutral Distribution from the OTC FX Option Market	12
2.1	Option prices and the risk-neutral distribution function	12
2.2	Main techniques for estimating risk-neutral PDF	15
2.2.1	Parametric PDF	15
2.2.2	Smoothed function	17
2.2.3	Other methodologies	19
2.3	Standard OTC FX Option Quotes and Malz's Method	20
2.4	Data and Implied Distribution	24
2.5	Excess Forward Returns	28
2.6	Summary	30
3	Models which Capture the FX Smile - A Review	31
3.1	Derivative Modelling - Theory and Practice	31
3.1.1	Modelling in Derivative Pricing and Hedging	31
3.1.2	Market Reality and Modelling Approach	31
3.2	Local Volatility Model	33
3.2.1	Introduction	33
3.2.2	Implied Volatility Function	33
3.2.3	Displaced Diffusions Model	35
3.2.4	CEV Model	36
3.2.5	Summary	39
3.3	Stochastic Volatility Model	40

3.3.1	Introduction	40
3.3.2	Literature Review	40
3.3.3	Option Pricing	42
3.3.4	Summary	44
3.4	Jump Model	45
3.4.1	Introduction	45
3.4.2	Jump Diffusion Model	45
3.4.3	Variance Gamma Model	47
3.4.4	Summary	50
3.5	Combined Model	51
3.5.1	Introduction	51
3.5.2	Bates Model	51
3.5.3	Summary	52
3.6	Carr's Stochastic Skewness Model	53
3.6.1	Modelling Stochastic Skewness - Motivation	53
3.6.2	Generalized Modelling Approach	54
3.6.3	Option Pricing under Stochastic Skewness	60
3.6.4	Summary	63
3.7	Summary	63
4	Spectral Methods in FX Modelling	64
4.1	Introduction	64
4.2	Generating Function in Spectral Theory	65
4.2.1	Continuous-time Markov Generator	65
4.2.2	Essential Principles in Functional Calculus	69
4.2.3	Exponential and Normality of Markov Generator	70
4.3	Model for the FX Rates	72
4.3.1	The Conditional Local Volatility Processes	73
4.3.2	Adding Jumps	77
4.3.3	Stochastic Volatility for Regime Switching	80
4.3.4	Deterministic Time Change	82
4.4	Option Pricing and Hedging	83
4.4.1	Pricing European Options	83

4.4.2	Hedge Ratios (Greeks)	85
4.4.3	Validation - The Black-Scholes' Case	86
4.5	Calibration	91
4.5.1	GBPUSD	92
4.5.2	USDBRL	98
4.6	Summary	100
5	Pricing FX Barrier Options	104
5.1	Barrier Options	104
5.1.1	Introduction	104
5.1.2	Pricing	105
5.2	Barriers on the Continuous-time Lattice	110
5.2.1	Barrier on the Markov Generator	110
5.2.2	Validation - Black-Scholes Case	112
5.3	Pricing Experiment	118
5.3.1	GBPUSD	118
5.3.2	USDBRL	119
5.4	Summary	120
6	Conclusion	131
	Appendix A Derivation of the Implied Pricing Kernel	134
	Appendix B Implied Distribution Examples	135
	Appendix C Proof of Theorems in Chapter 4	138

List of Tables

- 2.5.1 Regression Results of Model 2.5.1 29
- 2.5.2 Regression Results of Model 2.5.2 30
- 4.4.1 GBPUSD Option Implied Volatilities with Various Number of Lat-
tice Point N, in Black-Scholes Case (Bold type indicates convergence
to BS volatility) 88
- 4.5.1 Parameters for GBPUSD local volatility regimes and jump intensity 93
- 4.5.2 Parameters for USDBRL local volatility regimes and jump intensity 99
- 5.2.1 Modified Markov generator for Up-and-Out barrier options, with
barrier level H and the number of lattice point N 111
- 5.2.2 Barrier Options with $S > H$, 400 Lattice Points in Black-Scholes Case.114
- 5.2.3 Greeks for Barrier Options with $S > H$, 400 Lattice Points in Black-
Scholes Case (Bold type indicates the difference of Greeks from
vanilla options) 115
- 5.2.4 Barrier Options with $S < H$, 400 Lattice Points in Black-Scholes Case.116
- 5.2.5 Greeks for Barrier Options with $S < H$, 400 Lattice Points in Black-
Scholes Case (Bold type indicates the distinct difference of the
Greeks from the vanilla options) 117
- 5.3.1 GBPUSD European Options and Hedge Ratios with 76 Lattice
Points and 5 Regimes (Bolded numbers are compared with the bar-
rier options counterparts in the following tables) 121
- 5.3.2 GBPUSD 'Down-and-Call' Barrier Options and Hedge Ratios with
 $S > H$, 76 Lattice Points and 5 Regimes (Bolded numbers are com-
pared with the European calls counterparts, indicating the barrier
property, as explained in the text) 122

- 5.3.3 GBPUSD 'Down-and-put' Barrier Options and Hedge Ratios with $S > H$, 76 Lattice Points and 5 Regimes (Bolded numbers are compared with the European puts counterparts, indicating the difference due to barrier property, as explained in the text) 123
- 5.3.4 GBPUSD 'Up-and-call' Barrier Options and Hedge Ratios with $S < H$, 76 Lattice Points and 5 Regimes (Bolded numbers are compared with the European calls counterparts, indicating the difference of Greeks for options with strikes below the barriers) 124
- 5.3.5 GBPUSD 'Up-and-put' Barrier Options and Hedge Ratios with $S < H$, 76 Lattice Points and 5 Regimes (Bolded numbers are compared with the Down and In Puts counterparts, as explained in the text) . 125
- 5.4.1 USDBRL European Options and Hedge Ratios with 76 Lattice Points and 5 Regimes (Bolded numbers are compared with the barrier options counterparts in the following tables) 126
- 5.4.2 USDBRL 'Down-and-call' Barrier Options and Hedge Ratios with $S > H$, 76 Lattice Points and 5 Regimes (Bolded numbers are compared with the European calls and GBPUSD counterparts, indicating the distinct Greeks due to the barrier property, as explained in the text) 127
- 5.4.3 USDBRL 'Down-and-put' Barrier Options and Hedge Ratios with $S > H$, 76 Lattice Points and 5 Regimes (Bolded numbers are compared with the European puts and GBPUSD counterparts, indicating the distinct Greeks due to the barrier property, as explained in the text) 128
- 5.4.4 USDBRL 'Up-and-call' Barrier Options and Hedge Ratios with $S < H$, 76 Lattice Points and 5 Regimes (Bolded numbers are compared with the European calls and GBPUSD counterparts, indicating the distinct Greeks due to the barrier property, as explained in the text) 129
- 5.4.5 USDBRL 'Up-and-put' Barrier Options and Hedge Ratios with $S < H$, 76 Lattice Points and 5 Regimes (Bolded numbers are compared with the European puts and GBPUSD counterparts, indicating the distinct Greeks due to the barrier property, as explained in the text) 130

List of Figures

2.1.1 Payoff of ΔS_T times the Butterfly spread	13
2.3.1 Payoff for option combinations	21
2.4.1 Implied volatility smile (GBPUSD monthly/weekly 20/06/05) . . .	26
2.4.2 Option implied PDF (GBPUSD monthly)	26
2.4.3 Spot GBPUSD monthly FX rate and the higher moments of implied PDF	27
3.2.1 Term structure of option prices for GBPUSD	38
3.2.2 Term structure of option prices for EURUSD	39
3.4.1 The Jump Diffusion model implied volatility, with parameters: $S =$ $0.95, \sigma = 0.05, r = 0.05, rf = 0.03, \lambda = 0.5, \mu = 0.05, \nu = 0.1.$. . .	46
3.4.2 The Variance Gamma model implied volatility, with parameters: $S = 105, r = 0.05, \sigma = 0.1213, \theta = -0.436, \nu = 0.1686.$	50
3.6.1 1-Month 25-delta Risk Reversal and Strangle (Daily Data from 19/10/04 to 19/10/05)	54
4.3.1 Boundaries of Pseudospectra for the CEV Markov Generator \mathcal{L} . . .	79
4.4.1 Boundaries of Pseudospectra for the Markov Generator \mathcal{L} , Com- puted with the GBPUSD Parameters.	84
4.4.2 ATMF delta for 6-month, 1-year and 2-year, calculated with 300 lattice points in Black-Scholes case.	89
4.4.3 ATMF delta for 6-month, 1-year and 2-year, calculated using Black- Scholes closed-form formula.	89
4.4.4 ATMF gamma for 6-month, 1-year and 2-year, calculated with 300 lattice points in Black-Scholes case.	90

4.4.5 ATMF gamma for 6-month, 1-year and 2-year, calculated using Black-Scholes closed-form formula.	90
4.5.1 Term Structure of Implied Volatilities for GBPUSD.	92
4.5.2 Extrapolated Implied Volatilities for GBPUSD European Options using Generic Strikes.	95
4.5.3 GBPUSD Probability Distribution Function under the Forward Measure.	95
4.5.4 Deterministic Time Change $f(t)$ (in years) as a Function of Calendar Time t for GBPUSD.	96
4.5.5 GBPUSD ATMF delta for 6-month, 1-year and 2-year, calculated with calibrated parameters.	96
4.5.6 GBPUSD ATMF gamma for 6-month, 1-year and 2-year, calculated with calibrated parameters.	97
4.5.7 GBPUSD ATMF vega for 6-month, 1-year and 2-year, calculated with calibrated parameters.	97
4.5.8 Term Structure of Implied Volatilities for USDBRL.	98
4.6.1 Extrapolated Implied Volatilities for USDBRL European Options using Generic Strikes.	101
4.6.2 USDBRL Probability Distribution Function under the Forward Measure	101
4.6.3 Deterministic Time Change $f(t)$ (in years) as a Function of Calendar Time t for USDBRL.	102
4.6.4 USDBRL ATMF delta for 6-month, 1-year and 2-year, calculated with calibrated parameters.	102
4.6.5 USDBRL ATMF gamma for 6-month, 1-year and 2-year, calculated with calibrated parameters.	103
4.6.6 USDBRL ATMF vega for 6-month, 1-year and 2-year, calculated with calibrated parameters.	103
5.2.1 Boundaries of Pseudospectra for the Barrier Markov Generator \mathcal{L} , Computed with the Calibrated GBPUSD Parameters.	112

Chapter 1

Introduction

The current world economy, characterized by the continuous opening of various countries' local economies, has significantly widened the foreign exchange (FX) market, which is already the largest financial market in respect to trading volume. Daily trading volume has exceeded 1.5 trillion U.S. dollar, the upwaved trend continues due to the increase of economic integration and ease of communication. As a result, a better understanding and modelling of exchange rate dynamics is required not only for financial academics and practitioners, but also for policy makers.

The currency option market has recently become prosperous with the increasing needs for the market speculators and hedgers in the underlying exchange rate market. Especially, the over-the-counter (OTC) currency option market has obtained significant improvement in liquidity and depth. In the light of the dependency of the option value on the future prices of the underlying assets, currency option prices can be used to derive the conditional risk-neutral probability distribution, which reflects the market participants' future expectation in the underlying exchange rates' dynamic process.

In this thesis, we endeavor to identify the core sources of uncertainty in the exchange rates dynamics, and develop a model that can capture the main features of the smile surface, and is flexible enough to price both European and exotic options. Through the process, we have made three novel extensions or improvements to previous work, namely:

- Develop the Error Correction Model (ECM) of implied risk-neutral higher moments to analyze and forecast the exchange rates movements
- Propose an alternative robust algorithm to calculate the exponential of non-normal matrix in the Albanese and Mijatovic[4] model.
- Develop the pricing method for FX Barrier options in the Albanese and Mijatovic[4] framework.

We firstly investigate the implied risk-neutral distributions from the OTC currency options, and analyze the dynamics of the exchange rates in Chapter 2. The first section goes through the development of different techniques in implying risk-neutral distributions from the options prices. In section 2, Malz[65]’s method, which is designed specifically for FX options, is applied to two currency pairs, and the dynamics of the exchange rates are analyzed via the resulting implied conditional risk-neutral distribution. We identify three sources of uncertainty: the stochastic exchange rate process, which gives the random risk-neutral mean; the stochastic volatility, as reflected in both historical time series and implied distribution; and the stochastic skewness, which can be observed either from the implied higher moments or from its proxy measure – risk reversal. An Error Correction Model (ECM) is then proposed to help forecasting exchange rates movements, which is useful in exploiting excess returns.

Given these identified sources of uncertainty, we then review various models and develop the appropriate one for foreign exchange rates. Chapter 3 starts with a review of three individual popular models. The disadvantages of these models in capturing only certain features of the smile surface lead the literature to a combined approach. However, this suffers from a lack of tractability. The Levy processes model by Carr and Wu[25] can capture both stochastic volatility and stochastic skewness. Yet it only has semi-closed-form solution for vanilla options, while the extension to exotic options appears to be too challenging and remains untackled.

After considering all the pros and cons of various models, the model developed by Albanese and Mijatovic[4], which addresses all three sources of stochasticity with tractability, is adopted in Chapter 4. Within an innovative framework based

on spectral theory and functional analysis, a model combining local volatility and Variance Gamma jumps with regime-switching controlled by a stochastic volatility process, is defined on a continuous time lattice. This model is both rich enough to calibrate to the smile surface and flexible enough to price both European and exotic options. During the implementation, we improve this model by using a more stable methodology to calculate the exponential for the nonnormal matrix, given the results of normality tests.

In Chapter 5, we successfully develop the methodology to price FX barrier options within this lattice framework. The model achieves reasonable pricing results for both a developed market currency pair (GBPUSD) and an emerging market currency pair (USDBRL). Chapter 6 concludes the whole thesis and makes suggestion for future work.

Our work thus culminates in a robust pricing method for FX vanilla and barrier options, which provides both prices and hedge ratios. The whole pricing and hedging process for FX vanilla and barrier options can be both effectively speeded up and profitably improved. The practical benefits will occur in both derivative pricing and risk management. Such a rich model, nicely calibrated to the market in a nearly stationary manner, allows traders to quickly and reliably price derivatives of any maturity. This will greatly improve the trader's competitiveness and profitability in the market. Meanwhile, both traders and risk management team can easily control portfolio risk with the readily available hedge ratios, making the hedging programme much simpler.

Chapter 2

Implied Risk-neutral Distribution from the OTC FX Option Market

In this chapter, we will firstly illustrate the theory underpinning the practice of deriving the risk-neutral distribution implied by European option prices quoted in the market, and then briefly review the main techniques in this area. The most appropriate method for FX market will be identified and applied in two currency pairs. With the resulting implied distributions, we then analyze the dynamics of the exchange rates, and identify the key sources of uncertainty. Finally, an Error Correction Model is proposed to exploit excess returns.

2.1 Option prices and the risk-neutral distribution function

It is well-known that under the established risk-neutral valuation framework, the price of a European call option with the payoff at maturity T being $\max(S_T - K)$, where S_T is the time- T asset price and K represents the exercise or strike price, is the risk-free discounted expectation of its future payoff under the risk-neutral measure. From Cox and Ross[31], by denoting $C(S, K, t, T)$ as the observed market

value at time t of a European option, we have:

$$\begin{aligned} C(S, K, t, T) &= e^{-r(T-t)} E_Q \max(S_T - K) \\ &= e^{-r(T-t)} \int_K^\infty (S_T - K) \phi(S_T) dS_T \end{aligned} \quad (2.1.1)$$

where E_Q denotes the conditional expectation under the risk-neutral measure, and ϕ is the risk-neutral probability density function (PDF) of the underlying asset price at maturity, conditional on the time t price S_t .

Breeden and Litzenberger[18] then made an important step in demonstrating that the risk-neutral PDF is actually the second derivative of the market call option price with respect to the exercise price K . In the time-state preference framework, they developed a general approach to price a state-contingent claim (also known as an Arrow-Debreu security), which has a payoff \$1 for each state. By constructing a four option portfolio which sells two call options with strike price $K = S_T$, and simultaneously buys two call options with strike price $K = S_T - \Delta S_T$ and $K = S_T + \Delta S_T$, respectively, where ΔS_T is the step size between two adjacent call options, one can get what is called the “butterfly spread” centered on state $S_T = K$ with the payoff:

$$\frac{[C(S_T + \Delta S_T, \tau) - C(S_T, \tau)] - [C(S_T, \tau) - C(S_T - \Delta S_T, \tau)]}{\Delta S_T} \Big|_{K=S_T} = 1$$

where $C(S_T, \tau)$ denotes the price of a European call option with strike K and time to maturity $\tau = T - t$. The payoff pattern is shown in Figure 2.1.1.

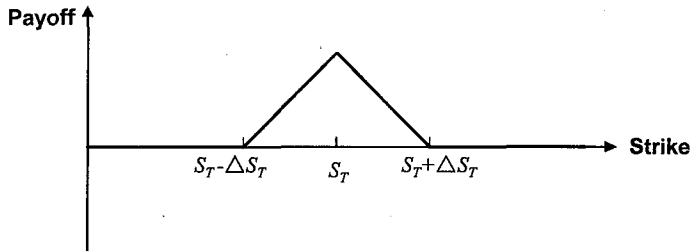


Figure 2.1.1: Payoff of ΔS_T times the Butterfly spread

From Figure 2.1.1 one can easily see that as ΔS_T tends to zero, the payoff tends to ΔS_T , which divided by ΔS_T yields 1, meaning that the butterfly spread becomes an Arrow-Debreu security paying \$1 at the state of $S_T = K$ and zero for all the other states.

Further differentiating the butterfly spread price with respect to ΔS_T , we arrive at a second-order difference quotient:

$$\frac{[C(S_T + \Delta S_T, \tau) - C(S_T, \tau)] - [C(S_T, \tau) - C(S_T - \Delta S_T, \tau)]}{(\Delta S_T)^2}$$

In the limit when ΔS_T tends to zero, the above expression tends to the second derivative of the call option price function with respect to the strike price at $K = S_T$.

$$\lim_{\Delta S_T \rightarrow 0} \frac{[C(S_T + \Delta S_T, \tau) - C(S_T, \tau)] - [C(S_T, \tau) - C(S_T - \Delta S_T, \tau)]}{(\Delta S_T)^2} = \frac{\partial^2 C(K, \tau)}{\partial K^2} \Big|_{K=S_T}$$

This, together with the alternative way of pricing an Arrow-Debreu security as payoff (\$1) multiplied by the risk-neutral probability density function at $S_T = K$, gives the final result¹:

$$\frac{\partial^2 C(K, \tau)}{\partial K^2} = e^{-r\tau} \phi(K) \quad (2.1.2)$$

This shows the existence of a one-to-one relationship between the option price and the risk-neutral PDF evaluated at the same strike K . Therefore, in order to get the continuous PDF, theoretically we need the prices of options across the full continuum of strikes. However, in reality, we can only get a few discrete option quotes, which is far from enough. This gives rise to a rich literature on various techniques to address this problem.

¹A more concise derivation of this result is shown in Appendix A.

2.2 Main techniques for estimating risk-neutral PDF

The empirical literature follows two main directions in the field of estimation techniques: one approximates the PDF directly using a parametric functional form for $\phi(K)$, the other starts from smoothing the volatility smile by interpolation and extrapolation before deriving PDF from a certain parametric specification of the option price function.

2.2.1 Parametric PDF

Parametric PDF methods make specific assumptions on the functional form of the Risk Neutral Distribution $\phi(K)$, and use Equation 2.1.1 to estimate the parameters by minimizing the difference between the observed option prices and those generated by the equation.

Melick and Thomas[68] pointed out that the parametric PDF approach is more general than starting from an assumption on the stochastic process, because a given stochastic process implied a unique PDF, but a given PDF is consistent with many different stochastic processes for the underlying asset. In practice, the observed asset price distributions are very close to a lognormal distribution. Therefore, it is plausible to follow Ritchey[78]'s suggestion that $\phi(K)$ ² can be represented as the weighted sum of k-component lognormal density functions:

$$\phi(K) = \sum_{i=1}^k \theta_i L(\alpha_i, \beta_i; K) \quad (2.2.1)$$

where $L(\alpha_i, \beta_i; K)$ is the i^{th} lognormal PDF:

$$L(\alpha_i, \beta_i; K) = \frac{1}{K\beta_i\sqrt{2\pi}} e^{[-(\ln K - \alpha_i)^2]/2\beta_i^2} \quad (2.2.2)$$

²Note that we are valuing the distributions at $S_T = K$. To be consistent with the previous discussion, we use K instead of S_T from the original paper.

with the parameters:

$$\begin{aligned}\alpha_i &= \ln K + \left(\mu_i - \frac{1}{2} \sigma_i^2 \right) \tau \\ \beta_i &= \sigma_i \sqrt{\tau}\end{aligned}$$

The probability weights θ_i satisfy the conditions:

$$\sum_{i=1}^k \theta_i = 1, \theta_i > 0 \text{ for all } i$$

The mixture PDF thus implicitly ensures that the call pricing function, which fits this PDF, is convex and monotonic decreasing in strike price, consistent with the arbitrage-free condition.

The most popular functional form is the so-called “Double Lognormal”, which uses a mixture of two lognormal distributions to approximate $\phi(S_T)$. This is because the small number of options traded in the market limits the number of distributional parameters that can be estimated from the data. The Double Lognormal contains only five parameters $(\theta, \alpha_1, \beta_1, \alpha_2, \beta_2)$, which gives the call option the following form:

$$C(S_t, K, t, T) = e^{-r(T-t)} \int_K^\infty (S_T - K) [\theta L(\alpha_1, \beta_1; S_T) + (1 - \theta) L(\alpha_2, \beta_2; S_T)] dS_T$$

Similarly, the put option can be represented as:

$$P(S_t, K, t, T) = e^{-r(T-t)} \int_K^\infty (K - S_T) [\theta L(\alpha_1, \beta_1; S_T) + (1 - \theta) L(\alpha_2, \beta_2; S_T)] dS_T$$

Both put and call options are priced using the same underlying PDF assumption, thus we can use both sets of data. In addition, under the arbitrage-free condition, the mean of the implied PDF must equal the forward price of the underlying asset. Therefore, the underlying asset can be viewed as a zero-strike option, thus the forward price provides an addition data point in the minimization

problem:

$$\min_{\alpha_1, \alpha_2, \beta_1, \beta_2, \theta} \sum_{i=1}^n \left[C(S_t, K_i, t, T) - \hat{C}_i \right]^2 + \sum_{i=1}^n \left[P(S_t, K_i, t, T) - \hat{P}_i \right]^2 \\ + \left[\theta e^{\alpha_1 + 1/2\beta_1^2} + (1 - \theta) e^{\alpha_2 + 1/2\beta_2^2} - e^{r(T-t)} S_t \right]$$

where \hat{C}_i and \hat{P}_i are the observed i^{th} prices, $\beta_1, \beta_2 > 0$, $0 \leq \theta \leq 1$, over the strike range K_i .

The Double Lognormal mixture can incorporate various possible functional forms, which can deal with a wide range of possible scenarios. Besides, by focusing directly on the possible future values of the underlying asset, this method can avoid specifying the dynamics of the underlying assets. Melick and Thomas[68] applied the Triple Lognormal technique to analyze the expectations on crude oil prices during the Gulf war.

Rubinstein[80] estimated the parametric PDF in another way to ensure it is closest to lognormal distribution in the least squares sense by forcing the present values of the underlying asset and all the options priced on it to fall between the respective bid and ask prices. This paper made a further step in converting the implied risk-neutral PDF to a “consensus subjective” PDF under the assumption that the representative agent maximizes his/her expected utility of wealth according to constant relative risk aversion (CRRA). The result showed that the difference between the two PDFs is negligible because the shape and higher moments are not significantly influenced by the risk aversion³. Jackwerth and Rubinstein[49] then employed different distance criteria in a similar method.

2.2.2 Smoothed function

More papers belong to a large category called “Smoothed Function”, which uses a smoothed parametric option pricing function or a volatility smile function to estimate risk-neutral PDF across the strikes.

The most intuitive attempt is to estimate the implied risk-neutral PDF by ap-

³Recent researches indicate that the difference is significant in forecasting the distribution of the realizations of the underlying asset.

plying the Breeden and Litzenberger[18] result directly to the call option pricing function 2.1.1, which is interpolated to yield a twice-differentiable smooth function that is also consistent with monotonicity and convexity conditions. To achieve this, one can either impose a parametric functional form on the call option price according to the observed values and solve a least squares problem to estimate the parameters, or use Nonparametric Kernel Regression, a statistical technique involving locally fitting polynomials across the call option pricing function⁴. However, since the intensive data requirement for nonparametric regression makes it impractical for the limited observed option market data, the first technique seems to be more practical. Bates[11] uses the cubic spline to interpolate the observed call option prices under monotonicity and convexity conditions. But in order to get accurate estimation, this method also requires lots of data because of the complex functional form needed for call pricing function.

Shimko[83] first developed an alternative methodology, which interpolates the implied volatility function instead of the call price function, based on the argument that the former is smoother than the latter. Under the assumption that implied volatility is a quadratic function of strike price in the traded range, he first interpolates the volatility smile curve and then obtains the call price function by using the Black-Scholes formula as a translation device. The risk-neutral PDF is then determined by twice differentiating the implied call option pricing function according to Equation 2.1.2. Note that since interpolation can only achieve the points between the lowest and highest observed prices, extrapolation is necessary to get the whole distribution. Shimko[83] extrapolates by imposing lognormal tails onto both endpoints of the observable density in such a way that the total cumulative probability equals one. However, this kind of extrapolation suffers from at least three shortcomings: (1) it arbitrarily imposes a constant volatility structure to the smile outside the observed strike range; (2) the transition from the observable part of the distribution to the tails may not be smooth; (3) the possibility of negative probability.

Among the various interpolation functions including piecewise linear, hyperbolic, parabolic, the best-fit polynomial and spline, the two knot points cubic spline seems to fit the data better than the others in most cases. Campa, Chang

⁴See Härdle[42], chapter 5.

and Reider[22] applies the smoothed spline function to estimate the volatility smile in currency options, while Bliss and Panigirtzoglou[16] tests the same technique on FTSE 100 index futures and options and concludes that it outperforms the Double Lognormal in estimating risk-neutral PDF when the average goodness-of-fit of both methods are comparable.

2.2.3 Other methodologies

Two other methodologies can be seen in the empirical literature. One is the so-called Nonparametric Method, which estimates the risk-neutral PDF without any parametric assumption on the call option pricing function, PDF, or underlying asset price dynamics. The other assumes a certain stochastic process for the underlying and then derives the option pricing function to imply the PDF. Art-Sahalia and Lo[1] uses the first method to estimate the PDF nonparametrically, while Malz[66] assumes FX rates follows a jump-diffusion process and recover the parameters using the quoted risk reversal prices. He obtains a closed-form solution for the implied PDF by assuming that the jump-diffusion is Bernoulli distributed, which means the jump size is either zero or one. His result shows that under such an assumption, the PDF takes the form of Double Lognormal.

In the field of FX options, however, the special way that the markets (mainly over-the-counter) package options provides an easier and more reliable technique to deal with the implied PDF. Malz[65] uses low-order polynomial functional forms to fit the volatility smile with only three points, thus shows that the existence of straddle, risk reversal and strangle enables us to infer the risk-neutral PDF using only limited option quotes. Campa, Chang and Reider[22] compare different estimation methods for implied risk-neutral PDF yet fail to find significant difference across the results. Bliss and Panigirtzoglou[16]’s test also provides strong support of the superior stability of Malz’s method over Double Lognormal method. We will illustrate Malz[65]’s method with applications to two main currency pairs in next section.

2.3 Standard OTC FX Option Quotes and Malz's Method

The OTC FX option prices are quoted in terms of deltas and volatilities, which come from the Black-Scholes/Garman-Kohlhagen formula:

$$C(S_t, K, t, T, \sigma, r_t, r_{f_t}) = e^{-r_{f_t}(T-t)} S_t \Phi \left[\frac{\ln(S_t/K) + (r_t - r_{f_t} + \sigma^2/2)(T-t)}{\sigma\sqrt{T-t}} \right] - e^{-r_t(T-t)} K \Phi \left[\frac{\ln(S_t/K) + (r_t - r_{f_t} - \sigma^2/2)(T-t)}{\sigma\sqrt{T-t}} \right] \quad (2.3.1)$$

where r_t and r_{f_t} are the domestic and foreign risk free interest rates, respectively.

Delta ($\delta \in [0, 1]$) represents the rate of change of the call option value with respect to the spot exchange rate S_t :

$$\delta_C(S_t, K, t, T, \sigma, r_t, r_{f_t}) = \frac{\partial C}{\partial S_t} = e^{-r_{f_t}(T-t)} \Phi \left[\frac{\ln(S_t/K) + (r_t - r_{f_t} + \sigma^2/2)(T-t)}{\sigma\sqrt{T-t}} \right] \quad (2.3.2)$$

$$\delta_P(S_t, K, t, T, \sigma, r_t, r_{f_t}) = \frac{\partial P}{\partial S_t} = 1 - \delta_C(S_t, K, t, T, \sigma, r_t, r_{f_t}) \quad (2.3.3)$$

As an alternative of the strike to measure the “Moneyness” of the option, delta abstracts the changes in the cash market (e.g. the fluctuations in the spot and forward FX rates), so dealers only need to recalculate their quotes when the implied volatilities change. The strike prices are then set such that delta equals a rounded number, e.g. 25 or 75 percent, using Equation 2.3.2 or 2.3.3.

Given that all the other parameters are the same, there exists a one-to-one relationship between the option price and volatility σ . The market thus can quote the options in units of so-called “Implied volatility”, which is obtained by converting the market determined option price through Black-Scholes/Garman-Kohlhagen formula⁵.

In the framework of these two concepts, the OTC FX option market mainly quotes the three options combinations: Straddle, Risk reversal and Strangle, the

⁵Note from the previous section that the formula is only a translation device, not necessarily to be accurate.

payoff patterns of which can be seen in Figure 2.3.1.

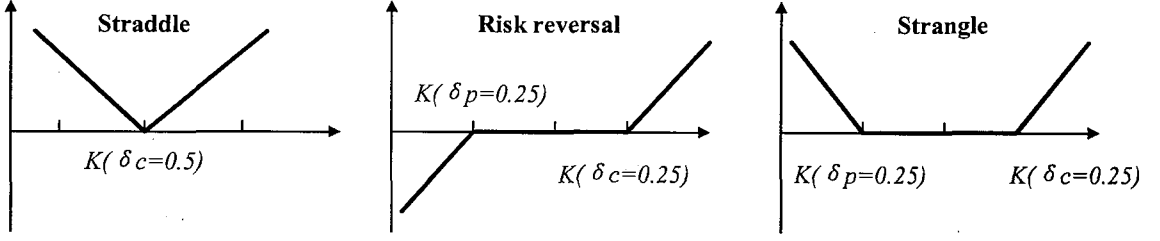


Figure 2.3.1: Payoff for option combinations

A standard quoted OTC Straddle is a combination of an at-the-money forward call and a put with the same maturity and strike price ($\delta_C = 0.5$), which is equal to the current forward price. The quote of the at-the-money forward call can be written as:

$$atm_t = \sigma_t^{(0.5)} \quad (2.3.4)$$

where $\sigma_t^{(0.5)}$ refers to the one-month 50-delta call.

The price of the straddle contains the information about the variance of the expected distribution for the FX rate. Quoted in volatility terms, a straddle price is called at-the-money implied volatility.

A standard quoted OTC Risk reversal is a combination of buying a 25-delta out-of-the-money call and selling a 25-delta out-of-the-money put option. The call and the put gain profits at the two directions of the FX rate movement, respectively. Therefore, risk reversals reflect the skewness of market expectation on the exchange rate distribution. It can be expressed as:

$$rr_t = \sigma_t^{(0.25)} - \sigma_t^{(0.75)}$$

where $\sigma_t^{(0.25)}$ and $\sigma_t^{(0.75)}$ refer to one-month 25-delta call and put, respectively.

A standard quoted OTC Strangle is a combination of 25-delta out-of-the-money call and put together with at-the-money call, which has the following payoff function:

$$str_t = 0.5 \left[\sigma_t^{(0.25)} + \sigma_t^{(0.75)} \right] - atm_t \quad (2.3.5)$$

The buyer of a strangle benefits from large movements of the underlying ex-

change rate, as shown in Figure 2.3.1. Therefore, the strangle prices indicate the kurtosis of the expected distribution.

Equation 2.3.4 to 2.3.5 can be rearranged to yield the expressions for the market prices of $\sigma_t^{(0.25)}$ and $\sigma_t^{(0.75)}$:

$$\sigma_t^{(0.25)} = atm_t + str_t + 0.5rr_t \quad (2.3.6)$$

$$\sigma_t^{(0.75)} = atm_t + str_t - 0.5rr_t \quad (2.3.7)$$

Malz[65] then obtains a continuous volatility smile by fitting the curve to a second-order Taylor approximation around the point $\delta_C = 0.5$:

$$\widehat{\sigma}(\delta_C)_t = b_0 atm_t + b_1 rr_t (\delta_C - 0.5) + b_2 str_t (\delta_C - 0.5)^2 \quad (2.3.8)$$

After simple algebraic manipulation of Equation 2.3.4 and 2.3.6 to 2.3.8, we have:

$$\widehat{\sigma}(\delta_C)_t = atm_t - 2rr_t (\delta_C - 0.5) + 16str_t (\delta_C - 0.5)^2 \quad (2.3.9)$$

This means that the volatility smile is constituted by a linear function of at-the-money volatility, a negative linear function of the risk reversal price and the difference of delta from 0.5, and a quadratic function of the strangle price and the difference of delta from 0.5. Given that the shape of any unimodal probability distribution can be asymptotically⁶ characterized by its second, third and forth central moments, Malz[65] points out that one is able to use these OTC options quotes to infer accurate risk-neutral probability distribution.

The volatility smile function provides the implied volatility for each delta, from which we can get the strike-volatility mapping:

$$\begin{aligned} \sigma_t = atm_t - 2rr_t \left\{ e^{-rf_t(T-t)} \Phi \left[\frac{\ln(S_t/K) + (r_t - rf_t + \sigma^2/2)(T-t)}{\sigma\sqrt{T-t}} \right] - 0.5 \right\} \\ + 16str_t \left\{ e^{-rf_t(T-t)} \Phi \left[\frac{\ln(S_t/K) + (r_t - rf_t + \sigma^2/2)(T-t)}{\sigma\sqrt{T-t}} \right] - 0.5 \right\} \end{aligned} \quad (2.3.10)$$

This equation is implicit for implied volatility, which can only be solved numerically. Then substitute the result into the Equation 2.3.1, we have the generalized

⁶Following the original paper, our research only centres on the first four moments.

Black-Scholes/Garman-Kohlhagen formula:

$$C(S_t, K, t, T, \sigma(K), r_t, rf_t) = e^{-rf_t(T-t)} S_t \Phi \left[\frac{\ln(S_t/K) + (r_t - rf_t + \sigma(K)^2/2)(T-t)}{\sigma(K) \sqrt{T-t}} \right] - e^{-r_t(T-t)} K \Phi \left[\frac{\ln(S_t/K) + (r_t - rf_t - \sigma(K)^2/2)(T-t)}{\sigma(K) \sqrt{T-t}} \right]$$

According to Equation 2.1.2, we differentiate the above equation twice with respect to K and multiply it by $e^{r_t(T-t)}$, which yields the risk-neutral PDF:

$$\phi(K) = e^{r_t(T-t)} \frac{\partial^2 C(S_t, K, t, T, \sigma(K), r_t, rf_t)}{\partial K^2} \quad (2.3.11)$$

This formula can be used to calculate the characteristic moments of the risk-neutral distribution. Note that the first moment is the forward price:

$$F_{t,T} = S_t e^{(r_t - rf_t)(T-t)}$$

The j^{th} central moment is defined as:

$$\mu_t^{(j)} = \int_0^\infty (K - F_{t,T})^j \phi(K) dK$$

The risk-neutral distribution for the percentage changes in FX rates has the following higher moments that characterize it:

The annualized second moment:

$$\sigma_t \equiv \sqrt{\frac{\mu_t^{(2)}}{T-t}}$$

Note that it is usually quite close to atm_t .

The standardized third moment (Skewness):

$$\alpha_t \equiv \frac{\mu_t^{(3)}}{[\mu_t^{(2)}]^{3/2}}$$

The standardized forth moment (Excess Kurtosis):

$$\kappa_t \equiv \frac{\mu_t^{(4)}}{[\mu_t^{(2)}]^2} - 3$$

These higher moments can help to extract the market expectations for the future exchange rate movement.

2.4 Data and Implied Distribution

We choose two main currency pairs: GBPUSD and EURUSD to which the Malz's method is applied. Historical daily OTC option data, including the quote for at-the-money forward (ATMF), 25-delta risk reversal and strangle prices, together with risk-free interest rate and underlying, are obtained from UBS Warburg⁷, from 23/06/2004 to 20/06/2005 with one-week and one-month maturity.

GBP and EUR are assumed to be the foreign currency on which the option is written, while the USD is the domestic currency.

Figure 2.4.1 displays an example of the smoothed implied volatility smile as a function of strike price (One-month forward rate) using Malz's polynomial functional form⁸. The one-week smile is lower, which is consistent with volatility term-structure, but the pattern is less 'smooth'; such curvature difference reflects that the impact of FX jumps on the volatility is more pronounced. This is because in the long term, the jumps caused by central banks' policy movements tend to 'average out', leaving less influence on the smile and making it much smoother.

Figure 2.4.2 shows the shape of the option-implied risk-neutral PDF of the GBPUSD calculated from one-month options data. It can be observed that the more dispersed shape of the one-month expected returns on 23rd June 2004 has changed to the more 'standard' bell shape distribution one year later. This may be

⁷UBS has a large share in currency options market. Therefore, we assume that the information extracted from UBS data is a good proxy for overall market expectation.

⁸The result is obtained by solving Equation 2.3.11 using the numerical method named Stefensen's Algorithm. Other numerical algorithm may be used to see if better approximation can be achieved. Note that the smile soon flattens out from about 5% change in one-month forward rate, which indicates that the potential errors of Malz's method for extreme values are small and negligible.

a reflection of more stable market expectations, which indicates a smooth market with less unexpected events. More examples of the volatility smile and implied distributions for GBPUSD and EURUSD are listed in Appendix B.

Figure 2.4.3 displays the one-year historical path of the spot FX rate and the calculated higher moments of the implied risk-neutral PDFs. The two periods of significant FX rate changes in the past one year are well reflected in the paths of higher moments. Between August and December 2004, the trend of GBP appreciation was accompanied by the continuous increase in the implied standard deviation, skewness and kurtosis, indicating the increase of uncertainty and bullish market expectations on the GBPUSD FX rate. And it can also be seen that, while the depreciation of GBP started since April 2005, the skewness trended all the way down to the negative zone, reflecting bearish market expectations. A similar correlation between the spot rate and higher moments in EURUSD can be observed from graphs in Appendix B.

The above analysis gives rise to two interesting research areas: 1. From the relationship between the spot FX rate and implied higher moments, a study of the explanatory power of the higher moments in excess forward returns can be carried out using econometric methods. This is done in the next section. 2. The historical paths of the higher moments show that they are stochastic, thus it is important to add such stochastic elements to our models for FX derivative pricing and risk management. A detailed analysis of the stochastic modeling is carried out in the main body of the thesis to reflect real world FX rate movements.

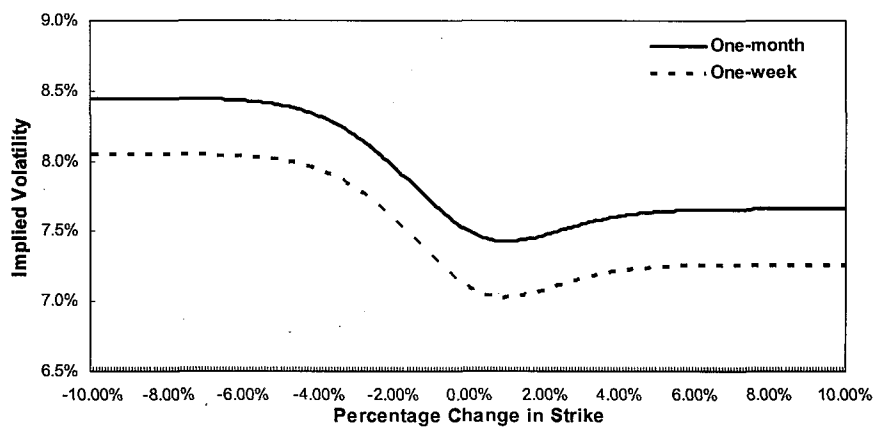


Figure 2.4.1: Implied volatility smile (GBPUSD monthly/weekly 20/06/05)

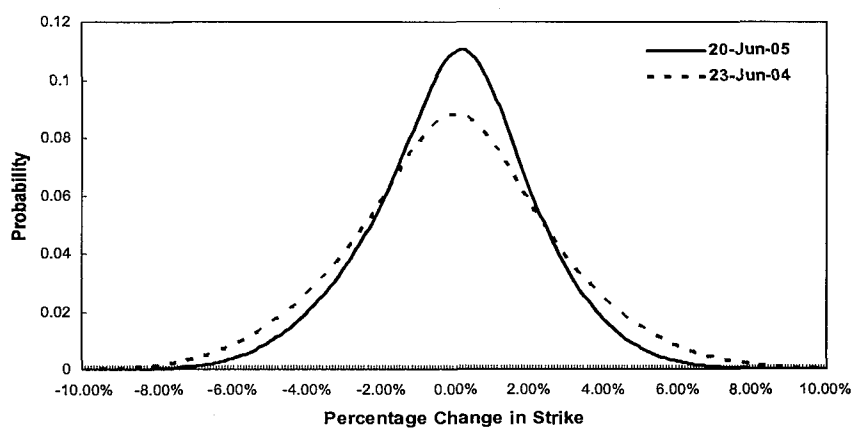


Figure 2.4.2: Option implied PDF (GBPUSD monthly)

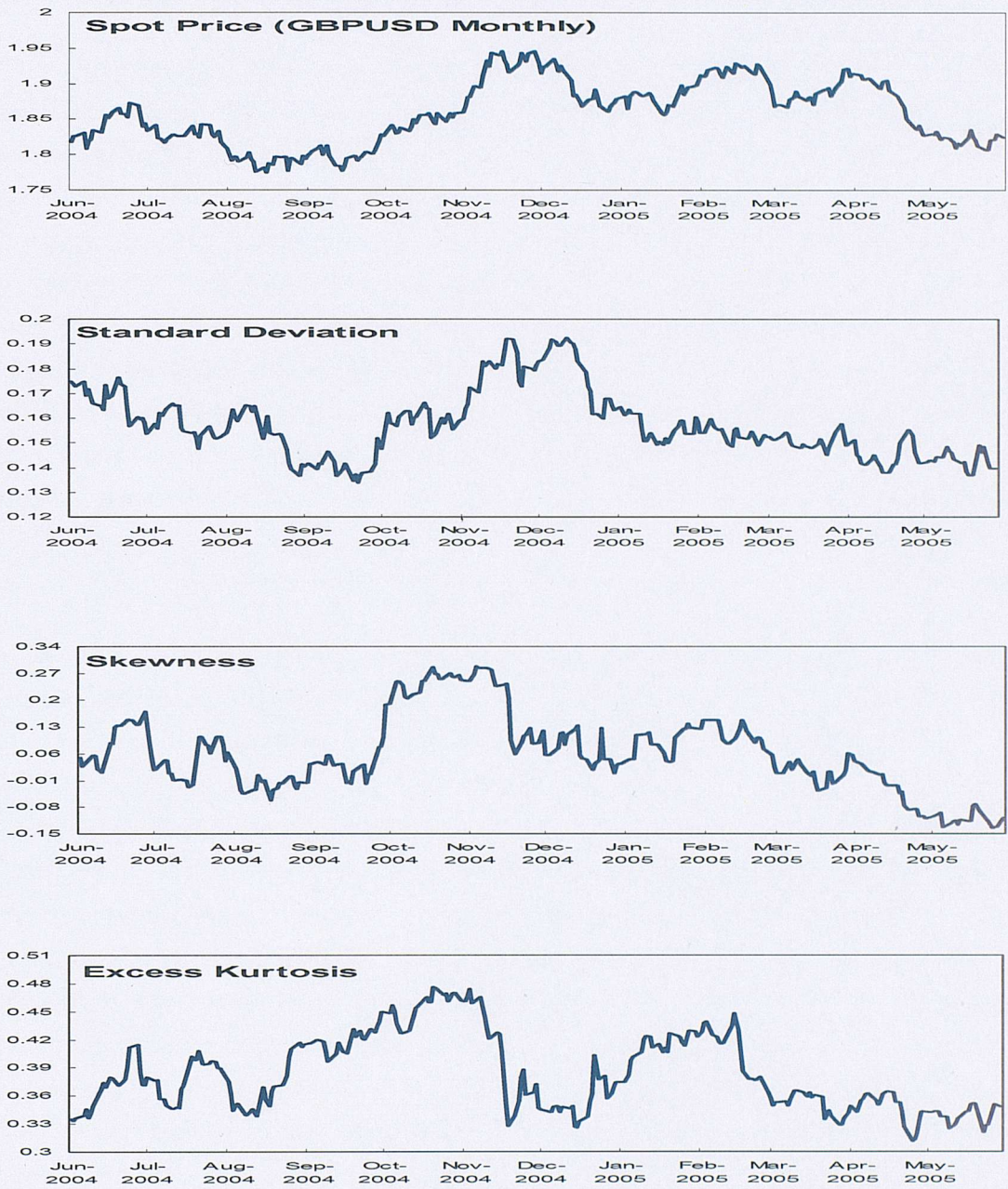


Figure 2.4.3: Spot GBPUSD monthly FX rate and the higher moments of implied PDF

2.5 Excess Forward Returns

The term ‘Forward Bias’ describes the fact that spot FX rates may turn out to be different from what forward rates have indicated. Mathematically, the bias, or excess forward return ζ_T , at time T can be defined as the difference between the spot FX rate at time T and the time t forward rate for T : $\zeta_T = S_T - f_t^T$.

Both research literature and empirical evidence have suggested that excess forward returns can be obtained in currency markets. Some researchers⁹ point out that this may due to the time-varying risk premium, thus it is logical to assume that the size of the excess return can be explained by the market expectations of the characteristic of the risk. Therefore, the most straightforward econometric model is to regress the level of the excess returns on the higher moments of the implied distribution:

$$\zeta_T = \alpha + \beta_1 std_t + \beta_2 skew_t + \beta_3 kurt_t + \varepsilon_t \quad (2.5.1)$$

where std_t , $skew_t$ and $kurt_t$ are the standard deviation, the skewness and the kurtosis of the option-implied PDFs of the currency pairs at time t .

Table 2.5.1 displays an example using GBPUSD one-month data. The data is overlapping as we are using daily data for one-month-ahead market expectations. Therefore, standard errors should be adjusted for the heteroskedasticity and autocorrelation effects using the method proposed by Newey and West [73]. Much previous research done on similar models concludes that the OLS estimated parameters are consistent, and the t-statistics are unbiased after the adjustment. Therefore, the results suggest that the skewness and the kurtosis are significant at 90% and 95% confidence level, respectively, while the standard deviation is insignificant. All three coefficients for the higher moments exhibit correct directions. The overall regression can explain 31.7% of the variation in changes of excess returns. However, as can be seen from the test summary part, this regression fails all tests, which means the data violate standard OLS assumptions and it is better to model them in a different way.

Noting that the data are all time-series, we turn to examine the stationarity

⁹See Lyons[61], Malz[65] and Gereben[39].

Table 2.5.1: Regression Results of Model 2.5.1

Variable	Coefficient	Std.Error	t-Statistic
Constant	-0.48123	0.22095	-2.1780**
std_t	0.60273	0.70148	0.85922
$skew_t$	-0.2363	0.13942	-1.6949*
$kurt_t$	1.0472	0.32376	3.2346**
R^2	0.31743	RSS	0.347699
Log-likelihood	436.862	DW	0.184
Number of observations	237	Number of parameters	4
Mean (Excess Return)	0.0020066	Var (Excess Return)	0.002149
AR 1-2 test:	$F(2, 231) = 526.78[0.0000]**$		
ARCH 1-1 test:	$F(1, 231) = 290.13[0.0000]**$		
Normality test:	$Chi^2(2) = 11.980[0.0025]**$		
Hetero test:	$F(6, 226) = 3.1311[0.0057]**$		

of the time-series data, which is necessary in order to get meaningful regression results. Our stationary tests show that the four time-series, namely excess return, standard deviation, skewness and kurtosis are all $I(1)$ processes¹⁰. In addition, the Augmented Dickey-Fuller (ADF) tests of the residuals indicate that the residuals of the above regression pass the tests at 90% confidence level. The ADF test is formulated as following:

$$\Delta\hat{\mu}_t = \gamma\hat{\mu}_{t-1} + \sum_{j=1}^k \delta_j \Delta\hat{\mu}_{t-j} + \varepsilon_t \quad H_0: \gamma = 0$$

The test results suggest that the time-series are cointegrated. According to the Granger Representation Theorem, there exists a valid long-run equilibrium relationship between these variables, and this relationship can be expressed as an Error Correction Mechanism (ECM). We then model the ECM as follows¹¹:

$$\begin{aligned} \Delta\zeta_t = & \beta_1\Delta\zeta_{t-1} + \beta_2\Delta std_t + \beta_3\Delta std_{t-1} + \beta_4\Delta skew_t + \beta_5\Delta skew_{t-1} \\ & + \beta_6\Delta kurt_t + \beta_7\Delta kurt_{t-1} + \beta_8\mu_{t-1} \end{aligned} \quad (2.5.2)$$

where Δ means first order difference, and $t-1$ indicates first order lag term. Table 2.5.2 shows the regression results.

¹⁰ $I(1)$ means the first-order difference of the time-series is stationary.

¹¹Theoretically, by following the General to Specific method, we should start as many lags as possible to pass the diagnostic tests. However, since financial time series data are usually 1st order autocorrelated, we directly start with only one lag for each variable, and the result of diagnostic tests indicates that such model is well-specified.

Table 2.5.2: Regression Results of Model 2.5.2

Variable	Coefficient	Std.Error	t-Statistic
$\Delta \zeta_{t-1}$	-0.031707	0.07126	-0.445
Δstd_t	-1.06986	0.3948	-2.71**
Δstd_{t-1}	0.676811	0.4084	1.66*
$\Delta skew_t$	0.0720503	0.05470	1.32
$\Delta skew_{t-1}$	-0.025522	0.05296	-0.482
$\Delta kurt_t$	-0.417942	0.1585	-2.64**
$\Delta kurt_{t-1}$	0.120419	0.1622	0.743
μ_{t-1}	-0.039904	0.02367	-1.69*
Sigma	0.0130445	RSS	0.03862
Log-likelihood	690.376	DW	1.96
Number of observations	235	Number of parameters	8
Mean (Excess Return)	-0.000115	Var (Excess Return)	0.000179
AR 1-2 test:	$F(2, 225) = 1.8264 0.1634$		
ARCH 1-1 test:	$F(1, 225) = 0.17891 0.6727$		
Normality test:	$Chi^2(2) = 0.034382 0.9830$		
Hetero test:	$F(16, 210) = 1.1215 0.3367$		

It can be seen from the test summary results that this model passes all OLS assumptions tests, indicating that the model is valid. However, only 4 out of the 8 parameters are significant at the 90% confidence level, suggesting further model improvement by omitting skewness from the long-run relationship.

2.6 Summary

With the Malz[65]’s method, which is specifically designed for FX market, we have estimated the implied risk-neutral distribution from option prices. The results are used in two research areas. Firstly, we follow the econometric method to investigate the explanatory power of the implied higher moments in excess forward returns. The resulting ECM model we proposed provides some econometric evidence of such explanatory power. However, more detailed econometric modeling and more data should be used before we can come to a robust conclusion. This gives rise to further research interest in the area beyond our thesis. Secondly, the stochasticity of the moments that characterize the distribution indicates that they are important sources of uncertainty, which should be considered in derivative pricing models and risk management. We will analyze the modelling techniques to capture the key features of the implied volatility smile and the implied distribution, namely the stochastic higher moments, in the rest of the thesis.

Chapter 3

Models which Capture the FX Smile - A Review

3.1 Derivative Modelling - Theory and Practice

3.1.1 Modelling in Derivative Pricing and Hedging

Black and Schole's seminal paper [15] initialized the practice of using mathematical formula to describe the stochastic process of the financial asset, from which the price of the derivative of the asset can be obtained. During the past 30 years, mathematical modelling has played a key role in derivative pricing and hedging: to value illiquid derivative securities whose prices are not observable in the market, and to calculate future hedging costs for derivatives.

By the end of 1990s, two types of model have been developed and existed in the market: models for forecasting, and models for replication. The first type is mainly used in Hedge funds, while the second type, used in derivative pricing and hedging, is our focus. We will investigate a modelling approach for FX option pricing which is consistent with the smile characteristic discussed in Chapter 2.

3.1.2 Market Reality and Modelling Approach

It is well-known that market incompleteness is a common fact rather than an exception. In addition, markets are not frictionless due to the existence of transaction

costs, bid-offer spreads, and discrete trading. These imply that in practice, perfect replication is impossible and traders have to consider both the initial hedging cost and the future re-hedging cost for pricing.

According to Rebonato[76], two main modelling approaches prevail currently: (1) The fundamental approach - if two models fit similarly to market plain-vanilla options, choose the model with the implied process closer to the statistically observed underlying process. (2) The instrumental approach - examine whether the model-implied option price evolution is consistent with reality. Under this approach, the trader will prefer a process that can produce the desired feature of the volatility smile surface. Some recent research even goes to the extreme of leaving process specification behind and directly modelling the dynamics of the volatility smile surface. Theoretically, the users of the instrumental approach who pay little attention to the true process of the underlying (which is difficult to find and justify) will be a 'money machine' for the other traders. However, in practice, the difficulty in trading for real arbitrages prevents them from playing this tragic role. Therefore, the instrumental approach is more widely used in the market.

In this thesis, we will follow the instrumental approach to find a process which can recover the current and future prices of the FX vanilla options in a plausible way. In other words, the process will be able to produce the proper dynamics of the FX smile surface. Empirical facts (e.g. the analysis of the first part of the thesis) show that the volatility smile for FX is more variable than that of equity and interest rates. It has stochastic skewness and kurtosis, and can even change to a 'smirk'. Therefore, neither pure diffusions nor pure jump processes can be sufficient to account for the asymptotic behavior the entire smile surface, especially the out-of-money option volatilities. Therefore, we should consider more than one mechanism in producing the FX smile, as suggested by Rebonato [76].

We will firstly review individually three popular models: the local volatility model, the stochastic volatility model and the jump diffusion model in the following sections. These models have different advantages in capturing the features of the FX volatility smile, but their disadvantages prevent them from working properly alone. Therefore, we will try to 'combine' these three models to produce a model capable of better capturing the smile dynamics, including stochastic volatility and skewness, and finally apply this model to price exotic options.

3.2 Local Volatility Model

3.2.1 Introduction

The local volatility model forms an important subclass in the stochastic volatility models. In such models, volatility is associated with the underlying variable at each state, hence the term "local". The volatility is uniquely determined conditional on the future realization of the underlying process. In other words, the volatility is restricted to change according to the functional dependence on the underlying, the so-called "Restricted-volatility". Mathematically, the stochastic process of the underlying can be described as:

$$dS_t = [r(t) - q(t)] S_t dt + \sigma_L(S_t, t) S_t dz_t \quad (3.2.1)$$

where S_t represents the time t underlying price, $r(t)$ is the time t instantaneous forward rate, $q(t)$ is dividend yield (or the time t instantaneous forward rate for the foreign country in FX market), $\sigma_L(S_t, t)$ is the local volatility which functionally depends on S_t and t , and dz_t is the increment of Wiener process.

As the volatility term is a deterministic function of the underlying, such a model specification does not require additional randomness to be covered, and the market is complete. Therefore, the whole local volatility model class has several advantages: (1) it can always recover the exogenous plain-vanilla option prices in the market (capture the current FX smile effect); (2) the ability to uniquely price exotic options by portfolio replication; (3) the possibility of producing closed-form solution due to its simplicity.

In the literature, there are three main modelling streams which differ in the way they specify the local volatility function $\sigma_L(S_t, t)$. We will review the key literature of these three models in the following sections.

3.2.2 Implied Volatility Function

The implied volatility function (IVF) model can be literally interpreted as implying the local volatility function from the market quoted plain-vanilla option prices - it is designed to fit exactly the current volatility surface. The model requires the

smooth option prices as input, thus depends on the successful interpolation of the observed discrete price points. Therefore, most of the literatures discussed in Chapter 2 make certain contribution in these area by either providing the possible interpolation methods or estimating the implied probability density for similar pricing purposes.

Derman and Kani[34][35], Rubinstein[80] extract the information for the local volatility function $\sigma_L(S_t, t)$ from observed and interpolated option prices by building an implied recombining binomial tree, which can recover the input prices exactly. Jackwerth[48] then generalizes this method by loosening the probability restrictions in Rubinstein[80]. However, as fully discussed by Rebonato[76], the implied tree model tends to suffer from numerical difficulties and comes up with very implausible estimates of the local volatility surface¹.

Rather than the binomial tree algorithm, Dupire[36] uses observed option prices to specify continuous implied stochastic dynamics for the underlying, and estimates the local volatility function $\sigma_L(S_t, t)$. The theoretical underpinning is Breeden and Litzenberger's [18] result² that the underlying PDF at a specific strike price and maturity date can be express as the compound second-order derivative of the option price with respect to the strike price. Starting from Equation 3.2.1 and using the forward (Fokker-Planck³) equation, both Dupire[36] and Andersen and Brotherton-Ratcliffe[7] show that $\sigma_L(S_t, t)$ can be expressed in a closed-form formula:

$$\sigma_L^2(K, T) = 2 \frac{\frac{\partial C(K, T)}{\partial T} + q(T) C(K, T) + K [r(T) - q(T)] \frac{\partial C(K, T)}{\partial K}}{K^2 \frac{\partial^2 C(K, T)}{\partial^2 K}} \quad (3.2.2)$$

Therefore, given the market plain-vanilla option price $C(K, T)$ with strike K and maturity T , this formula will give the relevant local volatility $\sigma_L(S, t)$ that will prevail when $S_t = K$ and $t = T$.

Compared with the implied tree, his method improves the numerical efficiency for the estimation of local volatility because it avoids numerical constraints such as

¹Rebonato[76] Chapter 12.

²See the discuss in Chapter 2 and Appendix A for Equation 2.1.2

³Given the drift and volatility of the process, Fokker-Planck equation describes the evolution of the future price (or distribution density).

imposing tree recombination. However, the term in the denominator, $\frac{\partial^2 C(K,T)}{\partial^2 K}$, can cause numerical trouble for both deep in-the-money and out-of-the-money options as $C(K,T)$ tends to be very small. Andersen and Brotherton-Ratcliffe[7] thus change Equation 3.2.2 to a new formula in terms of implied volatility. Yet the numerically better formula still has the same big problem as its previous version, as pointed out by Wilmott[90] and many others in their papers, and thoroughly discussed by Rebonato[76]. The task is ill-posed in practice since the estimated local volatility is unstable, and very sensitive to small changes in the input smile surface, which varies with the interpolation and extrapolation methods used. These numerical methods can easily generate numerical noise and financially introduce arbitrage. We have seen in Chapter 2 that even though there is a rich literature on interpolation for implying market information, none of them have demonstrated that it outperforms all the others in terms of stability. This persists as the fundamental disadvantage of the IMF method.

3.2.3 Displaced Diffusions Model

Displaced diffusion assumes that a new quantity, $S_t + a$, follows a geometric Brownian process rather than the original S_t :

$$\frac{d(S_t + a)}{S_t + a} = \mu_a dt + \sigma_a dz_t \quad (3.2.3)$$

where the constant a is the displacement coefficient, μ_a and σ_a are the percentage drift and volatility of $S_t + a$.

This modelling approach was first introduced by Rubinstein [79], and well-discussed in Marris [67]. It carries the advantages of simplicity and a possible link to CEV process. Generally there are two types of modelling formula for forward price which can simplify the diffusion process because of the absence of the drift. The one that links with the CEV is:

$$dF_t = [\gamma F_t + (1 - \gamma) F_0] \sigma_\gamma dz_t \quad (3.2.4)$$

as shown by Marris [67]. Rebonato[76] pointed out that if γ is set equal to the exponent β in CEV process (See next section), these two approaches will produce

extremely similar implied volatilities. Thus displaced diffusion can be a computational proxy for the CEV process. However, such an approximation fails with the deep out-of-the-money options.

3.2.4 CEV Model

Model Description

Constant Elasticity of Variance (CEV), discussed by Cox and Ross [31] in detail, is the most popular local volatility model, where the local volatility function is specified explicitly as an exponential function of the underlying:

$$dS_t = [r(t) - q(t)] S_t dt + \sigma_t S_t^\beta dz_t \quad (3.2.5)$$

where β is a positive constant and $\sigma_t S_t^{\beta-1}$ represents the volatility of the stock return, which is $\sigma_L(S_t, t)$ in formula 3.2.1. It includes two special cases: $\beta = 1$ for geometric Brownian motions and $\beta = 0$ for arithmetic Brownian motions.

In the range of $0 < \beta < 1$, CEV can capture the so-called "Leverage effect", introduced by Black[14] and widely discussed in many recent papers. According to empirical observation, the underlying price is negatively correlated with the volatility. Therefore, in the above specific range for β , which is a typical assumption in the equity case, the hedge ratios produced by CEV model reflect the ability to vega-hedge with the underlying asset. In the FX context, however, we need to know what will happen if the domestic and foreign countries are switched. In other words, the views from the investors from both countries are equally important. Therefore, it is necessary to consider the symmetric interval $[-1, 1]$ so that we can use a general functional form of the SDE which is invariant when changing between domestic and foreign markets:

$$dS_t = (r_t - r_{f_t}) S_t dt + \sigma_t (S_t)^\beta dz_t \quad (3.2.6)$$

One key advantage of the CEV model is its analytical tractability. With such a complicated SDE which can predict skews, it is still possible to get the closed-form solution for European options. A more convenient practice is to derive the

option pricing formula for $\beta \in (0, 1)$, and then apply the "Put-call symmetry"⁴ to finish the part $(-1, 0)$. The special case when $\beta = 1$ can be simply solved by Black-Schole's formula, and $\beta = 0$ can be solved using the formula for arithmetic Brownian motion.

By using Laplace transform and Fourier representation for modified Bessel functions⁵, we can get the resulting formula for the European call:

$$C(t, S) = e^{-rf_t(T-t)} S [1 - \chi^2(a, b + 2, c)] - e^{-r_t(T-t)} K \chi^2(c, b, a) \quad (3.2.7)$$

where $\chi^2(z, k, v)$ is the cumulative probability of a non-central χ^2 distributed variable, with noncentrality parameter v , k degree of freedom and quantile z . The variables a , b and c are given by:

$$a = \frac{[K e^{-(r_t - rf_t)T}]^{2(1-\beta)}}{(1-\beta)^2 \delta}, \quad b = \frac{1}{1-\beta}, \quad c = \frac{S^{2(1-\beta)}}{(1-\beta)^2 \delta}$$

The put price can then be derived by the put-call parity:

$$P(t, S) = e^{-r_t(T-t)} K [1 - \chi^2(c, b, a)] - e^{-rf_t(T-t)} S \chi^2(a, b + 2, c) \quad (3.2.8)$$

Finally, with the help of put-call symmetry, we can derive the pricing formula for the case $\beta \in (-1, 0)$: $C(\beta, t, S, K, \sigma, r, rf) = SKP(-\beta, t, 1/S, 1/K, \sigma, rf, r)$, and we apply the put-call parity again to get $P(\beta, t, S, K, \sigma, r, rf)$.

Data and Calibration

We apply the CEV model to historical GBPUSD and EURUSD exchange rate data on 19/10/2005. According to the discussion in Chapter 2, the quote in FX market allows us to imply the 25-delta call and put volatility from the quote of

⁴Put-call symmetry is a special case of Put-call duality, which is based on the change of numeraire through Girsanov's Theorem.

⁵For detailed derivations, see Schroder, M. 1989. Computing the Constant Elasticity of Variance Option Pricing Formula, *Journal of Finance*, Vol 44, No.1, and Lipton, A. 2001. *Mathematical Methods for Foreign Exchange*, Chapter 10.

ATM, 25-delta risk reversal and strangle, using formulas 2.3.6 and 2.3.7. We then calculate the strike and option prices from such quotes, and calibrate the CEV model by minimizing the sum of square of errors:

$$\min_{\beta, \sigma} \sum_{i=1}^3 \sum_{j=1}^{11} (V(S_0, K_{ij}, T_i, r_i, rf_i, \beta, \sigma) - V_{ij})^2 \quad (3.2.9)$$

where $V(S_0, K_{ij}, T_i, r_i, rf_i, \beta, \sigma)$ is the CEV model price for both call and put using the closed-form formula 3.2.7 and 3.2.8 respectively, and V_{ij} is the relevant market price, from 2-week to 30-month⁶. We find that for both currency pairs, the calibrated β is greater than 1, while volatilities are less than but close to the implied volatility. Figure 3.2.1 displays the market implied term structure of option price and the CEV model result for GBPUSD currency pair. Figure 3.2.2 shows the market data and the result for EURUSD. The merit of the CEV model is easily seen: both figures show that the model can fit the market data well.

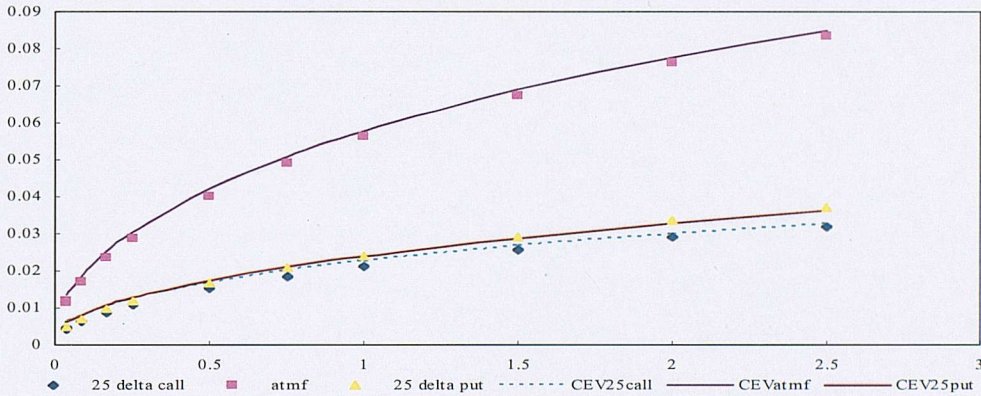


Figure 3.2.1: Term structure of option prices for GBPUSD

⁶The 1-week data are not quite consistent with the other data in the CEV model, so we only start from 2-week data. The 3-year and 4-year data from UBS are flat, which is not consistent with the normal smile. Thus we have 3 instruments (ATM, 25-delta call and 25-delta put), each of which has 11 terms.

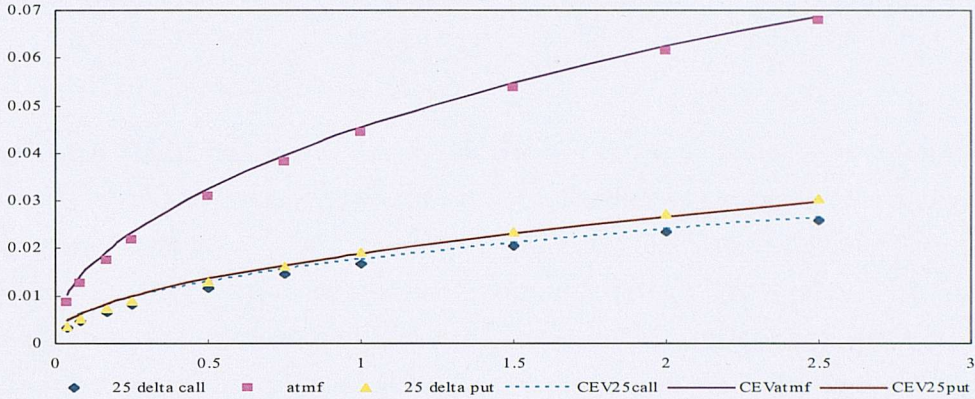


Figure 3.2.2: Term structure of option prices for EURUSD

3.2.5 Summary

Local volatility models are quite popular among practitioners in equity, FX and interest rate (CEV) modelling because of their ability to capture the smile effect and good fit to the market data, while keeping the tractability. However, as criticized by Andersen[6], Rebonato[76], Albanese[2] and many other researchers, such models suffer from the dynamic inconsistency. This can be explained in two ways: (1) The local volatility function is not stationary, implying that future smiles will be quite different from the current ones, and recalibration is necessary whenever the market data change. In reality, however, the market smile tends to be stationary. (2) The model implied volatilities of the same strike tend to stay the same while the underlying price changes. Empirically, the so-called "Sticky-strike" result only appears occasionally, yet the "Sticky-delta" phenomenon, in which the implied volatilities of the same delta stay approximately constant as the underlying evolves, is observed frequently in the normal market[33]. Therefore, pure local volatility models are not adequate for our modelling purpose, especially in FX, where the jump is a common phenomenon rather than an exception.

3.3 Stochastic Volatility Model

3.3.1 Introduction

Stochastic Volatility (SV) is the one of the key terms in financial economics. Empirical studies have demonstrated that the volatility of financial time series is not only non-constant, but also cannot be described by a deterministic function of time, or even a function of time and the underlying. The graphs in Chapter 2 vividly show the stochastic evolution of the standard deviation through one year. SV models specify an additional stochastic process for the volatility of the underlying, so as to better capture the dynamics of the option data or high frequency return data.

From the hedging perspective, the presence of the new uncertainty (risk) associated with stochastic volatility can only be neutralized by using an additional traded asset which depends on volatility. Otherwise, the market with the underlying only is incomplete, since volatility is not traded. Rebonato[76] shows that the strategy of hedging with the underlying and an option does not work because a no-arbitrage unique price can only be obtained if the hedger knows the full process, which is not practical at all. In addition, the complex specification results in the intractability of the model - a closed-form solution is only possible for special processes.

More recent research even shows that more and more complicated volatility dynamics are necessary to model financial data (see Rebonato[76] and Albanese and Kuznetsov[2] for example). At the same time, estimation issues generate another stream of literature, which includes much econometric work. We will briefly review these main fields in the next section, followed by a more detailed discussion of two tractable special cases and their application in option pricing.

3.3.2 Literature Review

Heterogeneity in the variance was accepted as a fact even at the time when Black and Scholes[15] published their seminal paper based on a homogeneity assumption. They point out that the evidence of non-stationary of variance should call for more future work. A rich literature ensues to address the issue, in which the first

published SV paper is written by Taylor[86]. In his discrete time model, the risky part of the daily returns is set to follow a product process.

Johnson and Shanno[51] studies the option pricing issue in time-varying variance models, while Wiggins[89] uses the stochastic volatility model to examine the option valuation. Among all the other similar works, Hull and White[47] seems to be the most widely-known one, which we will discuss in the next section.

In the last decade, SV extensions have been widely witnessed in the literature. Bates[13] influentially demonstrates that it is necessary to add jumps to the standard SV models, particularly under Markovian volatility. Eraker, Johannes and Polson[37] examine SV models incorporating jumps in both underlying and volatility process, and develop an efficient technique for parameter estimation. Furthermore, some researchers suggest a different jump modelling approach using Ornstein-Uhlenbeck (OU) type process. Barndorff-Nielsen and Shephard[10] study the financial application of the non-Gaussian OU-based models and possible closed-form solutions. Nicolato and Venardos[74] investigate the OU class in derivative analysis and the related market incompleteness, and derive a closed-form solution for vanilla options when the structure preserves Martingale property.

The other stream of literature extends the SV model by using a long-memory dynamic to describe σ . Breidt, Crato and Lima[19] propose incorporating an ARFIMA process into a standard SV process. This discretely models the log of volatility by fractional ARMA process. Comte and Renault[29] work on the continuous-time moving average fractional process, which reconciles ARMA and Brownian motion and thus uses fractional integration of Brownian to model the log of volatility.

In the field of estimating the SV model parameters, there are roughly two streams: Generalized Method of Moments (GMM), and the Markov Chain Monte Carlo (MCMC) simulation⁷ based approach.

Taylor[86] first calibrates his SV model using the method of moments. Melino and Turnbull[69] then use the GMM method to estimate the SV model parameters for FX data. Andersen and Sorensen[8] systematically study which moments should be heavily weighted in SV models using the GMM method, and similar

⁷MCMC samples from the last step of a constructed Markov chain, which has the desired distribution. The quality of such simulation improves with the increase of the number of steps.

studies are done by both Sorensen[84] and Hoffmann[45]. However, Ruiz[81] shows that in practice, GMM is not as efficient as Quasi-Maximum Likelihood (QML) combined with Kalman filter.

For MCMC, early application can be found in Jacquier, Polson and Rossi[50]. Subsequently, Kim, Shephard and Chib[55] widely discuss several types of MCMC algorithms. In addition, they introduce a "particle filter", the first filter in this field. This facilitates model comparison and model testing.

In summary, the literature for SV model is both extensive and intensive. In the following section, we will concentrate on the SV models in option pricing.

3.3.3 Option Pricing

By describing financial data in a more realistic manner, SV models provide a good basis for option pricing modelling. Important papers like Hull and White[47] appear as early as 1987. Stein and Stein[85] introduce the first analytic stock option pricing formula, while Heston[44] provides another closed-form solution and extends it for bond and FX options. In more recent research, Nicolato and Venardos[74] carry out a detailed study on OU SV models based on Barndorff-Nielsen and Shephard[10]. Of all these, Hull and White[47] and Heston[44] appear to be the most popular and influential through time.

Hull and White SV Model

Taking the leverage effect into account, Hull and White[47] assume that the underlying S and its variance V follow risk-neutral processes:

$$dS = (r - q) S dt + \sqrt{V} S dz_S \quad (3.3.1)$$

$$dV = \theta (V_L - V) dt + \xi V^\alpha dz_V \quad (3.3.2)$$

where the mean-reverting rate θ , long-term variance rate V_L , volatility of variance ξ and elasticity parameter α are all constants, and the Wiener processes z_S and z_V are correlated with coefficient ρ .

Hull and White show that their model can produce both a smile and a skew in option implied volatility, and the result is quite consistent with the FX market

implied volatility pattern. Their study indicates that by assuming constant rather than the real stochastic volatility, Black-Scholes tends to overprice at-the-money or close to the money options, and underprice deep in- or deep out-of-the-money options[47]. They also provide the analytic formula for vanilla call option when $\rho = 0$: $C_{HW} = \int_0^\infty c(\bar{V}) g(\bar{V}) d\bar{V}$, where \bar{V} is the average variance rate, $c(\bar{V})$ is the Black-Scholes price as the function of \bar{V} , and $g(\bar{V})$ is the risk-neutral probability density function.

Heston SV Model

Heston[44] points out that SV models assuming no correlation between volatility and the underlying asset (e.g. Wiggins[89]) can not capture the important skewness effect, which is generated by correlation. Compared with the Hull-White approach which has to rely on Monte Carlo simulation, he models the volatility rather than the variance and comes up with a general closed-form solution with the help of characteristic functions:

$$dS_t = \mu S_t dt + \sqrt{v_t} S_t dz_1 \quad (3.3.3)$$

$$d\sqrt{v_t} = -\beta \sqrt{v_t} dt + \delta dz_2 \quad (3.3.4)$$

where drift μ and β , volatility of volatility δ are constants, the Wiener processes z_1 and z_2 have correlation ρ ($dz_1 dz_2 = \rho dt$). The volatility actually follows an OU process, which is used in Stein and Stein[85].

Heston guesses the Black-Scholes type solution for the vanilla options, and subsequent researches show that the general formula for FX options is:

$$h(t) = \phi \left[e^{-rf\tau} S_t P_+(\phi) - K e^{-r\tau} P_-(\phi) \right] \quad (3.3.5)$$

where $P_+(\phi)$ and $P_-(\phi)$ are the conditional cumulative probabilities that the option expires in-the-money, solved via the inverse Fourier Transform of the characteristic functions.

This closed-form solution is used to calibrate to market vanilla options, the

resulting Heston model can then be applied to price exotic options via a finite difference method or, using Monte Carlo simulation.

Calibration

As mentioned in the literature review, it is quite common to estimate the parameters from a time series of historical data, using econometric techniques such as Generalized Method of Moments (GMM) and Monte Carlo (MCMC) simulation. In addition, Efficient Method of Moments (EMM) is also popular. These methods are used to fit the empirical return distributions to the marginal distributions, and suitable for intractable SV models. However, we cannot estimate the market price of risk. For those with closed-form solutions, a different smile-based method can be used: we can find the parameters by minimizing the sum of square of errors between the market and model implied volatility smile. For example, for Heston model, we need to solve the following optimization problem:

$$\min_{\kappa, \theta, \sigma, \rho, v_0} \sum_{i=1}^3 (\hat{\sigma}_i - \sigma_i(\kappa, \theta, \sigma, \rho, v_0))^2 \quad (3.3.6)$$

where $\hat{\sigma}_i$ is the market implied volatility for a single maturity. Since market price of risk is embedded in the volatility smile, this method frees us from estimating it.

3.3.4 Summary

Empirical testing of SV models shows that they can fit the market implied volatility smile for the medium maturities quite well, but fail for the short and extremely long maturities[88]. In particular, such models tend to have difficulties in producing smiles steep enough to capture the short-term behavior of the market implied volatilities, unless one assumes time-dependent parameters or large instantaneous volatilities. However, these remedies either generate a non-time-homogeneous smile surface or become inconsistent. Rebonato[76] also points out that it is not practical to overcome this shortcoming by using a high reversion rate and a high volatility of volatility, which is not a "free parameter". Therefore, pure stochastic volatility models are not suitable for our modelling purpose either.

3.4 Jump Model

3.4.1 Introduction

The FX market is quite sensitive to government policy and economic news. Historical market data of many currency pairs suggest that jumps usually occur in response to certain economic events. A jump model is devised to account for such possibility.

Literature in this field shows that two different modelling approach can be used to capture the market character: A jump diffusion model specifies both the continuous and discontinuous components presented in the dynamics of the exchange rates, such as the well-known model by Merton[71], and Bates[13]; the Variance-Gamma (VG) model uses stochastic time-change to reflect the impact of unpredictable events, as introduced by Madan and Seneta[62]. We will analyze the these models in the next two sections.

3.4.2 Jump Diffusion Model

A jump diffusion model is a mixture of jump process and Brownian motion diffusion. Merton[71] provides one of the earliest descriptions of the jump process in option pricing, while Glasserman and Kou[40] look at its application in interest rate modelling. In the FX context, Lipton[58] gives a detail description of one special case in Merton's general model, namely the log-normal jump amplitude, and models the FX spot rate with the SDE:

$$\frac{dS_t}{S_t} = (\alpha - \lambda\kappa) dt + \sigma dz_t + (e^J - 1) dN_t \quad (3.4.1)$$

where the Poisson process N_t is assumed to be independent of the Wiener process z_t , and the logarithm of jump size is described as an *i.i.d* distributed random number J with the probability density $f(J)$. The probability of more than one jump between t and $t + dt$ is assumed to be negligible. λ is the average number of jumps per unit time in the real world, $e^J - 1$ is the percentage change in the exchange rate before and after the jump, and κ represents the expected size of the percentage jump amplitude. One trivial advantage over the CEV model is that

the jump diffusion model is the same when switching between the domestic and foreign markets.

Assuming that jump amplitude J is normally distributed, we can get the vanilla call option pricing formula:

$$C_{JD}(S, K, \tau, \sigma, r, rf) = \sum_{n=0}^{\infty} \frac{e^{-\lambda'\tau} (\lambda'\tau)^n}{n!} C_{BS}(S, K, \tau, \sigma_n, r_n, rf) \quad (3.4.2)$$

with

$$\lambda' = \lambda e^{\mu + \nu^2/2}, \quad \sigma_n^2 = \sigma^2 + \frac{n\nu^2}{\tau}, \quad r_n = r + \lambda - \lambda' + \frac{n(\mu + \nu^2/2)}{\tau}.$$

Although Formula 3.4.2 results from the special distribution assumption, it is quite representative and can be used to analyze the implied volatility pattern of jump diffusion models. With certain experimental parameters, we evaluate implied volatilities for the call options, and the result is displayed in Figure 3.4.1.

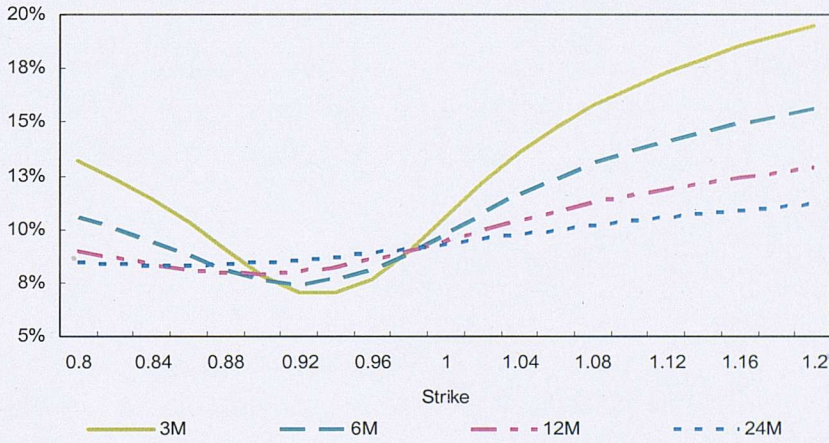


Figure 3.4.1: The Jump Diffusion model implied volatility, with parameters: $S = 0.95$, $\sigma = 0.05$, $r = 0.05$, $rf = 0.03$, $\lambda = 0.5$, $\mu = 0.05$, $\nu = 0.1$.

It is obvious that the model implied volatility smiles for the long maturities tend to flatten out very quickly, which is not consistent with the market data, and thus is the main shortcoming of the pure jump diffusion model.

3.4.3 Variance Gamma Model

Introduced by Madan and Seneta[62], the Variance Gamma (VG) model is a pure jump model without a diffusion component, yet it can fit the current option prices time-homogeneously, as well as stochastic volatility and/or jump diffusion models. VG is financially motivated by the idea that "economic time", which is affected by the irregular arrival of unpredictable events, does not flow evenly. Mathematically, this is translated into a stochastic time change, i.e. using a mechanism to randomly accelerate or slow down time. Importantly, as normal time flows, this mechanism must always increase the time. A good candidate for this is the gamma process: $\gamma = \gamma(t; 1, \nu)$, and the VG process is the Brownian motion evaluated at $t = \gamma(t; 1, \nu)$:

$$x(t; \theta, \sigma, \nu) = B(\gamma(t; 1, \nu); \theta, \sigma) = \theta \gamma(t; 1, \nu) + \sigma z(\gamma(t; 1, \nu)) \quad (3.4.3)$$

where θ is the Brownian motion drift, z is a Wiener process, and the mean 1 in the gamma process guarantees that when $\nu = 0$ the new time γ becomes the clock time t .

One key property of the gamma process is that it evolves discretely through the time with high (low) probability for small (large) increments. The increment g over a finite interval h , has the distribution:

$$f_h(g) = \left(\frac{\mu}{\nu}\right)^{\frac{\mu^2 h}{\nu}} \frac{g^{\frac{\mu^2 h}{\nu} - 1} e^{-\frac{\mu}{\nu} g}}{\Gamma\left(\frac{\mu^2 h}{\nu}\right)} \quad (3.4.4)$$

where $\Gamma(x)$ is the gamma function.

In their most important paper in the VG literature, Madan, Carr and Chang[64] systematically develop the VG framework and use it to model the logarithm of stock prices. According to their model construction, the VG process is a Brownian motion conditional on a particular time change g , thus it is normally distributed with density function $\phi(X | g)$:

$$\phi(X | g) = \frac{1}{\sigma \sqrt{2\pi g}} \exp \left[-\frac{(X - \theta g)^2}{2\sigma^2 g} \right] \quad (3.4.5)$$

We can then get the unconditional density function $f_t(X)$ over the time interval t by using Formula 3.4.4 with $\mu = 1$ to integrate Formula 3.4.5 over all time changes:

$$\begin{aligned} f_t(X) &= \int_0^\infty \phi(X | g) f_h(g) dg \\ &= \int_0^\infty \frac{1}{\sigma\sqrt{2\pi g}} \exp\left[-\frac{(X - \theta g)^2}{2\sigma^2 g}\right] \frac{g^{\frac{t}{\nu}-1} e^{-\frac{g}{\nu}}}{\nu^{\frac{t}{\nu}} \Gamma\left(\frac{t}{\nu}\right)} dg \end{aligned} \quad (3.4.6)$$

With the normally distributed variable $X(t)$, Mandan *et al* [64] specify the risk-neutral process of the stock price at time t as:

$$S_t = S_0 \exp[rt + X(t; \sigma_{rn}, \nu_{rn}, \theta_{rn}) + \omega_{rn}t] \quad (3.4.7)$$

where the subscript rn indicates that those are risk-neutral parameters, and $\omega_{rn} = \frac{1}{\nu_{rn}} \ln(1 - \theta_{rn}\nu_{rn} - \sigma_{rn}^2\nu_{rn}/2)$, which is set to ensure the equality between the expectation of the stock price return and the risk-neutral return.

Due to its linear dependence on the stock price, the payoff has the same probability as $X(t; \sigma, \nu, \theta)$, and the price of a vanilla call option with strike price K can thus be obtained by using Formula 3.4.6. Madan and Milne[63] further make use of the fact that the call price is normally distributed, conditional on the realized time change g , and give the Black price as:

$$\begin{aligned} C(g) &= S_0 (1 - c_1)^{\frac{t}{\nu}} \exp\left(\frac{g(\alpha + s)^2}{2}\right) \Phi\left(\frac{d}{\sqrt{g}} + (\alpha + s)\sqrt{g}\right) \\ &\quad - K \exp(-rt) (1 - c_2)^{\frac{t}{\nu}} \exp\left(\frac{g\alpha^2}{2}\right) \Phi\left(\frac{d}{\sqrt{g}} + \alpha\sqrt{g}\right) \end{aligned} \quad (3.4.8)$$

with

$$\begin{aligned}\alpha &= \zeta s, \quad \zeta = -\frac{\theta}{\sigma^2}, \quad s = \frac{\sigma}{\sqrt{1 + \left(\frac{\theta}{\sigma}\right)^2 \frac{\nu}{2}}} \\ d &= \frac{1}{s} \left\{ \ln \frac{S_0}{K} + rt + \frac{t}{\nu} \ln \left[\frac{1 - c_1}{1 - c_2} \right] \right\} \\ c_1 &= \frac{\nu(\alpha + s)^2}{2}, \quad c_2 = \frac{\nu\alpha^2}{2}\end{aligned}$$

The unconditional call price is finally calculated by numerically integrating over the density of g :

$$C_{VG}(S_t, K) = \int_0^\infty C(g) \frac{g^{\frac{t}{\nu}-1} e^{-\frac{g}{\nu}}}{\nu^{\frac{t}{\nu}} \Gamma\left(\frac{t}{\nu}\right)} dg \quad (3.4.9)$$

Using special functions, Madan, Carr and Chang[64] further develop a semi-closed form formula:

$$\begin{aligned}C_{VG}(S_0, K, t, r) &= S_0 \Psi \left(d \sqrt{\frac{1 - c_1}{\nu}}, (\alpha + s) \sqrt{\frac{\nu}{1 - c_1}}, \frac{t}{\nu} \right) \\ &\quad - K \exp(-rt) \Psi \left(d \sqrt{\frac{1 - c_2}{\nu}}, \alpha s \sqrt{\frac{\nu}{1 - c_2}}, \frac{t}{\nu} \right)\end{aligned} \quad (3.4.10)$$

with c_1 , c_2 and d defined as before, and the probability distribution function $\Psi(a, b, \gamma)$ is expressed in terms of the modified Bessel function of the second kind and the degenerate hypogeometric function of two variables, see Madan *et al* [64] for detailed description.

We apply Madan and Milne's method using parameters estimated in Madan *et al* [64] to examine the volatility smile produced by VG model. The result in Figure 3.4.2 shows that VG model can generate a steep enough volatility smile for short maturities, however, the smiles soon flatten out as the maturity increases. This is quite similar to what we have obtained from Jump diffusion model, indicating a general shortcoming of jump models.

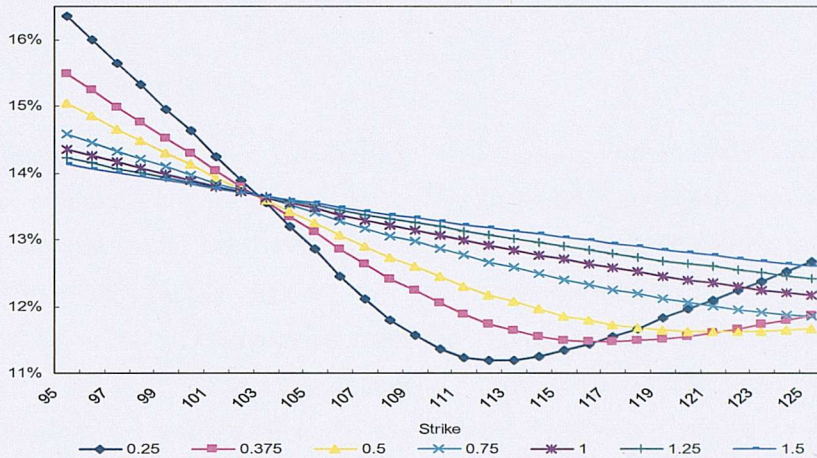


Figure 3.4.2: The Variance Gamma model implied volatility, with parameters: $S = 105$, $r = 0.05$, $\sigma = 0.1213$, $\theta = -0.436$, $\nu = 0.1686$.

3.4.4 Summary

With different mechanisms, both Jump diffusion and Variance Gamma models can capture the jump feature in the FX market, which appears as heavier left and right tails compared with the Black-Scholes model. This explains the growing popularity of jump models in FX and credit derivative modelling.

In contrast to the SV model, the Jump diffusion model generates deterministic future smiles which are independent of the future realization of the underlying price, because of the memoryless property of the Poisson process. It is then left to market reality and the trader's view to justify whether this is an appealing property. The VG model also produces perfectly deterministic smiles. However, as pointed out by many researchers and revealed in our numerical studies, implied volatility smiles produced by jump models tend to flatten out too rapidly, although the short-term skews are closed to those in the market. Therefore, pure jump models cannot fulfill the modelling demand of generating realistic market volatility smiles.

3.5 Combined Model

3.5.1 Introduction

The review of three popular FX smile modelling approaches leads us to the conclusion that although they are each appealing in some way, their disadvantages prevent them from being adequate individually. Therefore, the direction of research towards unifying volatility model, i.e. combining the models to take advantage of them, has been in the literature for a while. Bates[13] examines stochastic volatility model with jump, the most common practice in model unification. Carr *et al* [27] produce a leverage effect by specifying correlation between the jumps and the stochastic volatility factor in their time-changed Levy processes model. Furthermore, Britten-Jones and Neuberger[20] combine the local volatility, stochastic volatility and jump-diffusion models, Albanese and Kuznetsov[2] prove that the mixture of the three volatility models can capture the complex features of exotic option prices in a tractable way. We will briefly review the most representative Bates[13] model.

3.5.2 Bates Model

Bates[13] model combines the Heston[44] stochastic volatility model and the Merton[71] jump diffusion model:

$$\begin{aligned}\frac{dS}{S} &= (\mu - \lambda \bar{k}) dt + \sqrt{V} dz + k dN \\ dV &= (\alpha - \beta V) dt + \sigma_v \sqrt{V} dz_v \\ cov(dz, dz_v) &= \rho dt \\ prob(dN = 1) &= \lambda dt, \ln(1 + k) \sim N\left(\ln(1 + \bar{k}) - \frac{1}{2}\delta^2, \delta^2\right)\end{aligned}\tag{3.5.1}$$

where μ is the instantaneous expected appreciation of the FX rate, λ is the annual jump frequency, k is the random jump intensity conditional on a jump occurring. It generalizes the stochastic volatility model 3.3.3 by adding jumps dN , or generalizes the jump diffusion model 3.4.1 by allowing the diffusion volatility \sqrt{V} to be stochastic. Skewness can be captured either by the non-zero correlation ρ between

FX rate and volatility process, or by non-zero average jumps. Excess kurtosis can be generated by the volatility of volatility or sufficient jumps. Therefore, the disadvantage of one individual modelling approach can be compensated by the other: at short maturity, the steep smile pattern can be captured by the jump diffusion, while at the longer maturities, it is generated by the stochastic volatility specification.

Bates obtains the pricing kernel by firstly solving the moment generating functions $F_j(\Phi|V, T)$, then applying the inverse Fourier transform to the complex-valued characteristic function $F_j(i\Phi|S_0, T)$. However, the model suffers from certain deficiencies, the most severe of which is the parameter instability, especially with the term structure of implied volatilities. The model also fails to capture the different skewness across various maturities. Reasonable extensions or different modelling approaches are desired.

3.5.3 Summary

Combined models, by taking advantage of different individual models, can produce some of the implied volatility surface properties that fit the market observed data. However, there are many issues regarding the appropriateness of the combination and numerical implementation. For example, currently, the degree of mixture between the stochastic volatility and jump diffusion is still an important topic in consistently pricing exotic options. These richer models are usually very difficult to implement.

In addition, the combination of stochastic volatility and jump diffusion can generate only deterministic skewness for the risk-neutral distribution. The skewness in the market, either observed by its proxy - risk reversal, or implied from the quotes as shown in Part I, is actually stochastic. The ability of a model to capture this important feature is quite desirable. Within the existing combined models framework, we can obtain stochastic skewness by either randomizing the mean jump size (k) or the correlation between FX rates and increments in volatility (ρ), yet neither of these are tractable.

The deficiencies of the combined models and the difficulties in their extension lead us to escape the constraints of the current framework and look at the modelling

approach in a more general way, as well as to search for a more 'novel' idea in model specification, which can fit the market data well and produce a consistent volatility smile surface.

3.6 Carr's Stochastic Skewness Model

3.6.1 Modelling Stochastic Skewness - Motivation

Main Sources of Uncertainty

From the previous reviews and market observation, we can recognise at least three sources of uncertainty in FX rates and their implied distribution. These need to be considered and reflected in currency option pricing. The first source is the stochastic exchange rate process, which gives the random risk-neutral mean. The Black-Scholes/Garman-Kohlhagen model, which assumes constant volatility and interest rate, can account for this underlying uncertainty. The second source, stochastic volatility, is widely observed in the market from either historical time series data or implied from option quotes, and has become an essential requirement in modelling. Both stochastic volatility models (e.g. Heston[44]) and combined models (e.g. Bates[13]) can handle this issue in addition to the first and generate deterministic skewness. The third source is stochastic skewness, which reflects the random movement of the risk-neutral distribution asymmetry over time. Carr's model aims to address all three sources of uncertainty with tractability.

Evidence of Stochastic Skewness

From Figure 2.4.3 in Chapter 2, the skewness of the implied risk-neutral distribution is indeed stochastic. Alternatively, to avoid any distortion due to numerical instability, we can directly examine the market quote for risk reversal, which is a proxy for skewness. Figure 3.6.1 shows the historical quotes for a 25-delta risk reversal and strangle, in two currency pairs.

It can be observed that the risk reversal, which measures the skewness, varies randomly over calendar time. Thus the skewness of the risk-neutral distribution is stochastic and needs to be built into the model. It is interesting to point out that

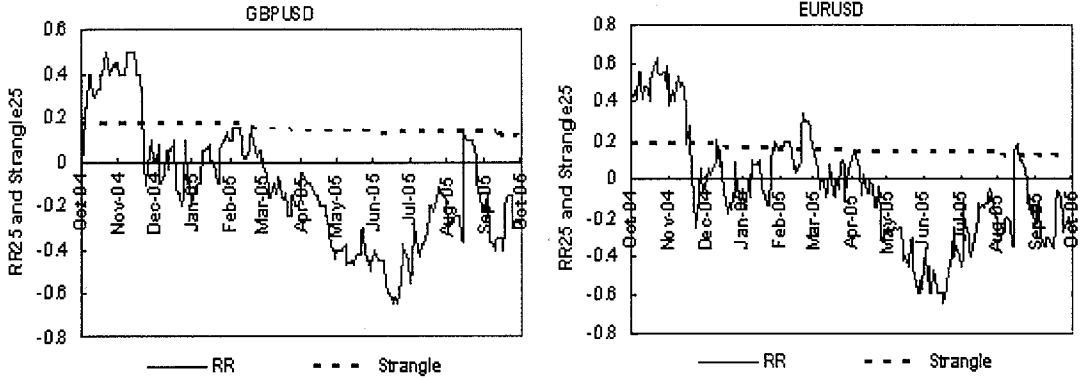


Figure 3.6.1: 1-Month 25-delta Risk Reversal and Strangle (Daily Data from 19/10/04 to 19/10/05)

the strangle, as a proxy for kurtosis, is quite stable over time, which contradicts the calculated kurtosis of the implied distribution. Due to the possible numerical instability of Malz's method, it is better to rely on the strangle observation and conclude that kurtosis is stable enough to be excluded as a source of uncertainty.

3.6.2 Generalized Modelling Approach

Instead of struggling in the tractability of the combined model, Carr and Wu[25] suggest looking at the option pricing issue in a more general framework, i.e. the wider class of Lévy Processes.

Lévy Processes

To generate an empirical non-Normal distribution for log returns of most financial assets more flexible stochastic processes, which generalize Brownian motion, are needed. Such processes, with independent and stationary increments, which give general infinitely divisible⁸ distributions, are called Lévy processes.

Definition 3.6.1 *A stochastic process $(X_t)_{t \geq 0}$ in \mathbb{R} is called a Lévy process if: (X_t) starts at zero and has independent and stationary increments, and the trajectories*

⁸If, for every positive integer n , the characteristic function of distribution $\phi(u)$ is also the n th power of a characteristic function, the distribution is *infinitely divisible*.

of (X_t) is càdlàg⁹.

For example, the arithmetic Brownian motion (ABM) is the only continuous Lévy process; the compound Poisson process, the pure jump Gamma process, and the generalization of pure jump CGMY[27] are all Lévy processes.

One of the key concepts in Lévy processes related calculation is the characteristic function:

Definition 3.6.2 *The characteristic function ϕ of a distribution, or a random variable X , is the Fourier transform of the distribution function $F(x) = P(X \leq x)$:*

$$\phi_X(u) \equiv \int_{-\infty}^{+\infty} e^{iux} dF(x) = E[e^{iuX}] \quad (3.6.1)$$

Equivalently, it can be defined as the Fourier transform of the probability density function (PDF) $q(x)$: $\phi_q(u) \equiv \int_{-\infty}^{+\infty} e^{iux} q(x) dx = E[e^{iuX}]$.

In option pricing, the pricing kernel $g(x)$ is actually the discounted risk-neutral PDF. The price V_0 of a claim paying $f(X_T)$ at maturity T can be obtained via risk-neutral valuation: $V_0 = \int_{-\infty}^{+\infty} f(k) g(k) dk$.

From the Inverse Fourier transform theorem, we can express the payoff function in terms of its Fourier transform: $f(k) = \frac{1}{2\pi} \int_{-\infty}^{+\infty} e^{-iuk} \phi_f(u) du = \phi_f(-u)$, thus V_0 can be recalculated as:

$$\begin{aligned} V_0 &= \int_{-\infty}^{+\infty} \frac{1}{2\pi} \int_{-\infty}^{+\infty} e^{-iuk} \phi_f(u) du g(k) dk \\ &= \frac{1}{2\pi} \int_{-\infty}^{+\infty} \phi_f(u) \phi_g(-u) du \end{aligned} \quad (3.6.2)$$

Here $\phi_g(-u) = B_0(T) \phi_q(-u)$, which is the product of the discount factor and the characteristic function.

The option pricing problem is thus rephrased in terms of the characteristic function and the Fourier Transform. As long as the characteristic function is

⁹In mathematics, a càdlàg function is a function defined on \mathbb{R} (or a subset of \mathbb{R}) that is everywhere right-continuous and has left limits. Càdlàg functions are important in the study of stochastic processes that include (or even require) jumps, unlike Brownian motion, which has continuous sample paths.

available in a closed form, the option price can be evaluated either in closed form or semi-closed form via a fast Fourier transform. Lévy processes, which provide more general and flexible model specification, are specified directly in terms of the characteristic function of the stochastic variable via the Lévy Khintchine Theorem. These processes open a new route to tractability for complicated models, which can generate stochastic volatility and skewness from the specification of characteristic functions.

Lévy Khintchine Theorem

Theorem 3.6.3 *All Lévy processes have a characteristic function:*

$$E[e^{iuX_t}] = e^{-t\psi(u)}, t \geq 0 \quad (3.6.3)$$

where the characteristic exponent $\psi(u)$ is given by:

$$\psi(u) = iau - \frac{\sigma^2 u^2}{2} + \int_{\mathbb{R} - \{0\}} (e^{iux} - 1) \ell(dx)$$

The Lévy process is specified by the Lévy triplet (σ, ℓ, a) , namely the diffusion coefficient (constant volatility) σ , the Lévy measure $\ell(dx)$ ¹⁰ and the constant drift rate a .

Without any restrictions, Lévy processes can go negative, while in practice futures prices must be nonnegative. Therefore, it is better to start with the assumption that the log of futures price relative, X_t , is a Lévy process which initiates from 0: $X_t = \ln(F_t/F_0)$. To avoid arbitrage, the futures price $F_t = F_0 e^{X_t}$ must be a positive martingale under the risk-neutral measure.

Assume there is another Lévy process L_t , which has 0 drift and the sample path of its jump component has finite variation. By the Lévy Khintchine theorem, we have:

$$E[e^{iuL_t}] = e^{t \left[-\frac{\sigma^2 u^2}{2} + \int_{\mathbb{R} - \{0\}} (e^{iux} - 1) \ell(dx) \right]} = e^{-t\psi(u)} \quad (3.6.4)$$

¹⁰The Lévy measure $\ell(dx)$ describes the arrival rate of jumps of size $(x, x + dx)$. It should be nonnegative and no measure for the origin: $\ell(\{0\}) = 0$, and integrate x^2 around the origin: $\int_{\mathbb{R} - \{0\}} x^2 1_{(|x| < 1)} \ell(dx) < \infty$.

where: $\psi(u) = -\ln E[e^{iuL_t}] = \frac{\sigma^2 u^2}{2} - \int_{\mathbb{R}-\{0\}} (e^{iux} - 1) \ell(dx)$.

Assuming finite expectation and evaluating the characteristic function 3.6.4 at $u = -i$, we get:

$$\begin{aligned} E[e^{L_t}] &= e^{t\psi(-i)} \\ E[e^{t\psi(-i)+L_t}] &= 1 \end{aligned} \tag{3.6.5}$$

Let $b \equiv \psi(-i) = -\frac{\sigma^2}{2} - \int_{\mathbb{R}-\{0\}} (e^x - 1) \ell(dx)$, and $X_t = bt + L_t$ is then a Lévy process with e^{X_t} being a positive martingale starting at 1. The spot price thus has the desired risk-neutral martingale property:

$$E_0[S_t] = S_0 e^{(r-q)t}, t \geq 0 \tag{3.6.6}$$

From the above analysis, we notice that the characteristic function of X_t is determined by the characteristic exponent $\psi(u)$, which is determined by the Lévy measure $\ell(dx)$. Model tractability then comes from carefully choosing $\ell(dx)$ so that $\int_{\mathbb{R}-\{0\}} (e^{iux} - 1) \ell(dx)$ can be evaluated in closed form, resulting in a closed form characteristic function.

Subordination

In general, there are three methods to define Lévy processes parametrically, namely subordination, direct measure specification and specifying the density of increments to be infinite. In Carr and Wu[25], as well as CGMY[27], stochastic volatility is obtained by using stochastic time as the subordinator.

Definition 3.6.4 *The Lévy process Z_t with monotonic increasing paths is called the subordinator. Let $(0, \ell, b)$ be a generating triplet for Z_t , then for each $u \leq 0$ moment generating function of Z_t has a form: $E[e^{uZ_t}] = e^{tl(u)}$, where $l(u) = bu + \int_0^\infty (e^{ux} - 1) \ell(dx)$ is called the Laplace exponent.*

A new Lévy process Y_t can be generated by subordinating the Lévy process $X_t(\sigma, \ell, a)$, of which the characteristic exponent is $\psi(u)$, with the subordinator

$Z_t(0, \ell, b)$, of which the Laplace exponent is $l(u)$. The resulting characteristic function for $Y_t \equiv X_{Z_t}$ is:

$$E[e^{iuY_t}] = e^{tl[\psi(u)]} \quad (3.6.7)$$

From the definition, Lévy processes have independent and stationary increments, hence squared returns are also independent. However, empirical research shows the opposite. Subordination has to be used to generate correlated increments. The most natural choice of subordinator is the time, thus the term 'Time-change'. Stochastic time-change means using a stochastic clock with correlated increments as the subordinator, consequently, the Lévy processes run on such a clock will inherit the correlation in their increments.

Let τ be a subordinator independent of the Lévy process X_t , for $Y_t \equiv X_\tau$, the characteristic function is:

$$\begin{aligned} \phi_{Y_t}(u) &\equiv E[e^{iuY_t}] = E[e^{iuX_{\tau_t}}] \\ &= E[e^{-\tau_t \psi_x(u)}] \\ &\equiv \mathcal{L}_{\tau_t}(\psi_x(u)) \end{aligned} \quad (3.6.8)$$

where $\mathcal{L}_{\tau_t}(\psi_x(u))$ is the Laplace transform of time τ_t , evaluated at the characteristic exponent of X_t . A closed form characteristic function is then available if both the Laplace transform and the characteristic exponent have closed form solutions.

Time-Change and Stochastic Volatility

For European options valuation, only total variance through the lives of the options matters, thus we can obtain stochastic volatility by randomizing the time on which the process is run, and the total variance is measured. The Heston[44] model can be viewed as stochastically time-changed Brownian motion:

$$\begin{aligned} \ln\left(\frac{S_t}{S_0}\right) &= (r_d - r_f)t + W_{T_t} - \frac{1}{2}T_t, \quad v_t \equiv \frac{\partial T_t}{\partial t}, \\ dv_t &= \kappa(\theta - v_t)dt + \sigma_v \sqrt{v_t}dZ_t, \quad dW_t dZ_t = \rho dt. \end{aligned} \quad (3.6.9)$$

where W_{T_t} is the time-changed Brownian motion, and the stochastic time-change is $T_t = \int_0^t v_s ds$.

For more general Lévy processes, stochastic volatility can be similarly induced by stochastically time-changing a Lévy martingale.

Stochastic Skewness

From the characteristic function definition of the Lévy Khintchine theorem, it can be seen that Lévy processes have a continuous component and a jump component. In modelling, it is more convenient to place the infinite activity in the jump component rather than in the continuous counterpart, because of the flexibility in jump process. For example, we can model the up and down moves separately and independently within finite variation. Taking advantage of this flexibility, Carr and Wu[25] model the positive and negative jumps separately using two independent Lévy martingales, so as to get skewness, and the stochasticity in both volatility and skewness is induced by time-changing the two Lévy martingales.

$$\begin{aligned} \ln \left(\frac{S_t}{S_0} \right) &= (r_d - r_f) t + \left(L_{T_t^R}^R - \xi^R T_t^R \right) + \left(L_{T_t^L}^L - \xi^L T_t^L \right) \quad (3.6.10) \\ L_{T_t^R}^R - \xi^R T_t^R &= \sigma \sqrt{v_t^R} dW_t^R + \int_0^\infty (e^x - 1) [\mu^R(dx, dt) - k^R(x) dx v_t^R dt] \leftarrow \text{Right skew} \\ L_{T_t^L}^L - \xi^L T_t^L &= \sigma \sqrt{v_t^L} dW_t^L + \int_{-\infty}^0 (e^x - 1) [\mu^L(dx, dt) - k^L(x) dx v_t^L dt] \leftarrow \text{Left skew} \end{aligned}$$

L_t^R is a Lévy martingale that generates positive skewness via a combination of diffusion and positive jumps, and L_t^L is the Lévy martingale that generates the negative counterpart. These two can generate the short-term smile effect in a implied volatility surface. Random clocks T_t^R and T_t^L subordinating the two Lévy martingales determinate stochastic total volatility $- [T_t^R + T_t^L]$ and stochastic skewness (measured by risk reversal) $- [T_t^R - T_t^L]$, thus the smile will persist, reducing the convergence to the normal distribution due to the Central Limit theorem. ξ^R and ξ^L are determined by the parameters of the two time-changed Lévy processes respectively. In addition, the market observed positive correlation between changes in risk reversal (ΔRR) and underlying returns can be captured by correlating the clock-driving Brownian motion and the Lévy diffusion component.

In the detailed expression, μ^R and μ^L are the counting measures assigning mass to the positive and negative jumps respectively. The Lévy density $k^R(x)$ has the

range $x \in (0, \infty)$, while $k^L(x)$ has the range $x \in (-\infty, 0)$. The activity rates, v_t^R and v_t^L , follow mean reverting square root processes and are chosen to have long run means of one:

$$dv_t^j = \kappa(1 - v_t^j)dt + \sigma_v \sqrt{v_t^j} dZ_t^j, \quad j = R, L. \quad (3.6.11)$$

3.6.3 Option Pricing under Stochastic Skewness

Choice of Lévy density $k(x)$

In order to get a closed form characteristic function, the Lévy density $k(x)$ has to be wisely chosen. Carr and Wu[25] suggest using the simple yet flexible exponentially dampened power law to model the Lévy density¹¹:

$$k^R(x) = \begin{cases} \lambda \frac{e^{-\frac{|x|}{v_J}}}{|x|^{\alpha+1}}, & x > 0, \\ 0, & x < 0. \end{cases}, \quad k^L(x) = \begin{cases} 0, & x > 0, \\ \lambda \frac{e^{-\frac{|x|}{v_J}}}{|x|^{\alpha+1}}, & x < 0. \end{cases} \quad (3.6.12)$$

For both up and down jumps, the model uses the same parameters $(\lambda, v_J) \in \mathbb{R}^+$, and the parameter α , which determines the fine structure of the sample paths, is set to be less or equal to 2 for parsimony¹². The characteristic exponents for the Lévy jump components $L_t^R - \xi^R t$ and $L_t^L - \xi^L t$ are calculated as:

$$\begin{aligned} \text{Right:} \quad & \psi^D + \lambda \Gamma(-\alpha) \left[\left(\frac{1}{v_J} \right)^\alpha - \left(\frac{1}{v_J} - iu \right)^\alpha \right] \\ & - iu \lambda \Gamma(\alpha) \left[\left(\frac{1}{v_J} - 1 \right)^\alpha \right] \\ \text{Left:} \quad & \psi^D + \lambda \Gamma(-\alpha) \left[\left(\frac{1}{v_J} \right)^\alpha - \left(\frac{1}{v_J} + iu \right)^\alpha \right] \\ & - iu \lambda \Gamma(\alpha) \left[\left(\frac{1}{v_J} + 1 \right)^\alpha \right] \end{aligned} \quad (3.6.13)$$

where $\psi^D = \frac{1}{2}\sigma^2(iu + u^2)$.

¹¹This specification comes from CGMY[27], which captures much of the market observed evidence in equities and exchange rates.

¹²The condition $\alpha \leq 2$ is necessary to maintain finite quadratic variation.

Therefore, the integral in the returns characteristic function:

$$\int_{\mathbb{R}-\{0\}} (e^{iux} - 1) \ell(dx) = \int_{\mathbb{R}-\{0\}} (e^{iux} - 1 - iux1_{|x|<1}) k(x) dx \quad (3.6.14)$$

can be evaluated in closed form.

Complex Change of Measure

According to the subordinator properties, if the two Lévy processes are independent of the stochastic clocks, i.e. the underlying processes are independent of the subordinators, the characteristic function of the return, which is the Laplace transform of the time evaluated at the characteristic exponent (as shown in formula 3.6.8), can be obtained in closed form. In Carr and Wu[25]'s model, however, the Lévy processes are correlated with the stochastic clocks so as to generate positive correlation between ΔRR and returns. According to Carr and Wu's previous paper[24], this correlation induces a new measure, which is defined as a complex-valued exponential martingale, to get the form of a Laplace transform for the stochastic clock:

$$\frac{dM}{dQ}|_t \equiv \exp \left[iu \left(L_{T_t^R}^R - \xi^R T_t^R \right) + iu \left(L_{T_t^L}^L - \xi^L T_t^L \right) + \psi^R T_t^R + \psi^L T_t^L \right] \quad (3.6.15)$$

Just as the change from P to Q builds risk aversion into the probabilities, the change from Q to M incorporates the required correlation into the probabilities. Under this measure, the characteristic function of the log return can be calculated as:

$$\begin{aligned} \phi(u) &\equiv E^Q \left[e^{iu \ln(S_t/S_0)} \right] \\ &= e^{iu(r_d - r_f)t} E^Q \left[e^{iu \left(L_{T_t^R}^R - \xi^R T_t^R \right) + iu \left(L_{T_t^L}^L - \xi^L T_t^L \right)} \right] \\ &= e^{iu(r_d - r_f)t} E^M \left[e^{-\psi^R T_t^R} \right] \equiv e^{iu(r_d - r_f)t} \mathcal{L}_T^M(\psi) \end{aligned} \quad (3.6.16)$$

Since the activity rates v_t^j are chosen to follow the special processes as in formula

3.6.11, the Laplace transforms for the stochastic time are exponential affine:

$$\mathcal{L}_T^M(\psi) = \exp \left(-b^R(t) v_0^R - c^R(t) - b^L(t) v_0^L - c^L(t) \right), \quad (3.6.17)$$

where:

$$\begin{aligned} b^j(t) &= \frac{2\psi^j (1 - e^{-\eta^j t})}{2\eta^j - (\eta^j - \kappa^j) (1 - e^{-\eta^j t})}, \\ c^j(t) &= \frac{\kappa}{\sigma_j^2} \left[2 \ln \left(1 - \frac{\eta^j - \kappa^j}{2\eta^j} (1 - e^{-\eta^j t}) \right) + (\eta^j - \kappa^j) t \right], \\ \eta^j &= \sqrt{(\kappa^j)^2 + 2\sigma_v^2 \psi^j}, \quad \kappa^j = \kappa - iu\rho^j \sigma \sigma_v, \quad j = R, L \end{aligned}$$

Therefore, the characteristic function 3.6.16 for exchange rates returns is available in closed form.

Parameters Estimation

Model parameters are estimated using quasi-maximum likelihood method. To capture the time-series dynamics of implied volatility, the exchange rates returns and activity rates dynamics must be specified under the objective measure P . Using an unscented Kalman filtering method¹³, which can generate efficient forecasts and updates on the conditional mean and variance for both states and measurement series, Carr and Wu[25] construct the likelihood function based on the assumption of normally distributed estimation errors:

$$\begin{aligned} \mathcal{L}(\Theta) &= \sum_{t=1}^N l_{t+1}(\Theta) \\ &= -\frac{1}{2} \sum_{t=1}^N \left[\ln |\bar{A}_t| + \left((y_{t+1} - \bar{y}_{t+1})^T (\bar{A}_{t+1}) (y_{t+1} - \bar{y}_{t+1}) \right) \right] \end{aligned} \quad (3.6.18)$$

¹³Kalman filter is a recursive estimator which can estimate the current state of a dynamic system with only the estimated state from the previous time step and the current measurement. Compared with the widely used Extended Kalman Filter (EKF), the Unscented Kalman Filter (UKF) avoids the linearization steps by using a set of discretely sampled points that can capture the mean and variance of the state distribution. UKF is more efficient and accurate than EKF in nonlinear estimation. See Julier and Uhlmann[53].

where Θ is the parameter set, and $\{y_t\}_{t=1}^N$ is the time series data set.

3.6.4 Summary

Carr and Wu[25]’s stochastic skewness model can, in principle, capture the key observed features of an implied volatility surface across both moneyness and maturity over time. The advantage is easily seen from the results of both the log likelihood ratio test and the root mean squared pricing errors. In both tests, the model outperforms the ’traditional’ models like Heston’s stochastic volatility model and Merton’s jump diffusion model.

However, for tractability, several assumptions are made about the parameters of the complicated time-changed Lévy processes, which restrict model flexibility in capturing the asymmetry on FX rate distributions, and more importantly, flexibility in calculating exotic options prices.

The parsimony of this model is achieved by assuming asymptotic conditional symmetry in the return distributions, resulting in using the same parameters for both the positive and negative Lévy components. This assumption can be strongly rejected for emerging market exchange rates. Estimation using different parameters displays large standard errors, thus such an extension requires further research.

The bigger issue comes from the fact that the analytical tractability of this model only exists for European options. For the increasingly actively traded exotic options, whether the necessary pricing formulae, in terms of characteristic functions, are available in closed form or semi-closed form is still unknown to the authors. It is clear that any small changes in the option payoff functions will induce technical difficulties in getting the characteristic function.

3.7 Summary

Our review of the main models demonstrates that the individual models fail to capture the various features of a FX implied volatility surface, while combined models and the Lévy processes based model suffers from a lack of tractability. We need a model that can capture the statistical features of the volatility surface and that is flexible enough to be extended to price exotic options.

Chapter 4

Spectral Methods in FX Modelling

4.1 Introduction

Stochastic skewness in the risk-neutral distribution of FX log returns, as displayed and discussed in both Chapter 2 from the implied PDF and Chapter 3 from the time series data of risk reversal (as the skewness measure), is the extra uncertainty that needs to be modelled in addition to the stochastic underlying and the volatility. However, it can not be specified explicitly, as with the stochastic volatility process, because this may induce internal model arbitrage. The dynamics of a model have to be rich enough to capture the stochasticity in skewness intrinsically so as to be arbitrage-free. The combined models can not tackle this with tractability.

Carr and Wu [25] go beyond Brownian motion and jump diffusion, and propose using Lévy processes which is defined by a characteristic function, thus the Fourier transform and the Laplace transform could possibly achieve tractability given the complicated model specification. They use two Lévy processes to model up and down jumps separately, and capture the stochastic volatility and skewness by randomizing the time underneath. However, the analytical tractability of such a model is restricted to pricing only vanilla options.

In the area of stochastic calculus, there are many technical difficulties likely to

arise in the development of a proper and flexible model. Albanese and Mijatović[4] thus innovatively move away from the stochastic calculus framework, which has dominated the mathematical finance ever since Black, Scholes and Merton published their seminal paper, to spectral theory and functional analysis. This new modelling framework is naturally built on the continuous-time lattice, one of the efficient numerical methods that can handle lots of exotic structures simultaneously. Therefore, one only need to focus on the model specification to capture various features of implied volatility surface, then the pricing task is relatively straightforward.

The main idea of this new method is to choose a generator of the Markov chain so that in the limit of an infinite number of states, it converges to the generator of the underlying continuous process. As proved by Albanese and Mijatović[5], under the Black-Scholes model, the probability kernel of the process in the discrete state-space converges to the PDF of the continuous state-space at the rate of $O(h^2)$, and delta and gamma converge at the same rate as option prices under a certain discretization scheme. The model starts from specifying the FX forward rates by the CEV process, described by a corresponding Markov generator, which is discretized to be applied on a continuous-time lattice. Jumps are then added to capture the short-dated skew and a stochastic volatility process is specified to govern the switch between different local volatility regimes, thus obtaining stochastic volatility and stochastic skewness simultaneously.

We will firstly review the essential mathematics of the continuous-time Markov generator and functional analysis in spectral theory in Section 4.2. The model is explained in Section 4.3, with vanilla option pricing and Greeks in Section 4.4. Calibration is carried out for two currency pairs in Section 4.5.

4.2 Generating Function in Spectral Theory

4.2.1 Continuous-time Markov Generator

A stochastic process is Markovian if the conditional probability distribution of the future states only depends on the current state and not any of the past states. Due to the central role of conditional probability in derivative pricing, the Markov

property provides a mathematically convenient tool.

Definition 4.2.1 *The stochastic process $\{X_t\}_{t \geq 0}$, which takes values in some countable state space Ω , has the Markov property if*

$$P(X_{t_n} = y | X_{t_1} = x_1, \dots, X_{t_{n-1}} = x_{n-1}) = P(X_{t_n} = y | X_{t_{n-1}} = x_{n-1})$$

for all $y, x_1, \dots, x_{n-1} \in \Omega$ and any sequence of times $t_1 \leq t_2 \leq \dots \leq t_n$.

One well-known example of Markov process is stock prices under risk-neutral measure. Another concept closely related to conditional probability is the transition probability.

Definition 4.2.2 *The transition probability $p(x, s; y, t)$ is defined as:*

$$p(x, s; y, t) = P(X_t = y | X_s = x)$$

for any $x, y \in \Omega$ and $s \leq t$. The set of all transition probabilities for fixed time s and t is called the Markov probability kernel.

The Markov chain is called *time homogeneous* if:

$$P(X_t = y | X_s = x) = P(X_{t-s} = y | X_0 = x)$$

for all s, t, x, y . In this framework, we assume all Markov chains are time homogeneous.

Let \mathbf{P}_t be an $N \times N$ matrix with $\mathbf{P}_t(x, y) = p(x, 0; y, t)$, the family $\{\mathbf{P}_t : t \geq 0\}$ is called the *transition semigroup* of the chain X_t .

Theorem 4.2.3 *The family $\{\mathbf{P}_t : t \geq 0\}$ is a stochastic semigroup which satisfies the following conditions:*

1. $\mathbf{P}_0 = \mathbf{I}$, the identity matrix.
2. \mathbf{P}_t has non-negative entries (i.e. $p(x, 0; y, t) \geq 0$ for all $x, y \in \Omega$).
3. \mathbf{P}_t has row sums equal to 1 (i.e. $\sum_{y \in \Omega} p(x, 0; y, t) = 1$ for all $x \in \Omega$).

4. \mathbf{P}_t satisfies the Chapman-Kolmogorov equation (i.e. $\mathbf{P}_{t+s} = \mathbf{P}_t \mathbf{P}_s$).

The proof of this theorem is shown in Appendix C.

The Markov generator can be defined, conditional on the assumption of continuity of the transition probabilities $p(x, 0; y, t)$ with respect to time t , for all $x, y \in \Omega$.

Definition 4.2.4 A stochastic semigroup $\{\mathbf{P}_t\}$ is called standard if

$$\lim_{t \rightarrow 0} \mathbf{P}_t = \mathbf{I},$$

equivalently,

$$\begin{aligned} \lim_{t \rightarrow 0} p(x, 0; x, t) &= 1, \text{ for all } x \in \Omega \\ \lim_{t \rightarrow 0} p(x, 0; y, t) &= 0, \text{ for all } x, y \in \Omega, x \neq y \end{aligned}$$

The semigroup is standard if and only if its elements $p(x, 0; y, t)$ are continuous functions of t .

In order to understand the local behaviour of a Markov chain, we need to understand the behaviour of the Markov probability kernel $p(x, 0; x, t)$ for small time interval δt .

Assuming the probability of two or more jumps in the time interval $(0, \delta t)$ is $o(\delta t)$, two scenarios can be identified¹: (1) Nothing happens, with probability $p(x, 0; x, \delta t) + o(\delta t)$, the error term caters for the possibility that the chain may move out and then back to state x ; (2) The chain moves to state y , with probability $p(x, 0; y, \delta t) + o(\delta t)$, the error term now accounts for the possibility of several jumps occurring within δt .

Theorem 4.2.5 For the standard stochastic semigroup $\{\mathbf{P}_t\}$, there exists an $N \times N$ matrix $\mathcal{L} = \mathcal{L}(x, y)$ such that the following holds for small time interval δt :

1. $p(x, 0; y, \delta t) = \mathcal{L}(x, y)\delta t + o(\delta t)$, for all $x, y \in \Omega, x \neq y$.
2. $p(x, 0; x, \delta t) = 1 + \mathcal{L}(x, x)\delta t + o(\delta t)$, for all $x \in \Omega$.

¹For detailed proof, see Grimmett and Stirzaker [41].

The matrix \mathcal{L} is called the Markov generator of the semigroup $\{\mathbf{P}_t\}$, a proof of its existence can be found in Chung[28].

Corollary 4.2.6 *Let $x, y \in \Omega$ and \mathcal{L} be the Markov generator of the Markov chain X . Then the following holds:*

1. $0 \leq \mathcal{L}(x, y) \leq \infty$ if $x \neq y$.
2. $-\infty \leq \mathcal{L}(x, y) \leq 0$ if $x = y$.
3. All row sums equal to 0.

Therefore, for square matrix \mathcal{L} , all the elements off the diagonal are nonnegative, while all the elements on the diagonal are non-positive. This theorem gives us an intuition into the relationship between Markov generator and the transition probability. In derivative pricing, the exact functional relationship is established by Kolmogorov's equations.

Theorem 4.2.7 (Kolmogorov's equations) *Let $\{\mathbf{P}_t\}$ be a standard transition semigroup with a Markov generator \mathcal{L} , then it is a unique solution to the:*

1. forward equation: $\mathbf{P}'_t = \mathbf{P}_t \mathcal{L}$,
 2. backward equation: $\mathbf{P}'_t = \mathcal{L} \mathbf{P}_t$,
- subject to the boundary condition $\mathbf{P}_0 = \mathbf{I}$. Furthermore, we can express \mathbf{P}_t in the following way:

$$\mathbf{P}_t = \sum_{n=0}^{\infty} \frac{t^n}{n!} \mathcal{L}^n = e^{t\mathcal{L}} \quad (4.2.1)$$

Formula 4.2.1 provides the functional form of the conditional probability density function for the Markov chain in terms of the Markov generator, on which the pricing model is specified. Therefore, we can summarize the properties of the Markov generator:

Corollary 4.2.8 *A real $N \times N$ matrix $\mathcal{L} = \mathcal{L}(x, y)$ is a Markov generator of a semigroup $\mathbf{P}_t = e^{t\mathcal{L}}$ if and only if*

$$\mathcal{L}(x, y) \geq 0 \text{ for } x \neq y \text{ and } \sum_y \mathcal{L}(x, y) = 0 \text{ for all } x.$$

4.2.2 Essential Principles in Functional Calculus

In the modelling process, we need to calculate various functions of the Markov generator \mathcal{L} , which is a real matrix (a linear operator). Functional calculus, as a theory allowing one to apply mathematical functions to mathematical operators, is then required.

Assume \mathcal{L} is defined on the N -dimensional Euclidean space, and admits a complete set of eigenvectors such that it can be expressed as $\mathcal{L} = U\Lambda U^{-1}$, where Λ is a diagonal matrix with eigenvalues $\lambda_0, \dots, \lambda_N$:

$$\Lambda = \begin{pmatrix} \lambda_0 & \cdots & 0 \\ \vdots & \ddots & \vdots \\ 0 & \cdots & \lambda_N \end{pmatrix}$$

The matrix U maps eigenvector u_i (associated with eigenvalue λ_i) into the i th element for each index i in $\{1, \dots, N\}$.

Let $\phi(x)$ be a real function of a real variable x , given by its Taylor series $\phi(x) = \sum_{n=0}^{\infty} a_n x^n$. If the convergence radius of the series is larger than the norm of \mathcal{L} , one can define:

$$\begin{aligned} \phi(\mathcal{L}) &= \sum_{n=0}^{\infty} a_n \mathcal{L}^n \\ &= \sum_{n=0}^{\infty} a_n (U\Lambda U^{-1})^n \\ &= U \left(\sum_{n=0}^{\infty} a_n \Lambda^n \right) U^{-1} \\ &= U \phi(\Lambda) U^{-1} \end{aligned} \tag{4.2.2}$$

Formula 4.2.2 is the basis of functional calculus, which plays a key role in this framework for the Markov generator.

4.2.3 Exponential and Normality of Markov Generator

According to formula 4.2.1, the transition probability matrix \mathbf{P}_t is calculated as the exponential of the Markov generator. In practice, there are many methods for calculating the exponential of a matrix, including the matrix eigenvalues, approximation theory, the matrix characteristic polynomial, and differential equations, as reviewed by Moler and VanLoan[72].

Matrix Diagonalization and Normality

Albanese and Mijatović[4] use the matrix diagonalization method and apply the functional calculus formula 4.2.2. The key is to find an Λ for which $e^{t\Lambda}$ is easy to compute, and:

$$e^{t\Lambda} = \begin{pmatrix} e^{t\lambda_1} & \dots & 0 \\ \vdots & \ddots & \vdots \\ 0 & \dots & e^{t\lambda_N} \end{pmatrix}$$

However, the validity of this method depends on the symmetry, or normality, of matrix \mathcal{L} . In linear algebra, matrix A is symmetric if: $A^T = A$, where A^T is the matrix transpose. The *finite-dimensional spectral theorem* is concerned about the property of this type of matrix:

Theorem 4.2.9 *Any symmetric matrix whose entries are real can be diagonalized by an orthogonal matrix. In other words, the eigenvectors of a symmetric matrix are orthogonal.*

If \mathcal{L} is not symmetric, i.e. \mathcal{L} does not have a complete set of linearly independent eigenvectors, we cannot diagonalize it as $\mathcal{L} = U\Lambda U^{-1}$, because any round-off errors from eigenvalue computation will be magnified in the calculation for $e^{t\Lambda}$. Therefore, we need to check the symmetry of \mathcal{L} first. Since a symmetric real matrix is a normal matrix², several measures for matrix normality can be used. For example, the condition number, defined by $\kappa = \|A^{-1}\| \cdot \|A\|$ in any consistent norm, indicates nonnormal matrix when it is large. Another measure, pseudospectra, is introduced by Trefethen[87]. It looks at the eigenvalue movement on the

²A real matrix is normal if: $A^T A = A A^T$. For a symmetric matrix, $A^T = A$, thus it is naturally a normal matrix.

pseudospectrum space, at the perturbation of a small positive number ϵ . A matrix with large condition number is not normal. But the rule for 'how large is enough' is not clear. In comparison, the decision rule for pseudospectra is quite clear and straightforward. In the model building section, we will use the EigTool software designed by Wright[91] to get the pseudospectra for the Markov generator in this model, and analyze the relevant matrix normality.

Scaling and Squaring

For a non-normal matrix, the exponential has to be calculated by alternative methods (see [72]). One of the most effective methods, which is used by Matlab, is called scaling and squaring, based on a Taylor or a Padé approximation. We propose using this method to replace the diagonalization scheme in the original paper when it is necessary, so as to achieve robust results and improve efficiency.

In a small time interval δt , the transition probability matrix can be approximated by a first-order Taylor expansion:

$$P_{\delta t} = e^{\delta t \mathcal{L}} \approx \mathbf{I} + \delta t \mathcal{L} \quad (4.2.3)$$

where \mathbf{I} is the identity matrix, and the error is of order $(\delta t)^2$.

As \mathcal{L} is time homogeneous, P_T can be approximated by:

$$P_T \approx (P_{\delta t})^{\frac{T}{\delta t}}$$

where $\frac{T}{\delta t}$ is an integer. The method can be quite reliable and efficient if an integer m just larger than $\frac{T}{\delta t}$ is chosen so that is a power of 2, thus P_T can be calculated by repeated squaring.

To implement this algorithm, we firstly need to choose a time interval t , which is small enough so that P_t , calculated by Taylor expansion 4.2.3, satisfies all four conditions specified in Theorem 4.2.3. Then an integer n is found such that 2^n is just larger than the value $\frac{T}{t}$. Finally a new small time interval $\tau = \frac{t}{2^n}$ is used in Formula 4.2.3 to get the transitional probability matrix P_τ , and P_T can be

calculated by repeated squaring:

$$\begin{aligned}
P_{2\tau} &= P_{\tau} \cdot P_{\tau} \\
P_{4\tau} &= P_{2\tau} \cdot P_{2\tau} \\
&\vdots \\
P_T &= P_{(n-1)\tau} \cdot P_{(n-1)\tau}
\end{aligned}$$

where $n = \log_2 \left(\frac{T}{\tau} \right)$ times of matrix multiplication is computed.

A New Algorithm

Clearly, if T is large, the computation time is long. In calibration, however, we have to calculate the transitional probability matrix for maturities ranging from 1 week to 5 year. If the above methodology is applied to each maturity, the program will be very inefficient.

Based on the time homogeneous property of \mathcal{L} , we develop an innovative algorithm, which uses the calculated P_T for the previous maturities, and minimizes the matrix multiplication time. We start with the smallest maturity available, 1 week, for which we use the full Scaling and Squaring method to obtain P_{1W} , then $P_{2W} = P_{1W} \cdot P_{1W}$. For 1 month, we can make use of P_{1W} and P_{3W} , the rest of the time interval ($31 - 7 - 21 = 3$ days) is small enough to use Scaling and Squaring again in a fraction of the time (for just a few matrix multiplication), and the final result is the product of these three matrices.

This algorithm makes maximum use of the calculated probability matrix, so that the need for duplicated matrix multiplication is minimized and the whole routine is efficient.

4.3 Model for the FX Rates

The FX spot rate X_t is described by a stochastic process with local volatility, jumps and stochastic switching between different volatility regimes, which is triggered by FX rate getting certain levels. Assuming that both domestic and foreign interest rates are deterministic functions of time, $r^d(t)$ and $r^f(t)$ respectively, the

actual modeled quantity is the FX forward rate: $F_t = e^{-(r^d(t)-r^f(t))t} X_t$, since it is numerically more convenient to simulate a driftless stochastic process (i.e. Martingale) on a lattice. The building block is the Markov generator, for which functional analysis is applied.

4.3.1 The Conditional Local Volatility Processes

Markov Generator for the CEV Process

The model consists of m local volatility regimes³. It starts with specifying a local volatility process in one regime α , which governs the local dynamics of the forward rate F_t . CEV is chosen for modelling F_t , which is defined by the following stochastic differential equation (SDE):

$$dF_t = v_\alpha(F_t) dW_t, \text{ where } v_\alpha(F_t) = \max\left(\sigma_\alpha F_t^{\beta_\alpha}, \bar{\sigma}_\alpha\right) \quad (4.3.1)$$

where W_t is the standard Brownian motion, and contents σ_α , β_α and $\bar{\sigma}_\alpha$ are determined by calibration for each regime α . The parameter σ_α is relevant to the size of the instantaneous variance of the process in 4.3.1, and $\bar{\sigma}_\alpha$ is used to cap the local volatility.

In order to carry out economically sensible calibration with a view to the market pricing, it is worth noting the influence of β_α in skewness. $\beta_\alpha = 1$ will give the Black-Scholes case, in which the smile is flat. If $\beta_\alpha < 1$, the implied volatility is a decreasing function of strike, or equivalently, the risk-reversal is negative. In the case when $\beta_\alpha > 1$, the risk-reversal becomes positive, making the implied volatility surface slop upwards.

Since the probability kernel of a diffusion process can be expressed in terms of Markov generator, the above CEV process has the following differential operator (Markov generator), for any twice differentiable real function u of F :

$$(\mathcal{L}_\alpha u)(F) = \frac{v_\alpha(F)^2}{2} \frac{\partial^2 u}{\partial F^2}(F) \quad (4.3.2)$$

³The original paper uses only 5 volatility regimes to calibrate the market implied volatility surface, and empirically demonstrates the adequacy.

The transition probability density function $p(G, t; F, T) = P(F_T = F | F_t = G)$ is the solution of the backward Kolmogorov PDE:

$$\frac{\partial p}{\partial t} + \mathcal{L}p = 0 \quad (4.3.3)$$

with boundary condition $p(G, T; F, T) = \delta(G - F)$, where $\delta(x)$ is the Dirac delta function⁴. This PDE implies that all the information needed to obtain $p(G, t; F, T)$ is contained in the Markov generator defined by 4.3.2.

To get enough flexibility in pricing both vanilla and exotic options, the model is built on the continuous-time lattice. From the definition and properties of Markov generator in the last section, we can see that it is easy to generalize it to this situation. Firstly, discretization of the forward rate is needed so that a lattice can be built to approximate the process by a natural discretization of the Markov generator \mathcal{L}_α . Let Ω be a finite set $\{0, \dots, N\}$ which contains the first N integers with 0, and let $F : \Omega \rightarrow \mathbb{R}$ be a non-negative function satisfying the following two conditions: $F(0) \geq 0$ and $F(x) > F(x - 1)$ for all x in $\Omega - \{0\}$. Thus the forward rate process F_t can take any of the values $F(x)$, where time $t < T$.

To ensure that the dynamics of the discretized forward rate process corresponds to the dynamics specified by the SDE 4.3.1, we need to reinterpret the Markov generator given by 4.3.2 in a discrete setting. Since \mathcal{L}_α is equal to a Laplace operator multiplied by a scalar function, its discrete version $\mathcal{L}_\alpha^\Omega$ can be obtained by the natural discretization of Laplace operator:

$$(\Delta^\Omega u)(x) = \begin{cases} u(x+1) + u(x-1) - 2u(x) & \text{for } x \in \Omega - \{0, N\}, \\ 0 & \text{for } x \in \{0, N\}, \end{cases} \quad (4.3.4)$$

for all functions u on Ω . This definition imposes absorbing boundary conditions on the Markov chain, at both end of the domain Ω . The boundary conditions make it easy to detect if the size of the domain Ω , which is one of the model parameters, is not large enough. Thus we can specify a sufficient size to calibrate to the market

⁴A Dirac delta function $\delta(x)$ is defined as:

$$\delta(x) = \begin{cases} \infty, & \text{for } x = 0 \\ 0, & \text{for } x \neq 0 \end{cases}.$$

data, preventing the process ever reaching the boundary.

Given the discrete version in 4.3.4, the generator $\mathcal{L}_\alpha^\Omega$ can be defined as a $(N + 1) \times (N + 1)$ tridiagonal matrix with elements $\mathcal{L}_\alpha^\Omega(x, y)$, where $x, y \in \Omega$. According to the Markov generator properties, $\mathcal{L}_\alpha^\Omega$ must satisfy the conditions:

$$\sum_{y \in \Omega} \mathcal{L}_\alpha^\Omega(x, y) = 0, \quad (4.3.5)$$

$$\sum_{y \in \Omega} \mathcal{L}_\alpha^\Omega(x, y) (F(y) - F(x)) = 0, \quad (4.3.6)$$

$$\sum_{y \in \Omega} \mathcal{L}_\alpha^\Omega(x, y) (F(y) - F(x))^2 = v(F(x))^2. \quad (4.3.7)$$

Condition 4.3.5 guarantees probability conservation, as shown in Corollary 4.2.8, over the infinitesimal time interval δt . It is actually the first-order derivative of the equation $\sum_{y \in \Omega} P(F_s^\Omega = F(y) | F_t^\Omega = F(x)) = 1$ with respect to time t . The remaining two conditions are there to match the instantaneous first and second moments⁵ of the discretized process F_t . Equation 4.3.6 insures that the dynamics of the forward rate is Martingale, i.e. it is driftless, while equation 4.3.7 is there to make sure that the instantaneous variance of the discretized forward process is the same as the diffusion defined in the SDE 4.3.1.

In addition, we need to specify the process at the boundary, following 4.3.4, so that the process F_t^Ω satisfies the boundary conditions if it goes that far. This can be achieved by setting all the elements in the top and bottom row of the matrix $\mathcal{L}_\alpha^\Omega$ to be 0:

$$\mathcal{L}_\alpha^\Omega(x, y) = 0, \text{ for all } y \in \Omega, x \in \{0, N\}.$$

which does not intervene with the three conditions above and thus is a well-defined generator for the Markov chain F_α^Ω .

⁵It is commonly accepted that the first two instantaneous moments of any diffusions determine its finite-dimensional distribution functions completely [54]. Therefore, once the two moments are matched, the discretized version F_t^Ω becomes a valid approximation for F_t .

Probability Kernel

With the above defined Markov generator, one can obtain the probability kernel by applying the spectral theory for operator. For this framework, it is sufficient to use only the spectral resolution method in the special case of the finite-dimensional matrix $\mathcal{L}_\alpha^\Omega$. Firstly we take the eigenvalue problem for matrix $\mathcal{L}_\alpha^\Omega(x, y)$:

$$\mathcal{L}_\alpha^\Omega u_n = \lambda_n u_n \quad (4.3.8)$$

where the vectors u_n are the eigenvectors of the linear operator $\mathcal{L}_\alpha^\Omega$ and λ_n are the relevant eigenvalues. The next crucial step in constructing this model is to check the normality of the matrix $\mathcal{L}_\alpha^\Omega$. If it is normal, we can diagonalize it as $\mathcal{L}_\alpha^\Omega = U\Lambda U^{-1}$ and apply an arbitrary function ϕ , which is defined on the spectrum of the generator by the formula:

$$\phi(\mathcal{L}_\alpha^\Omega) = U\phi(\Lambda)U^{-1} \quad (4.3.9)$$

Then the calculation of $\phi(\Lambda)$ is quite simple:

$$\phi(\Lambda) = \begin{pmatrix} \phi(\lambda_0) & \cdots & 0 \\ \vdots & \ddots & \vdots \\ 0 & \cdots & \phi(\lambda_N) \end{pmatrix} \quad (4.3.10)$$

Formula 4.2.1 implies that the transition probability matrix $P_{T-t} = e^{(T-t)\mathcal{L}_\alpha^\Omega}$ is the solution for the backward Kolmogorov equation, with the boundary condition $P_0 = \mathbf{I}$, where \mathbf{I} is the identity matrix. Therefore, the probability kernel $p(x, t; y, T) = P(F_T = F(y) | F_t = F(x))$ can be expressed in terms of the generator as:

$$p(x, t; y, T) = \left(e^{(T-t)\mathcal{L}_\alpha^\Omega} \right) (x, y) = \sum_{n=0}^N e^{\lambda_n(T-t)} u_n(x) v_n(y), \quad (4.3.11)$$

where the vectors v_n are the columns of the matrix U^{-1} .

However, if the matrix $\mathcal{L}_\alpha^\Omega$ fails the normality test, we have to use the Scaling and Squaring method mentioned in last section to calculate the exponential $e^{\mathcal{L}_\alpha^\Omega}$.

4.3.2 Adding Jumps

It has been generally discussed and accepted that pure diffusion models cannot explain smiles in short-dated implied volatility smile effects, as studied in Chapter 3 of this thesis. Unexpected jumps are certainly presented in the FX market and influence the prices for short-term out-of-the-money options. In order to successfully calibrate to the market implied volatility surface, jumps must be introduced to the pure diffusion CEV process.

With spectral theory, this can be easily done in a general way. Since the market expectations for up and down jumps are known to market makers and are almost always quite different from each other, we need to have different distributions of jump sizes for them in the model. The Variance Gamma[62] (VG) model can capture such market features because its characteristic function is complex. Therefore, Albanese and Mijatović[4] try to impose the infinite-activity jump⁶ in their model, by subordinating the diffusions using stochastic time changes, which is given by a non-decreasing stationary process T_t with independent increments:

$$E_0 [e^{-\lambda T_t}] = e^{-\phi(\lambda)t} \quad (4.3.12)$$

where $\phi(\lambda)$ is a Bernstein function that characterizes the subordinator T_t .

In the VG model, the function $\phi(\lambda)$ takes the form:

$$\phi(\lambda) = \frac{\mu^2}{v} \log \left(1 + \lambda \frac{v}{\mu} \right) \quad (4.3.13)$$

with the mean-reversion rate μ (usually taken to be 1) and variance rate v . This model adds the VG jump and thus uses $\phi(\lambda)$ defined in 4.3.13.

Phillips [75] has shown that, given a general Markov processes X_t with generator \mathcal{L} and the subordinator T_t , the time-changed process X_{T_t} has the Markov generator $\mathcal{L}' = -\phi(-\mathcal{L})$, where ϕ is the Bernstein function for T_t .

Based on the previous CEV process with generator $\mathcal{L}_\alpha^\Omega$, we can produce asymmetric jumps by specifying two VG Bernstein functions with different parameters

⁶As mentioned in Chapter 3, building infinite activity into the jump component rather than into the diffusion part will give us more flexibility to model the up and down jumps separately and independently.

μ_+ and v_+ for the up jump, and μ_- and v_- for the down jump. Then the two Markov generators can be computed separately:

$$\mathcal{L}_\pm = -\phi_\pm(-\mathcal{L}_\alpha^\Omega) = -U_\pm \phi_\pm(-\Lambda) U_\pm^{-1} \quad (4.3.14)$$

where Λ is the diagonal matrix with eigenvalues λ_n and the Bernstein functions ϕ_\pm are given by:

$$\phi_\pm(\lambda) = \frac{\mu_\pm^2}{v_\pm} \log \left(1 + \lambda \frac{v_\pm}{\mu_\pm} \right). \quad (4.3.15)$$

To compute the matrix logarithm, we need to check matrix normality using pseudospectra, as with the matrix exponential. If the matrix is normal, we can diagonalize it and follow the functional calculation 4.3.9.

With the above mentioned MatLab library EigTool, we computed the eigenvalues and perturbations of a small positive number ϵ , for the input generator matrix, which is a pure CEV process (with $\sigma = 8.9\%$, $\beta = 3$, $\bar{\sigma} = 60\%$). In Figure 4.3.1, the dots around 0 are the eigenvalues of the matrix, the coloured boundaries represent the distance that a small positive perturbation $\epsilon = 10^\alpha$ can move the eigenvalue to, where $\alpha = 0.4, 0.6, 0.8$ and 1 in our example. According to Trefethen[87], if a matrix is normal, the perturbation ϵ will not move the eigenvalue to a distance greater than ϵ . Graphically, the value of the boundary on the Y-coordinate should be less or equal to ϵ . For this CEV generator matrix, it can be seen clearly that each perturbation ϵ cannot move the eigenvalues of \mathcal{L} by a distance greater than ϵ . For example, the outmost curve shows that the perturbations of norm 10^1 will only move the eigenvalues to a distance roughly within 10. This result is not accidental, since the Markov generator of a pure CEV process is a tri-diagonal matrix, in which the elements of the upper-diagonal and lower-diagonal are very close to each other. Therefore, we can safely conclude that the matrix is normal, or very close to normal, for which diagonalization can be applied to calculate the matrix logarithm with formula 4.3.15.

Thus we have two diffusion processes, corresponding to two different generator \mathcal{L}_+ and \mathcal{L}_- , each of which is a square matrix. The upper diagonal matrix \mathcal{L}_+ contains the (scaled) probabilities of jumping up in the infinitesimal time interval δt , while the lower diagonal matrix \mathcal{L}_- is for the probabilities of down jumps. A

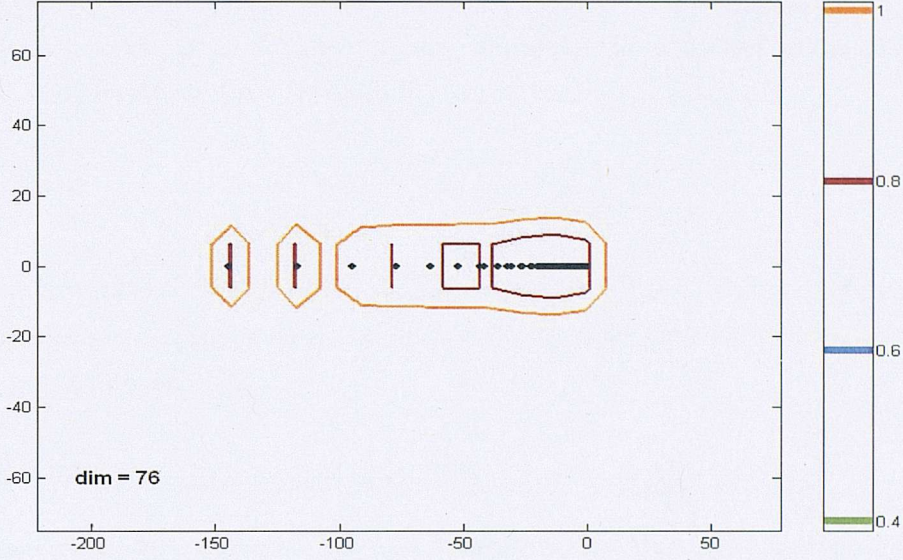


Figure 4.3.1: Boundaries of Pseudospectra for the CEV Markov Generator \mathcal{L} .

new combined generator can then be defined from \mathcal{L}_+ and \mathcal{L}_- :

$$\mathcal{L}_\alpha^\Omega = \begin{pmatrix} d(0,0) & \mathcal{L}_+(0,1) & \cdots & \mathcal{L}_+(0,N-1) & \mathcal{L}_+(0,N) \\ \mathcal{L}_-(1,0) & d(1,1) & \cdots & \mathcal{L}_+(1,N-1) & \mathcal{L}_+(1,N) \\ \vdots & \vdots & \ddots & \vdots & \vdots \\ \mathcal{L}_-(N-1,0) & \mathcal{L}_-(N-1,1) & \cdots & d(N-1,N-1) & \mathcal{L}_+(N-1,N) \\ \mathcal{L}_-(N,0) & \mathcal{L}_-(N,1) & \cdots & \mathcal{L}_-(N,N-1) & d(N,N) \end{pmatrix}. \quad (4.3.16)$$

The new process with jumps would satisfy the Martingale condition 4.3.6 by adjusting the elements just above and below the diagonal of the matrix $\mathcal{L}_\alpha^\Omega$. For example, if the x -row has a positive drift, we can add some probability to the element $\mathcal{L}_\alpha^\Omega(x, x-1)$ so as to satisfy condition 4.3.6; when the drift is negative, we can add probability to the element $\mathcal{L}_\alpha^\Omega(x, x+1)$.

Notice that a linear deterministic time change, which comes along with the stochastic time change, may distort the instantaneous variance by a constant factor. We need to multiply each row of the new generator by a constant which is chosen to make condition 4.3.7 hold. In this way, we can eliminate the effect of the deterministic time change since the starting instantaneous variance $v(F(x))^2$

is recovered.

The last constraint is for the diagonal elements $d(x, x)$, which should be chosen so that the condition 4.3.5 (probability conservation) is satisfied:

$$d(x, x) = - \sum_{y \in \Omega - \{x\}} \mathcal{L}_\alpha^\Omega(x, y) \quad (4.3.17)$$

Now, we have a well-defined Markov generator $\mathcal{L}_\alpha^\Omega$ for a diffusion process with jumps, which is a martingale and thus suitable to model the FX forward rate under a risk-neutral measure.

4.3.3 Stochastic Volatility for Regime Switching

Stochastic volatility and skewness are obtained by stochastically switching between different jump-diffusion regimes, controlled by a stochastic volatility process. The stochasticity of volatility is sensitive to the current level of the underlying, therefore it is possible to relate the model to particular market views (e.g. smile and skew features of the implied volatility surface), commonly based on expected future trading levels of the underlying. In this model, such levels can be set explicitly as the volatility regimes, each of which are modeled separately by a corresponding jump-diffusion that can describe the volatility surface.

Let V be the set $\{0, \dots, m-1\}$ of all possible volatility regimes. For each regime $\gamma \in V$, a Markov generator \mathcal{L}_γ^V is defined by the matrix element $\mathcal{L}_\gamma^V(\alpha, \beta)$, where $\alpha, \beta \in V$, so that the continuous-time diffusion process given by \mathcal{L}_γ^V mean-reverts to the state γ .

In addition, a single global stochastic volatility Markov generator, which will favour a certain regime γ given the level of the FX forward rate F_t , can be specified by using the so-called *partition of unity* method. We choose a strictly increasing sequence F_γ of the forward rate levels such that if the forward rate process F_t is close to the level F_γ , the market views of the smile and skew agree with the ones implied by the process $\mathcal{L}_\gamma^\Omega$ from last section. The partition of unity is then defined

as a sequence of m functions $\epsilon_\gamma : \mathbb{R} \rightarrow [0,1]$, with the important property:

$$\sum_{\gamma=0}^m \epsilon_\gamma(F) = 1 \text{ for all } F \in \mathbb{R}. \quad (4.3.18)$$

With the sequence of forward rate levels F_γ , such a function can be explicitly defined as piecewise linear functions in the following form:

$$\epsilon_\gamma(F) = \begin{cases} \frac{F-F_{\gamma-1}}{F_\gamma-F_{\gamma-1}} & F \in [F_{\gamma-1}, F_\gamma] \\ \frac{F_{\gamma+1}-F}{F_{\gamma+1}-F_\gamma} & F \in [F_\gamma, F_{\gamma+1}] \\ 0 & \text{otherwise.} \end{cases} \quad (4.3.19)$$

At the boundary when $\gamma \in \{0, m-1\}$, this definition needs to be slightly modified as:

$$\epsilon_0(F) = \begin{cases} 1 & F \leq F_0 \\ \frac{F_1-F}{F_1-F_0} & F \in [F_0, F_1] \\ 0 & F \geq F_1, \end{cases} \quad \epsilon_{m-1}(F) = \begin{cases} 0 & F \leq F_{m-2} \\ \frac{F-F_{m-2}}{F_{m-1}-F_{m-2}} & F \in [F_{m-2}, F_{m-1}] \\ 1 & F \geq F_{m-1}. \end{cases} \quad (4.3.20)$$

We can thus define the global Markov generator, which is able to change its properties conditioned on a substantial move of the forward rate:

$$\mathcal{L}_x^V(\alpha, \beta) = \sum_{\gamma=0}^{m-1} \epsilon_\gamma(F(x)) \mathcal{L}_\gamma^V(\alpha, \beta) \quad (4.3.21)$$

where $\alpha, \beta \in V$ and $F(x)$ is forward rate process function defined on Ω .

As in any other stochastic volatility model, the Markov generator \mathcal{L} should specify the probabilities of going from any state (x, α) in $\Omega \times V$ to any other state (y, β) of the same set in the infinitesimal time interval δt . This can be achieved by using the *Kronecker delta* function:

$$\delta_{xy} = \begin{cases} 1 & \text{if } x = y, \\ 0 & \text{otherwise.} \end{cases} \quad (4.3.22)$$

Finally, the Markov generator for the dynamics of FX forward rate in this

model is specified as:

$$\mathcal{L}(x, \alpha; y, \beta) = \mathcal{L}_\alpha^\Omega(x, y) \delta_{\alpha\beta} + \mathcal{L}_x^V(\alpha, \beta) \delta_{xy} \quad (4.3.23)$$

From the properties of the Kronecker delta, the matrix \mathcal{L} is a genuine Markov generator, and by definition, it does not allow for simultaneous jumps of the regime and the volatility variables, thus ensuring that the forward process F_t^Ω , the dynamics of which is specified by \mathcal{L} , is still a martingale:

$$\begin{aligned} E_t^{(x, \alpha)} [dF_t^\Omega] &= \sum_{(y, \beta) \in \Omega \times V} (F(y) - F(x)) (\mathcal{L}_\alpha^\Omega(x, y) \delta_{\alpha\beta} + \mathcal{L}_x^V(\alpha, \beta) \delta_{xy}) \quad (4.3.24) \\ &= \sum_{y \in \Omega} (F(y) - F(x)) \mathcal{L}_\alpha^\Omega(x, y) + (F(x) - F(x)) \sum_{\beta \in V} \mathcal{L}_x^V(\alpha, \beta) = 0 \end{aligned}$$

4.3.4 Deterministic Time Change

Up to now, the model described is completely stationary, i.e. the implied volatility surface does not have explicit time dependence, thus the calibration result is not quite satisfying. To get a closer match to the 25- Δ and at-the-money implied volatilities, a minimal deterministic time change has to be introduced, which is achieved by specifying an increasing function $f : [0, T] \rightarrow [0, \infty)$ which deterministically transforms calendar time t to financial time $f(t)$.

For each currency, the deterministic time change function $f(t)$ is identified in such a way that for all quoted maturities, the at-the-money options are correctly priced. Then the entire interval between now and five years can be obtained by linear interpolation. We will see in next section that such deterministic time change will enter the probability kernel of the model in an isolated and controlled manner. Note that because the model can already capture the prominent features of the implied volatility surface before time change is introduced, the difference between the calendar time t and financial time $f(t)$ is quite small.

4.4 Option Pricing and Hedging

4.4.1 Pricing European Options

In this framework, which is defined under a risk-neutral measure⁷, the problem of pricing European options of maturity T is reduced to calculating the transition probability $p((x, \alpha), t; (y, \beta), T)$ for the FX forward rate process F_t^Ω , as defined in the last section in terms of Markov generator \mathcal{L} . Taking the deterministic time change into account, for which the financial time is defined as $s = f(t)$ (and $S = f(T)$ for calendar time T), the transition probabilities for going between the states (x, α) and (y, β) in the time interval $[s, S]$ can be expressed as $u((x, \alpha), s; (y, \beta), S)$, thus the stochastic matrix induced by the Markov generator is $U(u((x, \alpha), s; (y, \beta), S))$.

According to the model building process in Section 4.3.1 (see formula 4.3.3), the probability matrix U_s satisfies the backward Kolmogorov equation:

$$\frac{\partial U_s}{\partial s} + \mathcal{L}U_s = 0 \quad (4.4.1)$$

with the boundary condition $U_S = \mathbf{I}$ (\mathbf{I} is the identity matrix on the vector space \mathbb{R}^k where $k = m(N+1)$). The solution of equation 4.4.1 can then be expressed as $U_{S-s} = e^{((S-s)\mathcal{L})}$, which can be explicitly calculated by either the spectral decomposition or the scaling and squaring method of the operator \mathcal{L} , which is a $k \times k$ matrix.

If the matrix decomposition is available, we can calculate the transition probability, which depends on the calendar time, in terms of financial time as follows:

$$\begin{aligned} p((x, \alpha), t; (y, \beta), T) &= e^{(f(T)-f(t))\mathcal{L}}((x, \alpha), (y, \beta)) \\ &= \sum_{n=1}^{m(N+1)} e^{\lambda_n(f(T)-f(t))} u_n(x, \alpha) v_n(y, \beta) \end{aligned} \quad (4.4.2)$$

where u_n is the eigenvector, and v_n is the inverse of the eigenvector matrix.

The important and surprising fact from formula 4.4.2 is that, the pricing kernel

⁷Under risk-neutral measure, the value of any security at time t is equal to the discounted expectation of the value of the same security at time T , for all $t \leq T$.

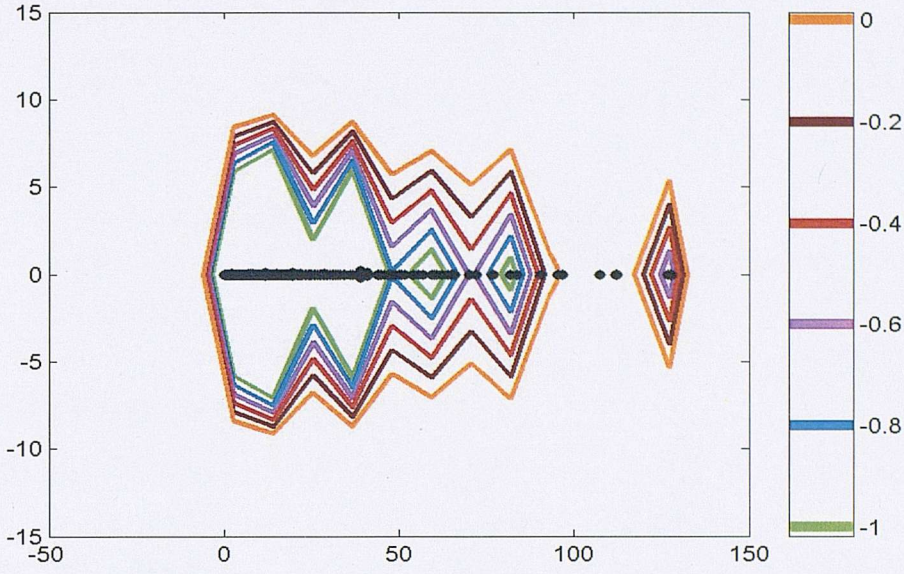


Figure 4.4.1: Boundaries of Pseudospectra for the Markov Generator \mathcal{L} , Computed with the GBPUSD Parameters.

depends on the financial time in a very isolated way, which makes the pricing problem less difficult to cope with.

However, before using this formula, we have to check the normality of the matrix. This time the input matrix is the complete generator for this model, which results from 5 CEV processes coupled with Variance Gamma jumps and stochastic regime-switching in between. We use certain parameters for the GBPUSD currency pair as a test. From Figure 4.4.1, we can see that the each perturbation ϵ ($\epsilon = 10^{-1}, 10^{-0.8}, 10^{-0.6}, 10^{-0.4}, 10^{-0.2}, 1$) can move the eigenvalues of \mathcal{L} by a distance greater than ϵ . For example, the inmost curve shows that the perturbations of norm 10^{-1} will move the eigenvalues to a distance as large as 8, which is much greater than 0.1. This suggests that the matrix is not normal, thus diagonalization error will be severely increased in the calculation of matrix exponential. Therefore, we have to use the alternative Scaling and Squaring method to compute the transitional probability matrix, as shown in formula 4.2.3.

With the calculated probability matrix $P_{(T-t)}$, in which each element is $p((x, \alpha), t; (y, \beta), T)$, the current price C_t of a European option with payoff $h(X_T)$ at maturity T , where

X_t is the underlying FX rate at time t , can be calculated as:

$$C_t = e^{-(r^d(T)T - r^d(t)t)} \sum_{(y, \beta) \in \Omega \times V} p((x, \alpha), t; (y, \beta), T) h\left(e^{-(r^d(T) - r^f(T))T} F(y)\right) \quad (4.4.3)$$

where the point x from Ω is chosen in such a way that the forward-spot relation holds: $F(x) = X_t e^{(r^d(T) - r^f(T))T}$, and α in V is the volatility regime we are in at time t .

4.4.2 Hedge Ratios (Greeks)

The last task for building the model framework is to find the hedge ratios (i.e. Greeks) for the derivative C_0 , which appears to be quite simple because all the numerical work has been done by the above mentioned algorithm and the relevant pricing and hedging informations are available in the continuous-time lattice. The delta and gamma of C_0 can be defined using symmetric differences as follows:

$$\Delta(x, \alpha) = \frac{C_0(x+1, \alpha) - C_0(x-1, \alpha)}{F(x+1) - F(x-1)} \quad (4.4.4)$$

$$\Gamma(x, \alpha) = \frac{C_0(x+1, \alpha) + C_0(x-1, \alpha) - 2C_0(x, \alpha)}{4(F(x+1) - F(x-1))^2} \quad (4.4.5)$$

where x is the lattice point in Ω , corresponding to the spot level S_0 of the FX rate at time 0 ($S_0 = F_0$). For $C_t(x+1, \alpha)$, or any other value of $C_t(y, \alpha)$ with a different starting point y , the probability density function is given by a different row of the matrix U_x , which is directly available as the result of the previous pricing algorithm for $C_t(x, \alpha)$. Therefore, the entire delta and gamma profiles of C_t can be calculated by using matrix-vector multiplication and then applying the above formulae to piece the Greeks together.

Similarly, vega can be obtained by taking the symmetric difference in the stochastic volatility domain V :

$$v(x, \alpha) = \frac{C_0(x, \alpha+1) - C_0(x, \alpha-1)}{\sigma_{\alpha+1} - \sigma_{\alpha-1}} \quad (4.4.6)$$

which should be reasonably adjusted if it is in the volatility regime on the boundary

of the domain V^8 . Note that the parameter σ_α , in which α is in the domain V , is actually the base volatility in the CEV process defined in Section 4.3.1. We can get the whole vega profiles using the same techniques for delta and gamma, as mentioned before.

4.4.3 Validation - The Black-Scholes' Case

In financial modelling, a more complicated model is usually tested against the simple Black-Scholes model, which is encompassed by the new model. In this continuous-time lattice framework, we can produce the Black-Scholes benchmark by setting only one regime (no regime switching), in which the CEV process has parameter $\beta = 1$, and no jumps.

Model validation can be carried out using imaginary data. However, to have a better feeling for the market, useful for later calibration, we use the actual current GBPUSD currency implied volatility surface as the example⁹. The market quotes of Black-Scholes implied volatility for five strikes, namely 10 delta put, 25 delta put, at-the-money forward, 25 delta call and 10 delta call, with seven maturities are used as the volatilities for the CEV process with $\beta = 1$ in the model. The model thus computes the relevant option prices, and implied volatilities are then calculated and compared with the actual inputs.

Table 4.4.1 demonstrates the convergence of model implied volatilities to the Black-Scholes (market quoted) implied volatilities with the increasing number of lattice points. In most of the cases, the model can converge to a Black-Scholes closed-form solution at 1 basis point accuracy with only 300 lattice points, while 400 points can guarantee convergence of any case.

We further compute the hedge ratios (Greeks) for the at-the-money-forward (ATMF) options of three maturities, 6 months, 1 year and 2 year, using 300 lattice points. Figure 4.4.2 shows the delta of these European options, calculated with the lattice model, while in comparison, Figure 4.4.3 gives the delta calculated using Black-Scholes delta formula 2.3.2. It can be seen that the delta lines are

⁸On the boundary of domain V , there is no data available for $\sigma_{\alpha-1}$, we should calculate the vega with some other methods. In the current model with 5 regimes, such problem won't affect the results. Therefore, we can leave the alternative methods to the future research.

⁹Since the test result is not sensitive to the choice of data, any currency pairs can be used.

very similar at the ATMF points. Although the differences increase when the spot moves to the more out-of-the-money cases, taking into account of the fact that delta hedging is only effective with a small movement of the underlying, the model calculated delta actually converges to the Black-Scholes delta at around ATMF point. Similarly, Figure 4.4.4 displays the model computed gamma, which has nearly identical shape to the Black-Scholes' gamma in Figure 4.4.5, especially around the at-the-money point.

These test results thus validate the practicability of the model, we can now move on to calibrate it to the market volatility surface, in order to price exotic options.

Table 4.4.1: GBPUSD Option Implied Volatilities with Various Number of Lattice Point N, in Black-Scholes Case (Bold type indicates convergence to BS volatility)

Maturity	Strike	BS Vol	N = 75	100	200	300	400
1M	10- Δ -Put	7.20%	7.10%	7.15%	7.19%	7.19%	7.20%
	25- Δ -Put	7.03%	6.84%	6.98%	7.02%	7.02%	7.03%
	ATMF	7.08%	6.85%	7.02%	7.07%	7.07%	7.08%
	25- Δ -Call	7.38%	7.18%	7.32%	7.37%	7.37%	7.38%
	10- Δ -Call	7.65%	7.53%	7.60%	7.63%	7.64%	7.65%
3M	10- Δ -Put	7.03%	6.98%	7.00%	7.02%	7.03%	7.03%
	25- Δ -Put	6.85%	6.78%	6.82%	6.84%	6.85%	6.85%
	ATMF	6.93%	6.85%	6.90%	6.92%	6.93%	6.93%
	25- Δ -Call	7.25%	7.17%	7.22%	7.24%	7.25%	7.25%
	10- Δ -Call	7.63%	7.57%	7.60%	7.62%	7.63%	7.63%
4M	10- Δ -Put	7.25%	7.22%	7.23%	7.25%	7.25%	7.25%
	25- Δ -Put	6.90%	6.85%	6.88%	6.89%	6.90%	6.90%
	ATMF	6.95%	6.89%	6.93%	6.94%	6.95%	6.95%
	25- Δ -Call	7.27%	7.20%	7.24%	7.26%	7.27%	7.27%
	10- Δ -Call	7.86%	7.83%	7.84%	7.86%	7.86%	7.86%
6M	10- Δ -Put	7.01%	6.98%	6.99%	7.01%	7.01%	7.01%
	25- Δ -Put	6.80%	6.75%	6.78%	6.79%	6.80%	6.80%
	ATMF	6.90%	6.85%	6.88%	6.89%	6.90%	6.90%
	25- Δ -Call	7.25%	7.19%	7.22%	7.24%	7.25%	7.25%
	10- Δ -Call	7.66%	7.63%	7.64%	7.66%	7.66%	7.66%
9M	10- Δ -Put	7.00%	6.98%	6.98%	6.99%	7.00%	7.00%
	25- Δ -Put	6.81%	6.77%	6.79%	6.80%	6.81%	6.81%
	ATMF	6.90%	6.86%	6.88%	6.89%	6.90%	6.90%
	25- Δ -Call	7.29%	7.24%	7.26%	7.28%	7.29%	7.29%
	10- Δ -Call	7.70%	7.65%	7.67%	7.69%	7.70%	7.70%
1Y	10- Δ -Put	7.08%	7.06%	7.07%	7.08%	7.08%	7.08%
	25- Δ -Put	6.85%	6.82%	6.83%	6.85%	6.85%	6.85%
	ATMF	6.90%	6.87%	6.88%	6.89%	6.90%	6.90%
	25- Δ -Call	7.25%	7.22%	7.23%	7.25%	7.25%	7.25%
	10- Δ -Call	7.78%	7.75%	7.76%	7.78%	7.78%	7.78%
2Y	10- Δ -Put	7.23%	7.24%	7.24%	7.23%	7.23%	7.23%
	25- Δ -Put	6.95%	6.94%	6.94%	6.95%	6.95%	6.95%
	ATMF	7.00%	6.98%	6.99%	6.99%	7.00%	7.00%
	25- Δ -Call	7.40%	7.39%	7.39%	7.40%	7.40%	7.40%
	10- Δ -Call	7.88%	7.90%	7.90%	7.89%	7.88%	7.88%

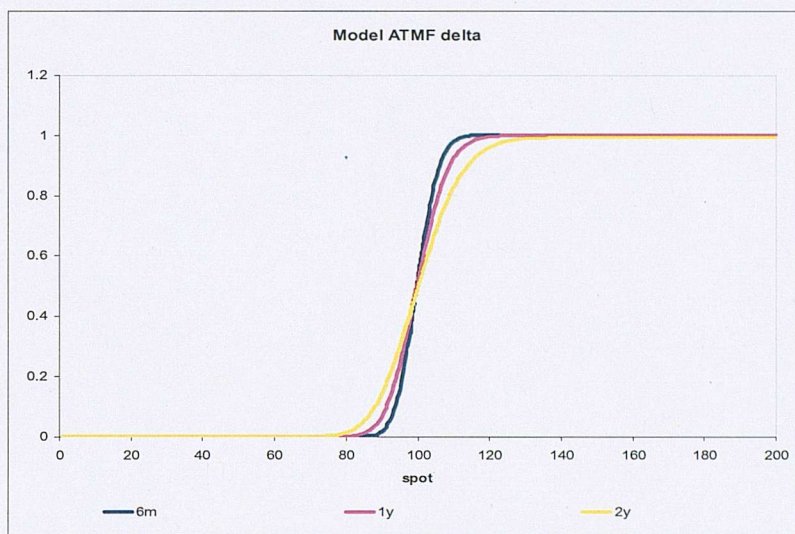


Figure 4.4.2: ATMF delta for 6-month, 1-year and 2-year, calculated with 300 lattice points in Black-Scholes case.

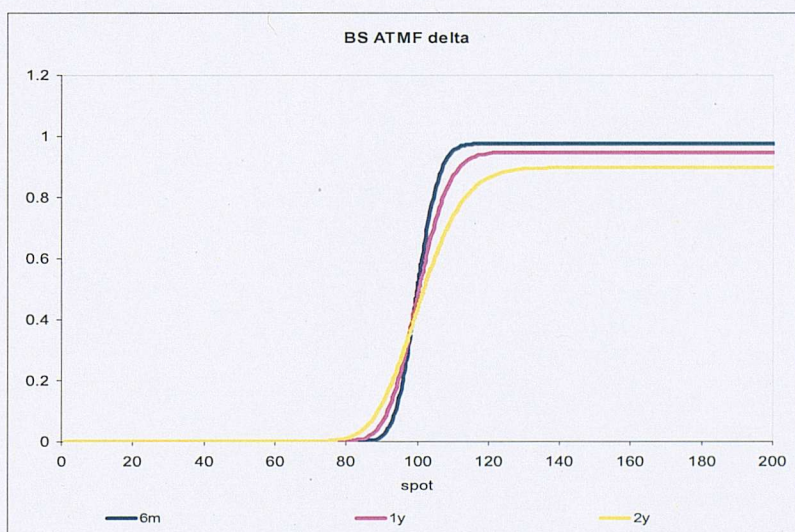


Figure 4.4.3: ATMF delta for 6-month, 1-year and 2-year, calculated using Black-Scholes closed-form formula.

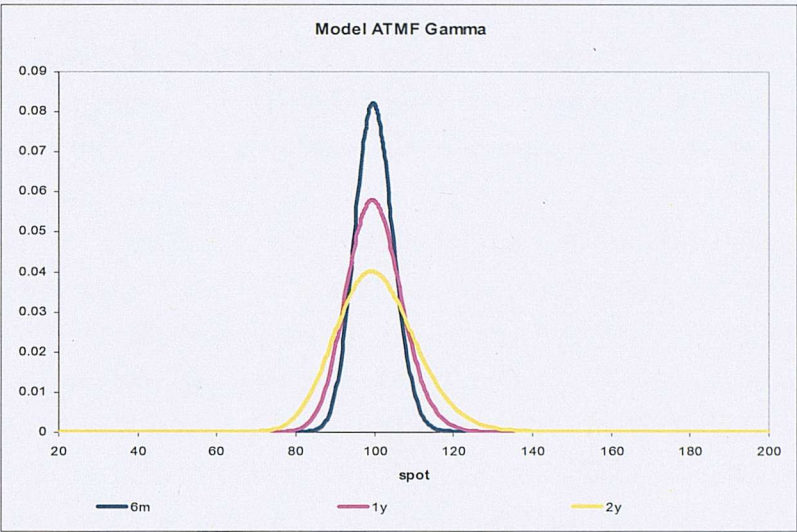


Figure 4.4.4: ATMF gamma for 6-month, 1-year and 2-year, calculated with 300 lattice points in Black-Scholes case.

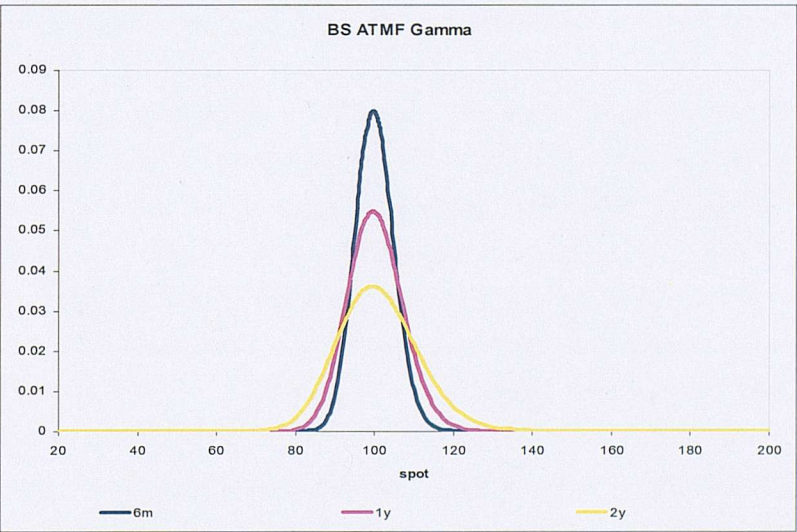


Figure 4.4.5: ATMF gamma for 6-month, 1-year and 2-year, calculated using Black-Scholes closed-form formula.

4.5 Calibration

The model should be calibrated for different currency pairs. Here we take one 'core' market currency pair GBPUSD and one 'emerging' market currency pair USDBRL as examples, to illustrate the calibration procedure and demonstrate model flexibility.

As explained in the first part of this thesis, the most liquidly traded instruments for certain maturity in the FX market are the at-the-money-forward call, the 25 delta call and the 25 delta put. We obtain market data for the entire implied volatility surface from Bloomberg on an arbitrary day (here 04-Jan-2007), and set the parameters in this model in such a way that the whole surface is reproduced by the model correctly. In order to preserve the correct smile and skew through time, in other words, to make sure that the model generated surface is stationary, we calibrate with main criterion of minimizing explicit time dependence. Such stationarity guarantees that the forward smile and skew will have the proper shape even after some movement of the underlying exchange rate.

In the calibration, we use an inhomogenous lattice with $76 = N + 1$ points, which is used to accommodate possible values of the forward rate F_t , and $m = 5$ local volatility regimes so as to capture the stochasticity of the skewness in these currency pairs.

The calibration procedure is different from the normal optimization method. It depends on the user's understanding of the market, so as to avoid the difficulty of explaining the non-sensible parameters that may result from a 'black box' optimization routine. Firstly, we calibrate the starting regime (2 in our case) and the neighbouring regimes to the short-term market implied volatilities (1-week to 6-month), based on the market information of certain parameters, and the user's judgement about the potential influence of different parameters. Then the regime 0 and regime 4 are calibrated to the longer term implied volatilities. The criterion is to minimize the difference between the model implied volatilities and the market implied volatilities¹⁰.

¹⁰A conditional optimization scheme, which translates the user's view of market to the restriction of certain parameters, can be carefully designed and implemented. However, due to the programming difficulty of dealing with such a large amount of parameters, we have to rely on this calibration method now, and leave the optimization routine to the future research.

4.5.1 GBPUSD

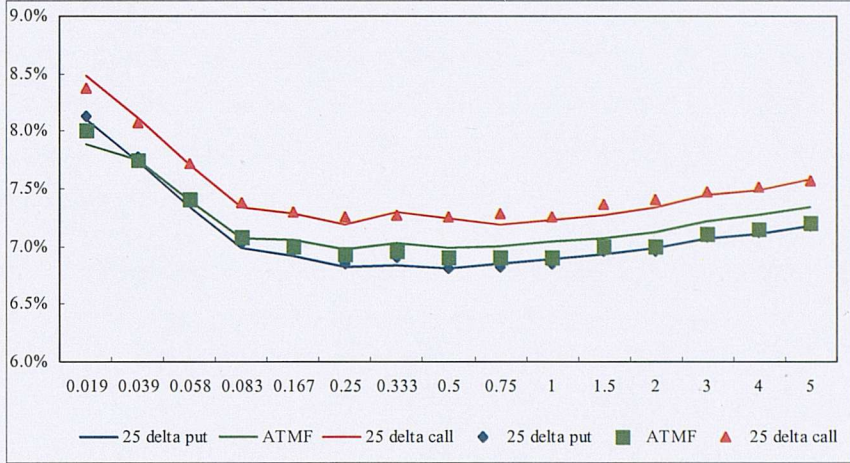


Figure 4.5.1: Term Structure of Implied Volatilities for GBPUSD.

The calibration is started with a detailed observation of the term structure of the implied volatilities plotted in Figure 4.5.1. As shown by the dots, the value of a risk reversal, which measures the skewness, is consistently positive through the maturities. This implies that the right-hand tail of the risk-neutral implied distribution must be fatter than the left, and suggests that the CEV parameter β_α should be positive. Especially for the starting regime, which has a dominant influence, β_α should be a number larger than 1 to keep the skews of the local volatility regimes decreasing in strike. However, there is almost no skew between the ATMF and 25 delta put, which means we need to consider compensating the positive skew introduced by the large β_α . This can be done by using a $\beta_\alpha < 1$ in the neighbouring regime to bounce back, or imposing a down jump by having non-zero jump intensity ν_α^- , or both.

In addition, a diffusion process cannot generate such a large skew for short maturity, due to the embedded expectation of sudden movement in the FX market. In order to produce the high volatility difference between 25 delta call and ATMF, an up jump is required, which is generated by non-zero jump intensity ν_α^+ . Also notice that with the increase of maturity, the price of the 25 delta call appreciates

relative to the ATMF price. This is due to the fact that vega risk for the out-of-the-money options increases with time. However, given the relative low volatility for this currency pair, this appreciation is not remarkable.

With such understanding of the risk-neutral dynamics of the FX rate, we can calibrate to the market step by step. Table 4.5.1 specifies the model parameters that optimally match the model implied volatilities to the market term structure of implied volatilities.

Table 4.5.1: Parameters for GBPUSD local volatility regimes and jump intensity

α	σ_α	β_α	$\bar{\sigma}_\alpha$	ν_α^-	ν_α^+	F_α
0	9.90%	0.4	60%	0.0%	1.5%	92
1	9.60%	1.5	60%	1.0%	5.0%	97
2	8.90%	3.0	60%	0.1%	0.5%	102
3	9.50%	0.6	60%	0.9%	5.0%	106
4	10.50%	1.0	60%	0.0%	2.0%	110

These parameters are chosen such that there is no explicit time dependence in their calculation, but the option prices can be approximately reproduced by the model. The final fitting of the result is then obtained by using a deterministic time change, as reported in Figure 4.5.4. The local volatility level σ_α are identified by investigating the ranges of the implied volatilities, changes in the skew, and underlying movements. The relative forward rate F_α (as percentage of the current level) is selected as the level on which regime-switching is most likely.

The GBPUSD spot exchange rate is 1.944 at the time of calibration. We start at regime 2, in which $\beta_\alpha = 3$ is relatively large. And β_α declines for the lower F_α regimes, while it goes down sharply to 0.6 for regime 3 and then comes back a little bit for regime 4. These changes are necessary to generate the positive skew between 25 delta call and ATMF, and nearly flat skew between ATMF and 25 delta put, since the five regimes interact.

In Figure 4.5.1, the lines are model implied term structure of volatilities. It can be seen that the calibration is quite good for shorter maturities. This is because in the FX market, a model without stochasticity in interest rates is efficient mainly for maturities shorter than 2 year, our calibration puts more weight on fitting the data for shorter maturities.

The extrapolated implied volatilities for out-of-the-money options are displayed

in Figure 4.5.2, while Figure 4.5.3 shows the model implied risk-neutral PDF. We can see that the right tail of the distribution is indeed fatter than the left. The hedge ratios, Delta, Gamma and Vega, for 6-month, 1-year and 2-year are reported in Figure 4.5.5, Figure 4.5.6 and Figure 4.5.7, respectively, all of which have the desired shapes.

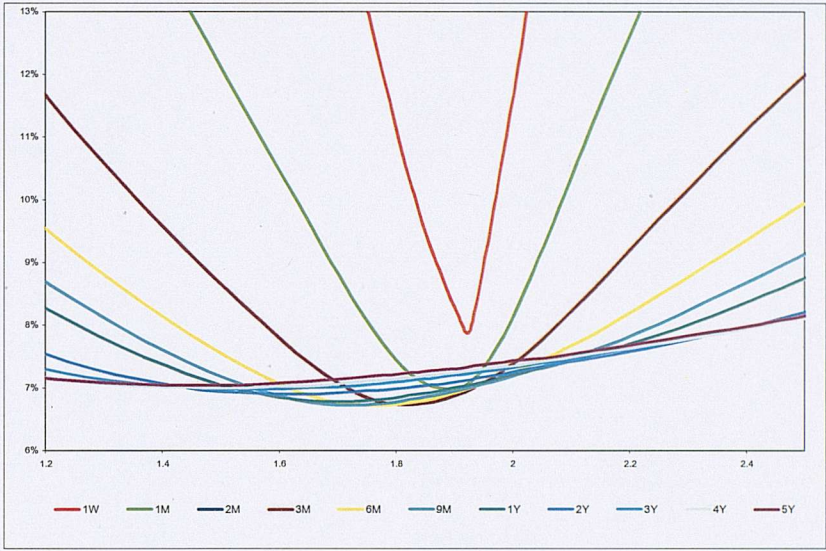


Figure 4.5.2: Extrapolated Implied Volatilities for GBPUSD European Options using Generic Strikes.

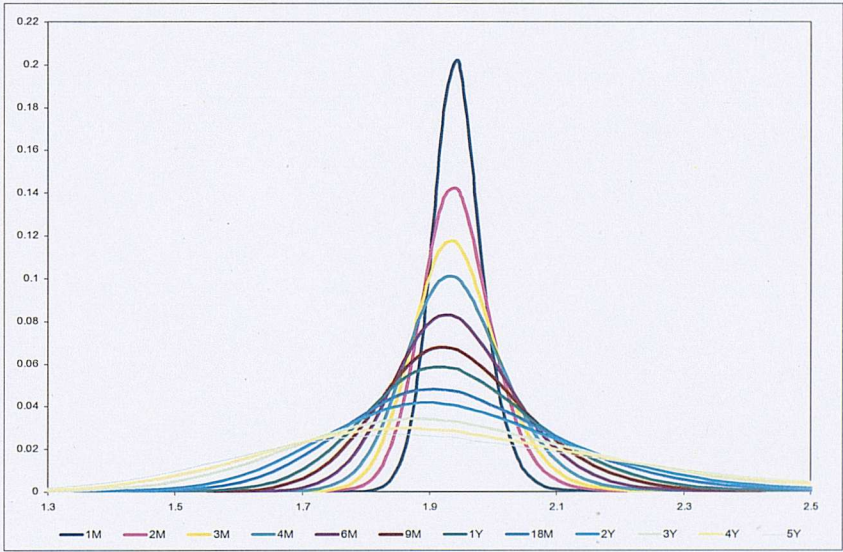


Figure 4.5.3: GBPUSD Probability Distribution Function under the Forward Measure.



Figure 4.5.4: Deterministic Time Change $f(t)$ (in years) as a Function of Calendar Time t for GBPUSD.

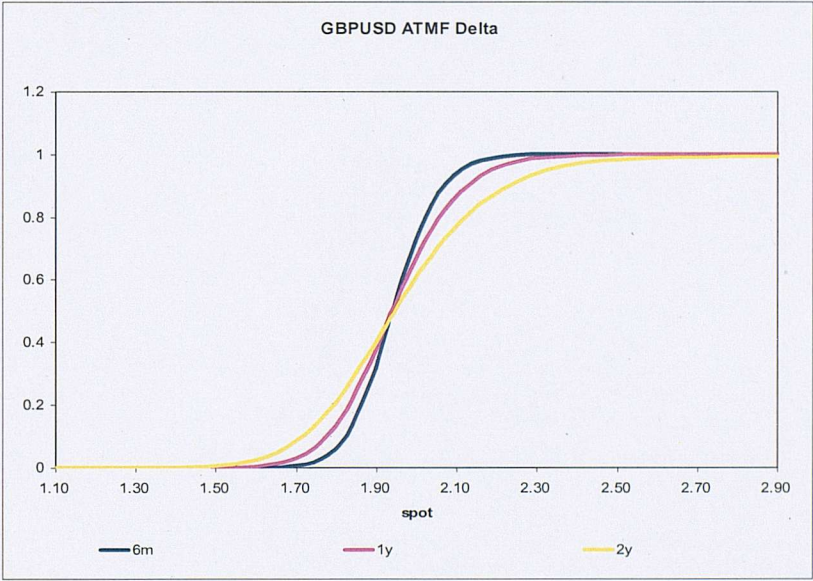


Figure 4.5.5: GBPUSD ATMF delta for 6-month, 1-year and 2-year, calculated with calibrated parameters.

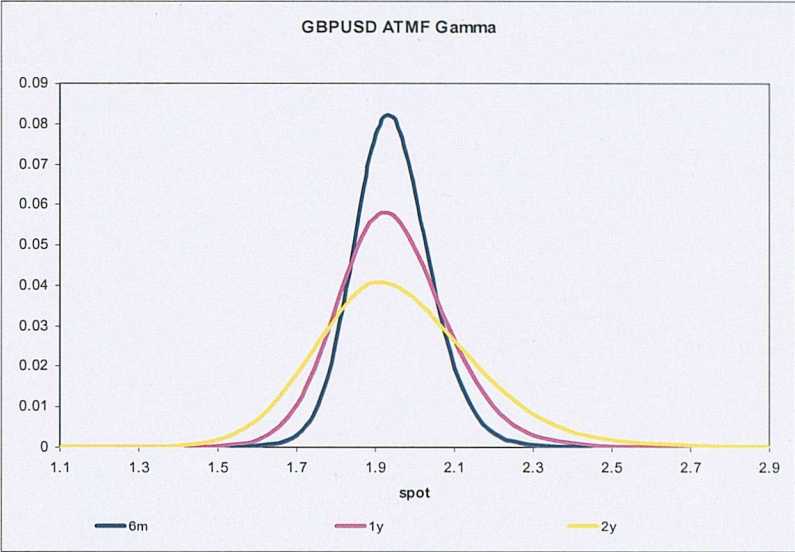


Figure 4.5.6: GBPUSD ATMF gamma for 6-month, 1-year and 2-year, calculated with calibrated parameters.

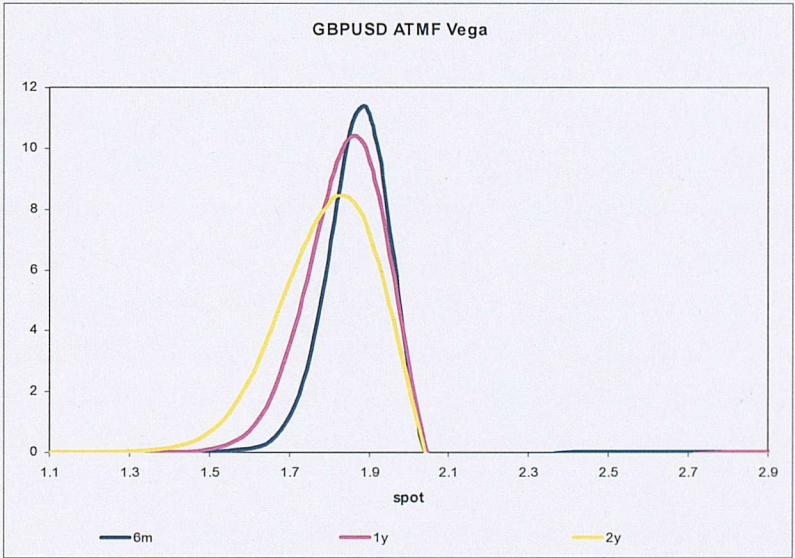


Figure 4.5.7: GBPUSD ATMF vega for 6-month, 1-year and 2-year, calculated with calibrated parameters.

4.5.2 USDBRL

To demonstrate the flexibility of the model, we also use it to calibrate one of the emerging market currency, Brazilian Lira (BRL), which is quoted against USD.

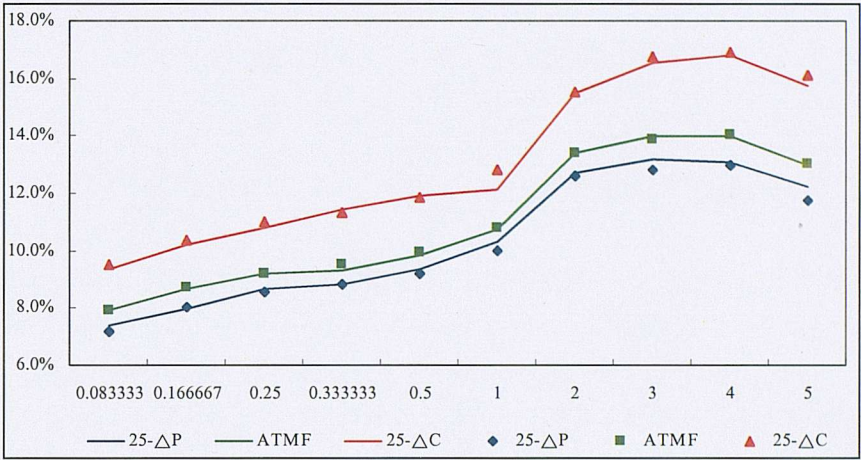


Figure 4.5.8: Term Structure of Implied Volatilities for USDBRL.

From Figure 4.5.8, we can clearly observe large positive risk-reversal through time. In particular, the skew between the 25 delta call and ATM is much greater than that between ATM and 25 delta put. This leads us to consider using β_α much larger than 1 to start with, coupled with a nonzero up jump intensity ν_α^+ much greater than those for GBPUSD. Notice that the price appreciation for 25 delta call against ATM with the increase of maturity is more obvious for this 'emerging' market currency, because of its much higher volatility. This suggests using a higher up jump intensity ν_α^+ for regimes with F_α further away from the current level. For the down jump intensity ν_α^- , since the high β_α and ν_α^+ can already generate a large positive skew between all three quotes, it is not necessary to have a value for ν_α^- .

Table 4.5.2 reports the parameters that work best¹¹ for USDBRL, which are also selected with no time dependence in their calculation. The external deterministic time change function, which is required to get exact fit, is shown in Figure

¹¹The resulting term structure of model implied volatilities fits the market quotes quite well in Figure 4.5.8.

4.6.3, which is quite different from that of GBPUSD, indicating the difference between 'core' market and 'emerging' market.

Table 4.5.2: Parameters for USDBRL local volatility regimes and jump intensity

α	σ_α	β_α	$\bar{\sigma}_\alpha$	ν_α^-	ν_α^+	F_α
0	30.0%	2.4	100%	0.0%	40.0%	88
1	20.0%	3.0	100%	0.0%	20.0%	95
2	10.0%	4.0	100%	0.0%	10.0%	100
3	20.0%	3.5	100%	0.0%	20.0%	110
4	30.0%	2.5	100%	0.0%	40.0%	128

The model implied term structure of volatilities are shown in terms of lines in Figure 4.5.8. Again, the calibration is putting more weight on the shorter maturities, yet the result for the long maturities is also satisfactory.

Figure 4.6.1 illustrates the extrapolated implied volatilities for out-of-the-money options. The strictly positive skew through all strikes is clear for maturities longer than 1-year. Figure 4.6.2 shows the model implied risk-neutral PDF, which is also well behaved in that they have only one maximum, indicating the risk neutral dynamics of the FX rate is completely controlled by the skewness and kurtosis of their tails. The hedge ratios, Delta, Gamma and Vega, for 6-month, 1-year and 2-year are reported in Figure 4.6.4, Figure 4.6.5 and Figure 4.6.6, respectively, all of which are different from those for GBPUSD. This may be explained by different underlying factors in these two markets, especially the policy risk in 'emerging' market.

4.6 Summary

In this chapter, we have introduced a spectral theory based modelling framework by Albanese and Mijatović[5], with a discuss of the financial underpinning and the mathematical derivation. During the numerical implementation, we propose the adoption of an alternative algorithm in calculating the exponential of non-normal matrix, and design a novel routine to improve the numerical efficiency. The model validation in Black-Scholes' case demonstrates its validity, and the model is calibrated to two very different currency pairs. The results, including the sensible implied volatilities surfaces, implied distribution functions and hedge ratios, show that this model can indeed capture the stochastic volatility and the stochastic skewness of the implied risk-neutral distribution in the FX market. Therefore, we will use the model and further extend it to price one of the exotic options - barrier options in next chapter.

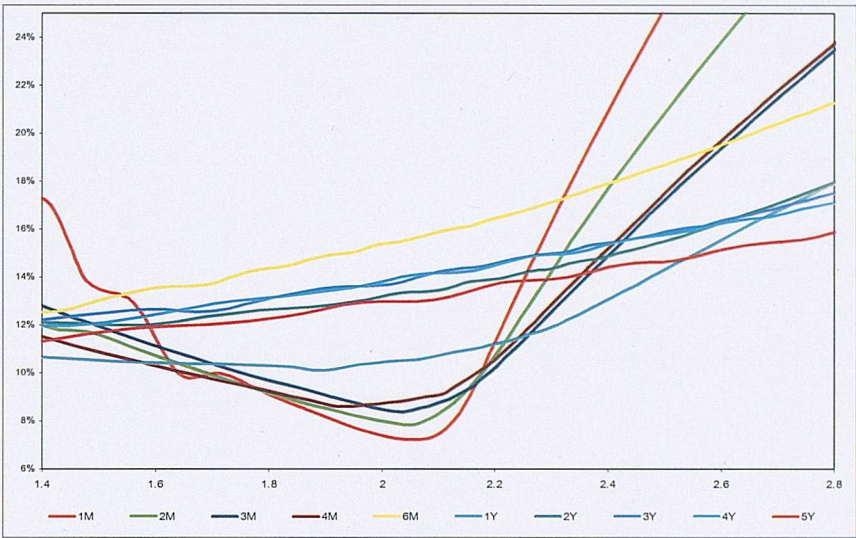


Figure 4.6.1: Extrapolated Implied Volatilities for USDBRL European Options using Generic Strikes.

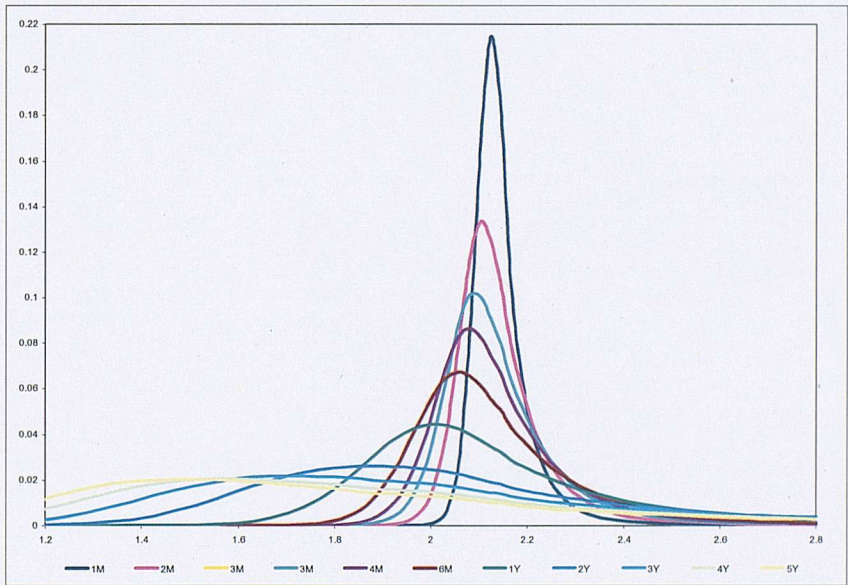


Figure 4.6.2: USDBRL Probability Distribution Function under the Forward Measure

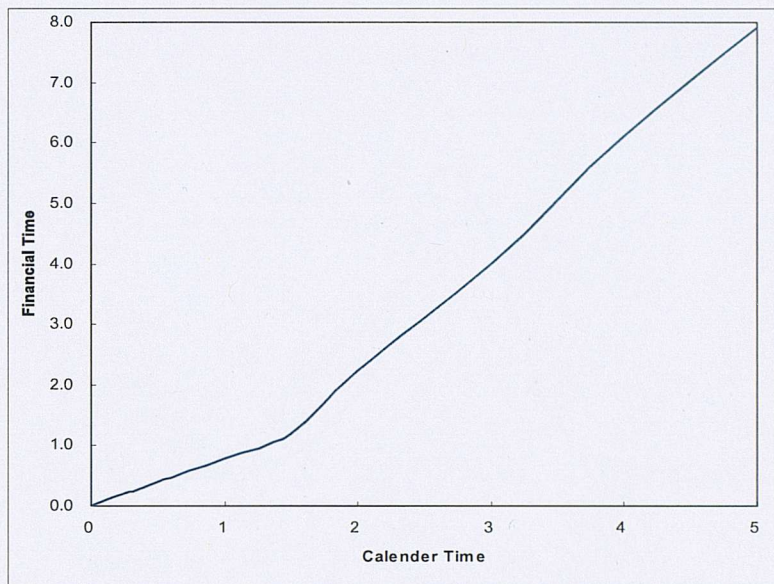


Figure 4.6.3: Deterministic Time Change $f(t)$ (in years) as a Function of Calendar Time t for USDBRL.

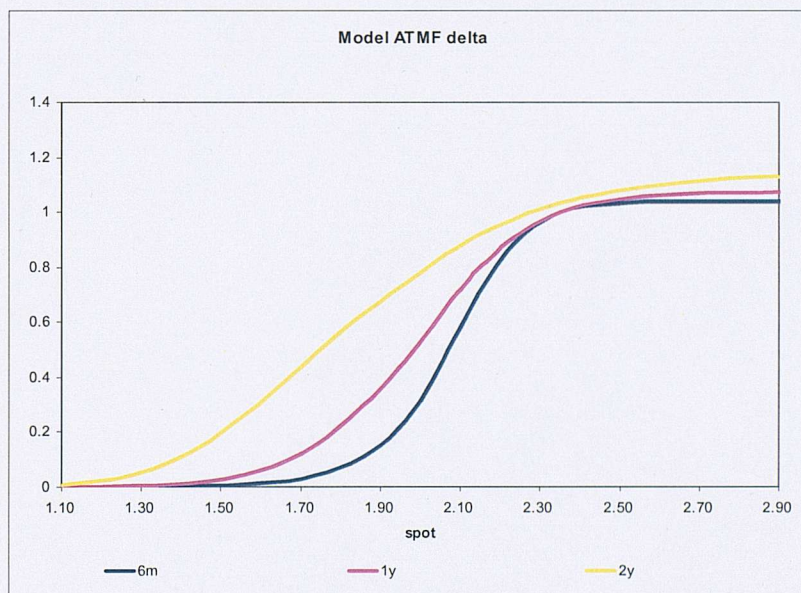


Figure 4.6.4: USDBRL ATM delta for 6-month, 1-year and 2-year, calculated with calibrated parameters.

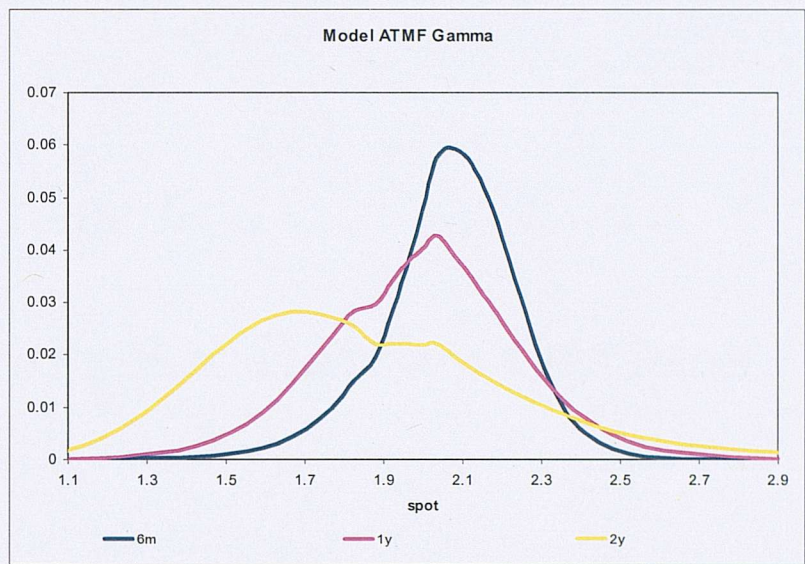


Figure 4.6.5: USDBRL ATMF gamma for 6-month, 1-year and 2-year, calculated with calibrated parameters.

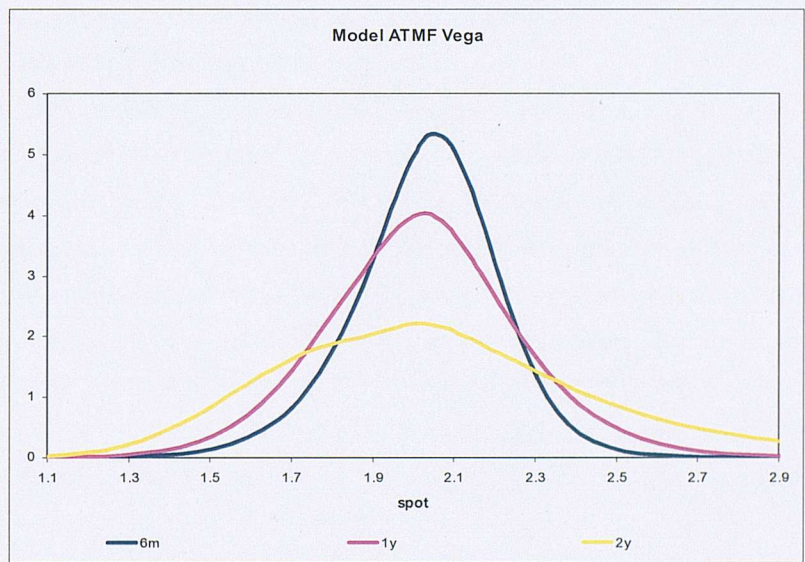


Figure 4.6.6: USDBRL ATMF vega for 6-month, 1-year and 2-year, calculated with calibrated parameters.

Chapter 5

Pricing FX Barrier Options

5.1 Barrier Options

5.1.1 Introduction

Barrier options are options that are initiated (knocked in) or terminated (knocked out) depending on whether the underlying asset's price reaches a certain barrier level. Thus they are called path-dependent options, whose payoffs are determined by the actual paths of the underlying assets.

In the OTC market, a number of barrier options are quite liquidly traded, mainly because of their barrier features, which make the options relatively cheaper than the standard ones, and more importantly, which give the investors the flexibility to incorporate their views about the future market movement in terms of the barriers. Especially in the FX market, most of the investors usually generate their views and forecast of the exchange rates movement from the macroeconomic factors such as government policy, interest rate differentials and GDP. These views thus have value for both a trading and hedging programme with options, coming from effectively selecting the cheaper 'right' barrier options according to the forecast.

There are various types of barrier options, based on their own characteristics. For the fundamental single barrier options, four types are widely traded and recognized, namely Up and In, Up and Out, Down and In, Down and Out, which total to eight in the form of calls and puts. More exotic forms of barriers, including dou-

ble barriers, Parisians, and partial time barriers, are also traded in the market to provide more flexibility. All these varieties can take either American or European forms.

In this chapter, we innovatively develop the pricing methodology for the FX single barrier European options within the Albanese and Mijatović[5] lattice framework, the idea of which can be applied to the more exotic types. We will modify the Markov generator to incorporate the barriers, and design the algorithm to price 16 barrier options simultaneously. The lattice pricing model is then validated in the Black-Scholes' case against the closed form solutions by Haug [43]. Finally we use the calibrated parameters from the previous chapter to price various barrier options for the previously mentioned two currency pairs.

5.1.2 Pricing

For path-dependent options, the lattice seems to be the most flexible and suitable pricing method, since it can store path information at lattice points. In the simplest Black-Scholes framework, however, analytical closed form formulae are available for 16 cases, depending on whether the barrier is greater or less than the strike price for the 8 types of options.

Closed Form Solution

Based on the lognormal assumption of the future probability distribution for the underlying asset price, Merton [70] firstly developed the closed form solution for the down and out call option. Reiner and Rubinstein [77] then provided the formulae for all 8 types of barrier options, which are generalized by Haug [43]. Here, we will summarize all 16 pricing formulae given by Haug [43], to serve as a model validation benchmark in the next section.

When the barrier H is less than or equal to the strike K , the 4 call options can

be priced using the following formulae:

$$\begin{aligned}
c_{di} &= S_0 e^{-rfT} \left(\frac{H}{S_0} \right) \Phi(y) - K e^{-rT} \left(\frac{H}{S_0} \right)^{2\lambda-2} \Phi(y - \sigma\sqrt{T}) \quad (5.1.1) \\
c_{do} &= c_{BS} - c_{di} \\
c_{ui} &= c_{BS} \\
c_{uo} &= c_{BS} - c_{ui} = 0
\end{aligned}$$

where

$$\begin{aligned}
\lambda &= \frac{r - rf + \sigma^2/2}{\sigma^2} \\
y &= \frac{\ln[H^2/S_0 K]}{\sigma\sqrt{T}} + \lambda\sigma\sqrt{T}
\end{aligned}$$

while the 4 relative put options are priced as:

$$\begin{aligned}
p_{di} &= -S_0 e^{-rfT} \left\{ \Phi(-x_1) - \left(\frac{H}{S_0} \right)^{2\lambda} [\Phi(y) - \Phi(y_1)] \right\} \quad (5.1.2) \\
&\quad + K e^{-rT} \left\{ \Phi(-x_1 + \sigma\sqrt{T}) - \left(\frac{H}{S_0} \right)^{2\lambda-2} [\Phi(y - \sigma\sqrt{T}) - \Phi(y_1 - \sigma\sqrt{T})] \right\} \\
p_{do} &= p_{BS} - p_{di} \\
p_{ui} &= p_{BS} - p_{uo} \\
p_{uo} &= -S_0 e^{-rfT} \left[\Phi(-x_1) - \left(\frac{H}{S_0} \right)^{2\lambda} \Phi(-y_1) \right] \\
&\quad + K e^{-rT} \left[\Phi(-x_1 + \sigma\sqrt{T}) - \left(\frac{H}{S_0} \right)^{2\lambda-2} \Phi(-y_1 + \sigma\sqrt{T}) \right]
\end{aligned}$$

where

$$\begin{aligned}
x_1 &= \frac{\ln(S_0/H)}{\sigma\sqrt{T}} + \lambda\sigma\sqrt{T} \\
y_1 &= \frac{\ln(H/S_0)}{\sigma\sqrt{T}} + \lambda\sigma\sqrt{T}
\end{aligned}$$

In the case when $H \geq K$, the call options can be valued with:

$$\begin{aligned}
c_{di} &= c_{BS} - c_{do} \\
c_{do} &= S_0 e^{-rfT} \left[\Phi(x_1) - \left(\frac{H}{S_0}\right)^{2\lambda} \Phi(y_1) \right] \\
&\quad - K e^{-rT} \left[\Phi(x_1 - \sigma\sqrt{T}) - \left(\frac{H}{S_0}\right)^{2\lambda-2} \Phi(y_1 - \sigma\sqrt{T}) \right] \\
c_{ui} &= S_0 e^{-rfT} \left\{ \Phi(x_1) - \left(\frac{H}{S_0}\right)^{2\lambda} [\Phi(-y) - \Phi(-y_1)] \right\} \\
&\quad - K e^{-rT} \left\{ \Phi(x_1 - \sigma\sqrt{T}) - \left(\frac{H}{S_0}\right)^{2\lambda-2} [\Phi(-y + \sigma\sqrt{T}) - \Phi(-y_1 + \sigma\sqrt{T})] \right\} \\
c_{uo} &= c_{BS} - c_{ui}
\end{aligned} \tag{5.1.3}$$

while for the put options:

$$\begin{aligned}
p_{di} &= p_{BS} \\
p_{do} &= p_{BS} - p_{di} = 0 \\
p_{ui} &= -S_0 e^{-rfT} \left(\frac{H}{S_0}\right) \Phi(-y) + K e^{-rT} \left(\frac{H}{S_0}\right)^{2\lambda-2} \Phi(-y + \sigma\sqrt{T}) \\
p_{uo} &= p_{BS} - p_{ui}
\end{aligned} \tag{5.1.4}$$

In addition, it is important to know the frequency of observation of the underlying price S to determine whether the barrier has been reached. All the previous 16 formulae are derived by assuming that S is monitored continuously, which is not always the case in reality. In some of the contracts, the terms may state that the asset price is only periodically measured, e.g. once a day. Broadie, Glasserman and Kou [21] come up with an adjustment for the barrier level, which effectively correct the formulae in the discrete sampling case:

$$H = H e^{\alpha\sigma\sqrt{T/m}} \tag{5.1.5}$$

where m is the number of times the underlying asset is observed, $\alpha = 0.5826$ for Up options, and $\alpha = -0.5826$ for Down options.

Lattice Methods

Lattice or trees can handle path-dependency property easily. For example, in the classic binomial tree method, introduced by Cox, Ross and Rubinstein [32], the up and down movements of barrier options are modelled the same as for other options:

$$\begin{aligned} d &= e^{-\sigma\sqrt{T}}, \quad u = \frac{1}{d} \\ p &= \frac{e^{(r-rf)T} - d}{u - d} \end{aligned} \tag{5.1.6}$$

where u and d represent the up and down magnitude of the movement respectively, p and $1 - p$ are the probability of moving up and down respectively.

The difficulty then comes from specifying the barrier on the tree. The real barrier, which is a straight line, does not lie on the 'zigzag' tree structure. Hull [46] illustrates the concept of inner and outer barriers on the tree, between which lies the true barrier. The price for the option with true barrier is the interpolation of the two prices obtained from assuming the inner and outer barrier are the true barrier.

Alternatively, when the initial price is not close to the barrier, the option can be valued by ensuring that the lattice nodes lie on the barrier, which is achieved by specifying conditions for u :

$$H = S_0 u^N \tag{5.1.7}$$

for some positive or negative N .

A more refined lattice, the trinomial framework, which is an extension of the binomial lattice, converges more quickly. For pricing barrier options, Ritchken and Kamrad [52] introduce a modified trinomial lattice, in which the up, middle and down magnitudes are modelled as:

$$u = \lambda\sigma\sqrt{T}, \quad m = 0, \quad d = -\lambda\sigma\sqrt{T} \tag{5.1.8}$$

with probabilities:

$$p_u = \frac{1}{2\lambda^2} + \frac{\mu\sqrt{T}}{2\lambda\sigma}, \quad p_m = 1 - \frac{1}{\lambda^2}, \quad p_d = \frac{1}{2\lambda^2} - \frac{\mu\sqrt{T}}{2\lambda\sigma}$$

where the drift $\mu = r - rf - \frac{1}{2}\sigma^2$, and the control term λ determines the space between the price layers. Levitan [57] further proposes the formula for λ :

$$\lambda = \frac{\ln(S/H)}{n_0\sigma\sqrt{T}} \quad (5.1.9)$$

where n_0 represents the number of consecutive down movements heading towards the lowest lattice point. Such a setting is demonstrated to have fast convergence towards the actual value.

Other Techniques

A popular alternative method to the standard lattice model is the adaptive mesh model, introduced by Figlewski and Gao [38], which can be used even when the initial price is close to the barrier. The geometry of the tree is designed so that the nodes lie on the barriers, and the probabilities on the branches are chosen to match the first two moments of the process. It is essentially a lattice transposed on top of another lattice, and can be implemented in a Monte Carlo framework. Because of the numerous paths constructed, a similar extension can be applied to American barrier option as well.

More advanced models incorporating jump diffusion, have been investigated in the literature. One important contribution is Leisen [56], who discretizes the underlying asset space instead of the usual time space to add jump risk. This bypasses the difficulty of specifying a barrier on the preset nodes. This is applied in our new framework.

In addition, the Monte Carlo framework is widely applied for valuing barrier options, in which various techniques are used to get faster convergence. For example, a Brownian bridge is used to limit the effects of high-dimensional components, variance reduction techniques such as importance sampling are used to reduce computational time.

5.2 Barriers on the Continuous-time Lattice

In this new framework, the valuation of barrier options is different from the majority of the techniques mentioned before, because of the different initial specification of the underlying diffusion process in terms of the Markov generator.

The Markov generator describes the behaviour of the diffusion process in infinitesimal time. The existence of a barrier restricts the movement of the underlying to certain states, thus modifies the behaviour of the process. Therefore, we need to modify the relevant Markov generator, which effectively describes the new process. Technically, this can be done by incorporating a barrier on the Markov generator.

5.2.1 Barrier on the Markov Generator

Modified Markov Generator

The various barrier options can be categorized into two groups: In and Out. There is a no-arbitrage relationship between their values V_{In} , V_{Out} and the vanilla option value V :

$$V_{In} + V_{Out} = V \quad (5.2.1)$$

On a lattice, it is relatively easier to specify the 'Out' barrier options, just by setting the value or probability of the nodes beyond the barrier to be zero. Then the corresponding 'In' barrier options can be calculated using formula 5.2.1. On this continuous-time lattice, we will similarly focus on valuing the 'Out' barrier options, for which the transitional probabilities of going to the points beyond the barrier should be zero.

However, as mentioned before, we should incorporate the barrier on the Markov generator to reflect the change of the diffusion process, rather than directly resetting the transitional probabilities, since the Markov generator is the driver of the process, while the transitional probabilities are the results. Theorem 4.2.5 establishes the relationship between the Markov generator $\mathcal{L}(x, y)$ and the transitional probability $p(x, 0; y, t)$ for a short time δt , for all $x, y \in \Omega$ and $t \in R_+$. It can be easily proved that for $\mathcal{L}(x, y) = 0$, the resulting $p(x, 0; y, t) = 0$. Therefore, to obtain zero transitional probabilities beyond the barrier, we can modify the relevant Markov generator to be zero.

Table 5.2.1: Modified Markov generator for Up-and-Out barrier options, with barrier level H and the number of lattice point N

0	1	2	...	$H-1$	H	...	N
1	$\mathcal{L}^\Omega(1,1)$	$\mathcal{L}^\Omega(1,1)$...	$\mathcal{L}^\Omega(1,H-1)$	0	...	0
2	$\mathcal{L}^\Omega(2,1)$	$\mathcal{L}^\Omega(2,2)$...	$\mathcal{L}^\Omega(2,H-1)$	0	...	0
\vdots	\vdots	\vdots	\ddots	\vdots	\vdots	\ddots	\vdots
$H-1$	$\mathcal{L}^\Omega(H-1,1)$	$\mathcal{L}^\Omega(H-1,2)$...	$\mathcal{L}^\Omega(H-1,H-1)$	0	...	0
H	0	0	...	0	0	...	0
\vdots	\vdots	\vdots	\ddots	\vdots	\vdots	\ddots	\vdots
N	0	0	...	0	0	...	0

The continuous-time lattice discretizes the underlying FX rate space, with the discrete Markov generator $\mathcal{L}^\Omega(x,y)$ describing the infinitesimal time movement from FX rate point x to point y . Therefore, the barrier level H , which is also a FX rate, can be specified directly on the lattice. If the barrier is not a lattice point, we can advisably choose a proper discretization scheme for the continuous Markov generator so as to make sure that one of the lattice point represents the barrier level. Then we can make the following modification to the generator:

$$\begin{aligned}
 \mathcal{L}^\Omega(x,H) &= 0, \text{ for } x \in \Omega \\
 \mathcal{L}^\Omega(H,y) &= 0, \text{ for } y \in \Omega
 \end{aligned}
 \tag{5.2.2}$$

Visually, Table 5.2.1 illustrates such changes for an Up-and-Out barrier option.

Transitional Probability Computation

According to Formula 4.2.1, the transitional probability can be calculated as the exponential of the matrix $t\mathcal{L}$. Among various method to calculate matrix exponential, the diagonalization method only works when the matrix is normal. However, as can be seen in Table 5.2.1, the matrix representing Markov generator is not symmetric, which is thus nonnormal. More valuably, we use the pseudospectra to check the normality. We test the matrix \mathcal{L} produced by the calibrated GBPUSD parameters as an example. Figure 5.2.1 reports the eigenvalues and perturbations computed by EigTool. It can be seen clearly that each perturbation ϵ can move the eigenvalues of \mathcal{L} by a distance greater than ϵ . For example, the outmost curve

shows that the perturbations of norm 10^1 will move the eigenvalues to a distance as large as 20. These indicate that the matrix is nonnormal, we cannot diagonalize matrix \mathcal{L} as $\mathcal{L} = U\Lambda U^{-1}$, and Formula 4.2.2 cannot be used to compute $e^{t\mathcal{L}}$. We have to use the alternative Scaling and Squaring method, as explained in the previous chapter.

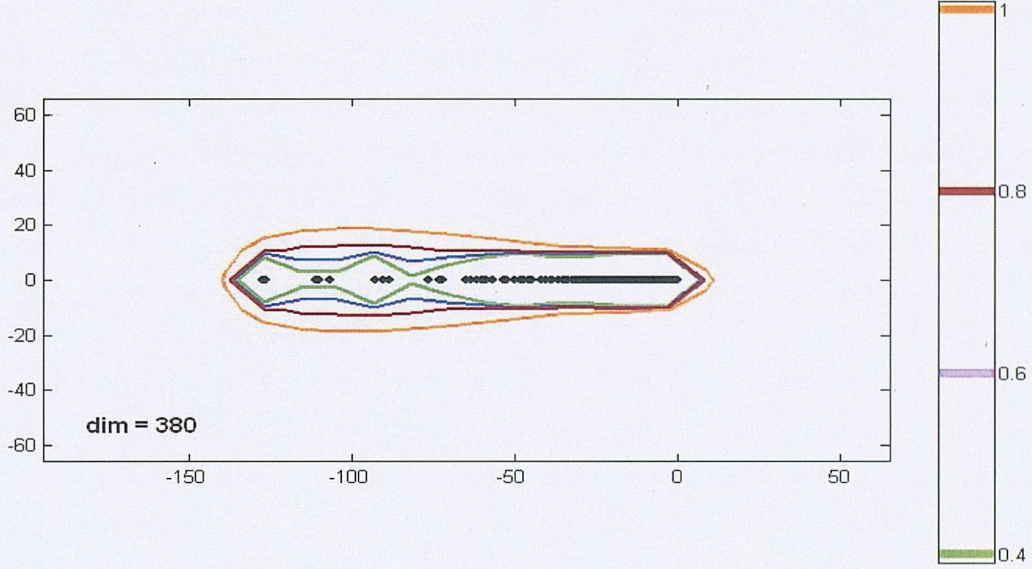


Figure 5.2.1: Boundaries of Pseudospectra for the Barrier Markov Generator \mathcal{L} , Computed with the Calibrated GBPUSD Parameters.

5.2.2 Validation - Black-Scholes Case

Before applying the calibrated model parameters, we firstly validate the modified Markov generator by pricing barrier options under Black-Scholes assumptions, and compare the results with those computed by the closed-form formulae in Section 5.1.2.

For validation purposes, we can use imaginary data as the input. We obtain the Black-Scholes case in the model by setting $\beta = 1$, one regime only. With other necessary parameters $S = 2$, $r = 5\%$, $rf = 5.5\%$, $\sigma = 20\%$, we firstly evaluate the barrier options with a lower barrier $H = 1.96$. Since $S > H$, the Up-and-Out call

and put options are both knocked out, and the Up-and-In call and put options become the normal European options. Therefore, we only need to focus on the Down-and-In and Down-and-Out options¹.

Table 5.2.2 shows the pricing results from the model and closed-form formulae². With only 400 lattice points, the model can price all the four 'down' barrier options with results very close to the closed-form formulae. As is the case with other lattice models, the result will be improved if we increase the lattice points, although this will increase the computational time.

As mentioned before, the Greeks, which are the important hedge ratios for model risk consideration, can be computed using finite difference methods, and these are reported in Table 5.2.3. They have some interesting differences from those of the vanilla options. For example, for Down-and-Out call options with strikes below the barrier, the gammas are negative; and for Down-and-In call options, the deltas are negative for all strikes.

Similarly, we examine the Black-Scholes case with the same parameters but a higher barrier $H = 2.02$. Now that $S < H$, the Down-and-Out call and put options have been knocked out, and the Down-and-In call and put options have become the European options. We only need to evaluate the Up-and-In and Up-and-Out options³.

Table 5.2.4 reports the pricing results, which are again very close to the closed-form solutions with only 400 lattice points. The relevant hedged ratios are reported in Table 5.2.5.

¹BSDOC: Closed-form Down-and-Out Call; DOC: Down-and-Out Call; BSDIC: Closed-form Down-and-In Call; DIC: Down-and-In Call; BSDOP: Closed-form Down-and-Out Put; DOP: Down-and-Out Put; BSDIP: Closed-form Down-and-In Put; DIP: Down-and-In Put.

²The strike is specified as the percentage of forward price.

³BSUOC: Closed-form Up-and-Out Call; UOC: Up-and-Out Call; BSUIC: Closed-form Up-and-In Call; UIC: Up-and-In Call; BSUOP: Closed-form Up-and-Out Put; UOP: Up-and-Out Put; BSUIP: Closed-form Up-and-In Put; UIP: Up-and-In Put.

Table 5.2.2: Barrier Options with $S > H$, 400 Lattice Points in Black-Scholes Case.

	Strike	BSDOC	DOC	BSDIC	DIC	BSDOP	DOP	BSDIP	DIP
1M	90%	0.0818	0.0824	0.1187	0.1176	0	0	0.0015	0.0015
	95%	0.0555	0.0558	0.0556	0.0547	0	0	0.0115	0.0116
	100%	0.0293	0.0293	0.0165	0.0162	0.0002	0.0002	0.0456	0.0460
	105%	0.0099	0.0099	0.0031	0.0030	0.0071	0.0074	0.1055	0.1059
	110%	0.0021	0.0021	0.0004	0.0004	0.0256	0.0263	0.1760	0.1761
2M	90%	0.0688	0.0694	0.1365	0.1348	0	0	0.0071	0.0073
	95%	0.0504	0.0507	0.0741	0.0727	0	0	0.0254	0.0258
	100%	0.0321	0.0321	0.0324	0.0317	0.0001	0.0001	0.0645	0.0653
	105%	0.0165	0.0164	0.0116	0.0113	0.0028	0.0030	0.1244	0.1255
	110%	0.0068	0.0067	0.0034	0.0033	0.0114	0.0120	0.1969	0.1981
3M	90%	0.0628	0.0634	0.1485	0.1463	0	0	0.0141	0.0144
	95%	0.0480	0.0483	0.0879	0.0861	0	0	0.0372	0.0381
	100%	0.0333	0.0333	0.0454	0.0443	0	0.0001	0.0786	0.0800
	105%	0.0200	0.0199	0.0207	0.0201	0.0015	0.0017	0.1378	0.1396
	110%	0.0105	0.0103	0.0084	0.0081	0.0067	0.0072	0.2094	0.2115
6M	90%	0.0544	0.0551	0.1746	0.1712	0	0	0.0345	0.0357
	95%	0.0445	0.0448	0.1181	0.1153	0	0	0.0652	0.0672
	100%	0.0345	0.0346	0.0752	0.0731	0	0	0.1097	0.1125
	105%	0.0250	0.0249	0.0454	0.0439	0.0005	0.0007	0.1672	0.1708
	110%	0.0170	0.0168	0.0260	0.0251	0.0025	0.0029	0.2351	0.2395
9M	90%	0.0504	0.0511	0.1939	0.1895	0	0	0.0524	0.0545
	95%	0.0425	0.0430	0.1402	0.1364	0	0	0.0868	0.0900
	100%	0.0347	0.0348	0.0978	0.0948	0	0	0.1324	0.1368
	105%	0.0271	0.0270	0.0660	0.0637	0.0003	0.0004	0.1888	0.1943
	110%	0.0203	0.0202	0.0433	0.0416	0.0013	0.0017	0.2542	0.2607
1Y	90%	0.0477	0.0485	0.2095	0.2044	0	0	0.0679	0.0712
	95%	0.0411	0.0416	0.1580	0.1534	0	0	0.1045	0.1090
	100%	0.0346	0.0348	0.1162	0.1124	0	0	0.1508	0.1567
	105%	0.0282	0.0282	0.0836	0.0806	0.0002	0.0003	0.2063	0.2136
	110%	0.0223	0.0222	0.0590	0.0566	0.0008	0.0011	0.2697	0.2783
2Y	90%	0.0415	0.0425	0.2526	0.2449	0	0	0.1149	0.1228
	95%	0.0374	0.0381	0.2071	0.2000	0	0	0.1549	0.1648
	100%	0.0333	0.0337	0.1682	0.1618	0	0	0.2015	0.2137
	105%	0.0292	0.0294	0.1356	0.1299	0	0.0001	0.2543	0.2688
	110%	0.0253	0.0254	0.1085	0.1036	0.0003	0.0004	0.3127	0.3294

Table 5.2.3: Greeks for Barrier Options with $S > H$, 400 Lattice Points in Black-Scholes
Case (Bold type indicates the difference of Greeks from vanilla options)

	Strike	DOCA	DOCT	DICA	DICT	DOPA	DOPT	DIPA	DIPT
1M	90%	2.0066	-0.0633	-1.0434	0.0758	0	0	-0.0323	0.0125
	95%	1.3710	-0.0235	-0.5559	0.0689	0	0	-0.1803	0.0454
	100%	0.7405	0.0153	-0.2339	0.0535	0.0050	-0.0010	-0.4938	0.0697
	105%	0.2648	0.0280	-0.0604	0.0210	0.1648	-0.0281	-0.9559	0.0771
	110%	0.0608	0.0138	-0.0094	0.0044	0.5964	-0.0821	-1.5405	0.1003
2M	90%	1.7102	-0.0228	-0.8118	0.0431	0	0	-0.0925	0.0202
	95%	1.2555	-0.0084	-0.5173	0.0474	0	0	-0.2527	0.0390
	100%	0.8029	0.0058	-0.2953	0.0425	0.0021	-0.0002	-0.4854	0.0486
	105%	0.4166	0.0143	-0.1339	0.0269	0.0705	-0.0062	-0.7786	0.0474
	110%	0.1746	0.0129	-0.0480	0.0125	0.2832	-0.0220	-1.1475	0.0474
3M	90%	1.5674	-0.0124	-0.7169	0.0341	0	0	-0.1358	0.0217
	95%	1.1981	-0.0045	-0.4989	0.0383	0	0	-0.2871	0.0338
	100%	0.8300	0.0033	-0.3222	0.0360	0.0012	-0.0001	-0.4798	0.0394
	105%	0.5009	0.0088	-0.1793	0.0267	0.0414	-0.0024	-0.7061	0.0380
	110%	0.2634	0.0098	-0.0860	0.0161	0.1732	-0.0094	-0.9821	0.0353
6M	90%	1.3661	-0.0043	-0.5999	0.0243	0	0	-0.2066	0.0200
	95%	1.1123	-0.0015	-0.4691	0.0267	0	0	-0.3296	0.0252
	100%	0.8591	0.0012	-0.3521	0.0262	0.0005	0	-0.4664	0.0274
	105%	0.6210	0.0036	-0.2463	0.0227	0.0162	-0.0005	-0.6144	0.0268
	110%	0.4211	0.0048	-0.1610	0.0178	0.0700	-0.0020	-0.7828	0.0246
9M	90%	1.2663	-0.0023	-0.5470	0.0199	0	0	-0.2403	0.0176
	95%	1.0652	-0.0008	-0.4501	0.0215	0	0	-0.3445	0.0207
	100%	0.8643	0.0007	-0.3597	0.0213	0.0003	0	-0.4553	0.0221
	105%	0.6722	0.0020	-0.2748	0.0196	0.0094	-0.0002	-0.5715	0.0218
	110%	0.5021	0.0029	-0.2011	0.0167	0.0404	-0.0008	-0.6990	0.0204
1Y	90%	1.2007	-0.0014	-0.5132	0.0172	0	0	-0.2590	0.0157
	95%	1.0314	-0.0005	-0.4352	0.0184	0	0	-0.3503	0.0179
	100%	0.8623	0.0005	-0.3607	0.0183	0.0003	0	-0.4452	0.0188
	105%	0.6990	0.0013	-0.2892	0.0173	0.0064	-0.0001	-0.5431	0.0187
	110%	0.5505	0.0020	-0.2249	0.0154	0.0272	-0.0004	-0.6481	0.0178
2Y	90%	1.0477	-0.0005	-0.4350	0.0117	0	0	-0.2832	0.0113
	95%	0.9395	-0.0001	-0.3903	0.0123	0	0	-0.3466	0.0121
	100%	0.8315	0.0002	-0.3458	0.0124	0.0001	0	-0.4102	0.0126
	105%	0.7259	0.0005	-0.3017	0.0121	0.0026	0	-0.4742	0.0126
	110%	0.6257	0.0008	-0.2596	0.0115	0.0106	-0.0001	-0.5403	0.0124

Table 5.2.4: Barrier Options with $S < H$, 400 Lattice Points in Black-Scholes Case.

	Strike	BSUOC	UOC	BSUIC	UIC	BSUOP	UOP	BSUIP	UIP
1M	90%	0.0120	0.0119	0.1885	0.1881	0.0009	0.0009	0.0006	0.0006
	95%	0.0026	0.0026	0.1084	0.1079	0.0056	0.0057	0.0059	0.0059
	100%	0	0	0.0458	0.0455	0.0172	0.0173	0.0287	0.0289
	105%	0	0	0.0131	0.0129	0.0313	0.0315	0.0813	0.0818
	110%	0	0	0.0025	0.0024	0.0455	0.0456	0.1561	0.1568
2M	90%	0.0054	0.0052	0.1999	0.1989	0.0030	0.0030	0.0041	0.0043
	95%	0.0010	0.0010	0.1235	0.1225	0.0088	0.0089	0.0166	0.0169
	100%	0	0	0.0645	0.0638	0.0179	0.0181	0.0466	0.0473
	105%	0	0	0.0281	0.0276	0.0281	0.0282	0.0991	0.1003
	110%	0	0	0.0102	0.0100	0.0383	0.0384	0.1701	0.1718
3M	90%	0.0032	0.0031	0.2081	0.2066	0.0047	0.0048	0.0094	0.0097
	95%	0.0006	0.0005	0.1353	0.1339	0.0104	0.0106	0.0268	0.0275
	100%	0	0	0.0787	0.0775	0.0182	0.0184	0.0604	0.0616
	105%	0	0	0.0407	0.0400	0.0266	0.0268	0.1127	0.1146
	110%	0	0	0.0188	0.0184	0.0350	0.0351	0.1811	0.1836
6M	90%	0.0013	0.0011	0.2278	0.2252	0.0077	0.0079	0.0268	0.0278
	95%	0.0002	0.0002	0.1623	0.1599	0.0127	0.0129	0.0526	0.0543
	100%	0	0	0.1097	0.1077	0.0185	0.0187	0.0912	0.0938
	105%	0	0	0.0704	0.0688	0.0245	0.0247	0.1431	0.1468
	110%	0	0	0.0430	0.0419	0.0306	0.0307	0.2070	0.2116
9M	90%	0.0007	0.0006	0.2436	0.2401	0.0093	0.0095	0.0431	0.0450
	95%	0.0001	0.0001	0.1826	0.1793	0.0136	0.0139	0.0731	0.0760
	100%	0	0	0.1324	0.1296	0.0185	0.0188	0.1139	0.1181
	105%	0	0	0.0931	0.0908	0.0235	0.0237	0.1656	0.1710
	110%	0	0	0.0636	0.0617	0.0285	0.0286	0.2270	0.2337
1Y	90%	0.0005	0.0004	0.2567	0.2525	0.0102	0.0105	0.0577	0.0607
	95%	0.0001	0.0001	0.1990	0.1950	0.0142	0.0145	0.0903	0.0945
	100%	0	0	0.1508	0.1472	0.0184	0.0187	0.1324	0.1380
	105%	0	0	0.1118	0.1087	0.0228	0.0230	0.1837	0.1908
	110%	0	0	0.0812	0.0787	0.0271	0.0273	0.2434	0.2521
2Y	90%	0.0002	0.0001	0.2938	0.2873	0.0118	0.0122	0.1031	0.1106
	95%	0	0	0.2444	0.2381	0.0147	0.0152	0.1401	0.1497
	100%	0	0	0.2015	0.1956	0.0178	0.0182	0.1837	0.1955
	105%	0	0	0.1648	0.1594	0.0209	0.0213	0.2335	0.2476
	110%	0	0	0.1338	0.1289	0.0240	0.0243	0.2890	0.3055

Table 5.2.5: Greeks for Barrier Options with $S < H$, 400 Lattice Points in Black-Scholes Case (Bold type indicates the distinct difference of the Greeks from the vanilla options)

	Strike	UOCA	UOCT	UICA	UICT	UOPA	UOPT	UIPA	UIPT
1M	90%	-0.5786	-0.0382	1.5418	0.0507	-0.0468	0.0062	0.0145	0.0063
	95%	-0.1236	-0.0103	0.9387	0.0557	-0.2880	0.0139	0.1077	0.0315
	100%	0	0	0.5072	0.0688	-0.8611	0.0039	0.3723	0.0649
	105%	0	0	0.2043	0.0490	-1.5567	-0.0163	0.7656	0.0654
	110%	0	0	0.0514	0.0182	-2.2529	-0.0366	1.3089	0.0549
2M	90%	-0.2570	-0.0098	1.1554	0.0300	-0.1533	0.0059	0.0609	0.0143
	95%	-0.0468	-0.0020	0.7850	0.0410	-0.4442	0.0065	0.1916	0.0325
	100%	0	0	0.5077	0.0484	-0.8986	0.0013	0.4153	0.0471
	105%	0	0	0.2827	0.0412	-1.3995	-0.0059	0.6914	0.0471
	110%	0	0	0.1266	0.0254	-1.9006	-0.0130	1.0363	0.0384
3M	90%	-0.1509	-0.0041	1.0015	0.0258	-0.2386	0.0044	0.1028	0.0173
	95%	-0.0257	-0.0008	0.7249	0.0346	-0.5265	0.0038	0.2393	0.0300
	100%	0	0	0.5079	0.0393	-0.9139	0.0007	0.4354	0.0386
	105%	0	0	0.3216	0.0355	-1.3269	-0.0032	0.6622	0.0388
	110%	0	0	0.1774	0.0259	-1.7399	-0.0071	0.9310	0.0330
6M	90%	-0.0561	-0.0008	0.8224	0.0208	-0.3911	0.0021	0.1845	0.0178
	95%	-0.0087	-0.0001	0.6520	0.0253	-0.6403	0.0014	0.3107	0.0237
	100%	0	0	0.5070	0.0274	-0.9281	0.0002	0.4622	0.0272
	105%	0	0	0.3747	0.0263	-1.2246	-0.0012	0.6264	0.0275
	110%	0	0	0.2601	0.0226	-1.5211	-0.0025	0.8084	0.0252
9M	90%	-0.0301	-0.0003	0.7494	0.0179	-0.4712	0.0013	0.2309	0.0164
	95%	-0.0044	0	0.6195	0.0208	-0.6894	0.0008	0.3449	0.0199
	100%	0	0	0.5046	0.0221	-0.9290	0.0001	0.4740	0.0220
	105%	0	0	0.3974	0.0216	-1.1729	-0.0006	0.6107	0.0222
	110%	0	0	0.3010	0.0196	-1.4168	-0.0014	0.7583	0.0210
1Y	90%	-0.0190	-0.0001	0.7065	0.0159	-0.5198	0.0008	0.2609	0.0149
	95%	-0.0027	0	0.5989	0.0179	-0.7156	0.0005	0.3653	0.0174
	100%	0	0	0.5016	0.0188	-0.9250	0	0.4801	0.0188
	105%	0	0	0.4098	0.0186	-1.1371	-0.0004	0.6004	0.0190
	110%	0	0	0.3256	0.0174	-1.3492	-0.0009	0.7284	0.0183
2Y	90%	-0.0057	0	0.6183	0.0113	-0.6015	0.0003	0.3183	0.0110
	95%	-0.0007	0	0.5499	0.0121	-0.7464	0.0002	0.3999	0.0120
	100%	0	0	0.4858	0.0126	-0.8957	0	0.4856	0.0126
	105%	0	0	0.4242	0.0126	-1.0456	-0.0002	0.5740	0.0128
	110%	0	0	0.3661	0.0123	-1.1955	-0.0003	0.6658	0.0126

5.3 Pricing Experiment

5.3.1 GBPUSD

With the parameters calibrated to the market, we can directly apply the previous validated model to price barrier options for GBPUSD currency pair. At the current spot level of 1.944, we try to price the 'Down' barrier options with a lower barrier 1.864 (approximately 96% of the spot price), and the 'Up' barrier options with a higher barrier 1.984 (about 102% of the spot price). In order to see the special properties of barrier options, we also produce the relevant European call and put option values and Greeks for comparison, listed in Table 5.3.1.

Table 5.3.2 shows the pricing results for Down and Out call and Down and In call, together with the delta, gamma and vega for hedging purposes. Several interesting barrier option properties can be observed clearly. For example, the price for the $k = 90\%$ (in-the-money for call) Down and Out call option decreases sharply with the maturity. This is because given the low volatility of GBPUSD (about 7%), the chances of hitting the barrier 96% is relatively small for a short maturity like one month, thus the in-the-money call still retains most of its value as the vanilla call. However, with the longer maturity, it is more likely that the barrier will be hit, thus the price decreases faster than that for vanilla options, creating a bigger difference between them. Another obvious difference is that the delta for Down-and-In call with strike below the barrier is negative, this is because with the decrease of the underlying, the option is more likely to be 'knock-in' and have value. Notice that the absolute value of delta also increases with maturity, the explanation is similar.

Table 5.3.3 reports the prices for Down-and-Out put and Down-and-In put options, together with their hedge ratios. Compared with the information in Table 5.3.1, we can see a few differences, the most obvious being the delta for Down-and-Out put option. Instead of the negative value for vanilla put delta, the deltas for maturities longer than six months are all positive. This can be explained by the trade-off between being in-the-money and being knocked-out. With the longer maturity, the put option has a higher probability of hitting the barrier and being knocked out. When the strike increases, on the one hand, the option value increases

because it is further away from the barrier and thus more likely to stay alive; on the other hand, the value decreases because it is less likely to be in-the-money. If the former effect is greater than latter one, the option value will have a positive relationship with the underlying, thus the delta is positive.

For the barrier higher than spot, Table 5.3.4 and Table 5.3.5 display the option values and Greeks for Up and Out and Up and In calls and puts, respectively. It is interesting to notice that the delta profile for Down and In put is quite similar to that for the Up and Out Put, while Down and In call and Up and Out call both have universal negative delta for in-the-money options. The absolute values of vega for deep in-the-money calls and puts are very large, due to the low volatility of this currency pair.

5.3.2 USDBRL

Similarly, we apply the model to price the USDBRL barrier options, with the parameters calibrated to the vanilla option quotes. For comparability with the GBPUSD results, we price the options with the same percentage barrier level, namely 96% for the 'Down' options and 102% for the 'Up' options. Based on the current market spot price of 2.145, we are effectively pricing with a lower barrier 2.056 and a higher barrier 2.190. For analytical convenience, we also display the corresponding European option prices and hedge ratios in Table 5.4.1. In comparison with the GBPUSD result in Table 5.3.1, we find that the volatility difference between these two currency pairs is most clear in the price for in-the-money put and its vega. For the low volatility GBPUSD, with the increase of maturity, the value decreased by the higher probability of getting closer to be out-of-the-money is not large enough to cancel out the increase of time value, thus the put option price rises. If the volatility increases, the option will more likely go out-of-the-money, thus the vega is negative. However, for USDBRL which has much higher volatility, the deep in-the-money put price is distinctly decreasing with the maturity, since the increase of time value cannot compensate for the sharp decrease of value due to the higher chances of being out-of-the-money. Given the already higher volatility, the small increase of volatility will however increase the option value, thus giving positive vega.

Table 5.4.2 provides the results for Down and Out call and Down and In call. The trend of both option value and hedge ratios are quite similar to those in GBPUSD case, except for the scale of vega profile. For Down and Out call, the vegas for both currency pairs increase with maturity for in-the-money options. However, due to the lower volatility, GBPUSD has a much larger vega increase, resulting in large positive vega in long maturity like 2-year, while USDBRL vega still remains negative. And opposite result can be seen in the vega for Down and In call. Also notice that for the short maturity out-of-the-money call in the Down and In case, GBPUSD has no value because of the small chance of getting knocked in with some value, while USDBRL can have none-zero value even at maturity as short as 2 months, because of much higher volatility. In comparison, in the Down and In put case, the short maturity out-of-the-money put for GBPUSD is easier to retain some value (e.g. $k = 95\%$ for 1-month), as can be seen in Table 5.4.3.

The pricing results for the Up and Out and Up and In calls and puts are shown in Table 5.4.4 and Table 5.4.5, respectively. As expected, the vegas for all four options are much smaller than their GBPUSD counterpart.

5.4 Summary

In this chapter, we innovatively develop the pricing methodology for the FX barrier options within the lattice framework proposed by Albanese and Mijatovic [4]. In calculating the exponential of the non-normal Markov generator matrix, we again apply the algorithm we proposed in the last chapter. The model is validated in the Black-Scholes' case against the closed-form pricing formulae provided by Haug [43]. The validity of our method is confirmed by the very small differences between the model prices and those from the closed-form solutions. Finally, with the parameters calibrated from last chapter, the model achieves reasonable pricing results for both a developed market currency pair (GBPUSD) and an emerging market currency pair (USDBRL).

Table 5.3.1: GBPUSD European Options and Hedge Ratios with 76 Lattice Points and 5 Regimes (Bolded numbers are compared with the barrier options counterparts in the following tables)

	Strike	Call	Call Δ	Call Γ	Call v	Put	Put Δ	Put Γ	Put v
1M	90%	0.1937	0.9958	0	10.7964	0	0	0	0
	95%	0.0970	0.9870	0.0088	11.3725	0.0001	-0.0088	0.0088	0.5774
	100%	0.0158	0.5001	0.1999	20.7495	0.0157	-0.4957	0.1999	9.9544
	105%	0.0004	0.0222	0.0186	1.6678	0.0970	-0.9736	0.0186	-9.1273
	110%	0	0.0007	0.0006	0.0542	0.1934	-0.9951	0.0006	-10.7409
2M	90%	0.1932	0.9912	0.0003	10.7662	0	-0.0003	0.0003	0.0172
	95%	0.0977	0.9584	0.0230	12.1516	0.0008	-0.0331	0.0230	1.4026
	100%	0.0223	0.5055	0.1402	16.2297	0.0217	-0.4860	0.1402	5.4807
	105%	0.0017	0.0630	0.0370	3.5235	0.0974	-0.9285	0.0370	-7.2255
	110%	0.0001	0.0045	0.0032	0.2940	0.1921	-0.9870	0.0032	-10.4550
3M	90%	0.1926	0.9859	0.0010	10.7633	0	-0.0013	0.0010	0.0611
	95%	0.0984	0.9275	0.0323	12.5329	0.0018	-0.0597	0.0323	1.8307
	100%	0.0269	0.5064	0.1148	14.2892	0.0262	-0.4808	0.1148	3.5869
	105%	0.0034	0.0991	0.0456	4.5704	0.0985	-0.8881	0.0456	-6.1318
	110%	0.0003	0.0115	0.0067	0.6390	0.1913	-0.9757	0.0067	-10.0632
6M	90%	0.1904	0.9620	0.0059	10.8807	0.0004	-0.0122	0.0059	0.3195
	95%	0.1018	0.8454	0.0422	12.4002	0.0064	-0.1288	0.0422	1.8390
	100%	0.0376	0.5040	0.0794	11.5533	0.0369	-0.4701	0.0794	0.9921
	105%	0.0094	0.1783	0.0506	5.8109	0.1033	-0.7959	0.0506	-4.7503
	110%	0.0018	0.0435	0.0166	1.7453	0.1903	-0.9307	0.0166	-8.8158
9M	90%	0.1881	0.9297	0.0112	10.9403	0.0015	-0.0314	0.0112	0.5207
	95%	0.1047	0.7871	0.0422	11.7684	0.0115	-0.1740	0.0422	1.3489
	100%	0.0449	0.4967	0.0639	10.2864	0.0453	-0.4644	0.0639	-0.1331
	105%	0.0149	0.2218	0.0475	6.0446	0.1087	-0.7394	0.0475	-4.3750
	110%	0.0041	0.0751	0.0218	2.4825	0.1914	-0.8860	0.0218	-7.9370
1Y	90%	0.1860	0.8945	0.0152	10.8600	0.0033	-0.0535	0.0152	0.5825
	95%	0.1072	0.7425	0.0401	11.1263	0.0168	-0.2056	0.0401	0.8488
	100%	0.0508	0.4885	0.0543	9.4627	0.0527	-0.4595	0.0543	-0.8148
	105%	0.0199	0.2491	0.0436	6.0443	0.1142	-0.6989	0.0436	-4.2331
	110%	0.0067	0.1024	0.0241	2.9554	0.1933	-0.8456	0.0241	-7.3220
2Y	90%	0.1770	0.7687	0.0205	9.9052	0.0137	-0.1282	0.0205	0.1824
	95%	0.1114	0.6240	0.0320	9.2167	0.0367	-0.2728	0.0320	-0.5060
	100%	0.0639	0.4472	0.0362	7.6266	0.0777	-0.4497	0.0362	-2.0962
	105%	0.0336	0.2841	0.0320	5.5359	0.1360	-0.6127	0.0320	-4.1868
	110%	0.0162	0.1612	0.0234	3.5424	0.2071	-0.7357	0.0234	-6.1804

Table 5.3.2: GBPUSD 'Down-and-Call' Barrier Options and Hedge Ratios with $S > H$, 76 Lattice Points and 5 Regimes (Bolded numbers are compared with the European calls counterparts, indicating the barrier property, as explained in the text)

	Strike	DOC	DOCA	DOCT	DOC _v	DIC	DICA	DICF	DIC _v
1M	90%	0.1886	1.2881	-0.2455	-4.8570	0.0050	-0.2923	0.2455	15.6534
	95%	0.0962	1.0370	-0.0349	8.5698	0.0008	-0.0501	0.0436	2.8027
	100%	0.0158	0.5003	0.1996	20.7309	0	0	0	0
	105%	0.0004	0.0222	0.0186	1.6674	0	0	0	0
	110%	0	0	0	0	0	0	0	0
2M	90%	0.1782	1.5081	-0.2685	-4.2354	0.0151	-0.5169	0.2687	15.0015
	95%	0.0948	1.0655	-0.0389	8.5644	0.0029	-0.1070	0.0619	3.5872
	100%	0.0223	0.5083	0.1378	16.0775	0.0001	-0.0028	0.0024	0.1523
	105%	0.0017	0.0631	0.0370	3.5186	0	0	0	0.0049
	110%	0.0001	0.0045	0.0032	0.2937	0	0	0	0
3M	90%	0.1687	1.5917	-0.2269	-0.1390	0.0238	-0.6058	0.2278	10.9024
	95%	0.0933	1.0741	-0.0334	9.0832	0.0052	-0.1466	0.0657	3.4497
	100%	0.0267	0.5152	0.1088	13.9242	0.0002	-0.0088	0.0060	0.3650
	105%	0.0034	0.0995	0.0453	4.5506	0	0	0	0
	110%	0.0003	0.0115	0.0067	0.6376	0	0	0	0
6M	90%	0.1477	1.5984	-0.1222	7.9589	0.0427	-0.6364	0.1281	2.9218
	95%	0.0894	1.0637	-0.0188	10.0935	0.0123	-0.2183	0.0609	2.3067
	100%	0.0360	0.5445	0.0622	10.6693	0.0016	-0.0405	0.0173	0.8840
	105%	0.0092	0.1834	0.0479	5.6592	0.0002	-0.0052	0.0027	0.1516
	110%	0.0018	0.0441	0.0162	1.7239	0	0	0	0.0214
9M	90%	0.1346	1.5258	-0.0753	10.7671	0.0535	-0.5961	0.0865	0.1731
	95%	0.0862	1.0376	-0.0116	10.3599	0.0184	-0.2505	0.0538	1.4085
	100%	0.0411	0.5688	0.0410	9.3098	0.0039	-0.0721	0.0229	0.9767
	105%	0.0142	0.2371	0.0414	5.7408	0.0007	-0.0153	0.0061	0.3037
	110%	0.0040	0.0780	0.0204	2.4127	0.0001	-0.0029	0.0013	0.0698
1Y	90%	0.1252	1.4512	-0.0510	11.8201	0.0608	-0.5566	0.0662	-0.9601
	95%	0.0835	1.0102	-0.0078	10.3553	0.0237	-0.2677	0.0479	0.7710
	100%	0.0442	0.5870	0.0290	8.5904	0.0066	-0.0985	0.0253	0.8723
	105%	0.0184	0.2774	0.0344	5.6471	0.0016	-0.0283	0.0092	0.3972
	110%	0.0064	0.1095	0.0214	2.8268	0.0003	-0.0071	0.0027	0.1287
2Y	90%	0.1025	1.2180	-0.0179	11.8318	0.0745	-0.4493	0.0384	-1.9267
	95%	0.0744	0.9010	-0.0019	9.6210	0.0371	-0.2770	0.0339	-0.4043
	100%	0.0476	0.5971	0.0121	7.4018	0.0163	-0.1500	0.0241	0.2248
	105%	0.0270	0.3558	0.0179	5.2289	0.0066	-0.0716	0.0141	0.3070
	110%	0.0138	0.1917	0.0163	3.3298	0.0024	-0.0306	0.0071	0.2126

Table 5.3.3: GBPUSD 'Down-and-put' Barrier Options and Hedge Ratios with $S > H$, 76 Lattice Points and 5 Regimes (Bolded numbers are compared with the European puts counterparts, indicating the difference due to barrier property, as explained in the text)

	Strike	DOP	DOP Δ	DOP Γ	DOP ν	DIP	DIP Δ	DIP Γ	DIP ν
1M	90%	0	0	0	0	0	0	0	0
	95%	0	0	0	0	0.0001	-0.0088	0.0088	0.5774
	100%	0.0120	-0.2856	0.0239	-1.2658	0.0036	-0.2101	0.1760	11.2202
	105%	0.0891	-0.5127	-0.3677	-33.7561	0.0080	-0.4609	0.3864	24.6288
	110%	0.1811	-0.2831	-0.5963	-48.7961	0.0123	-0.7119	0.5970	38.0552
2M	90%	0	0	0	0	0	0	0	0
	95%	0	0	0	0	0.0008	-0.0331	0.0230	1.4026
	100%	0.0108	-0.1145	-0.0528	-5.2866	0.0108	-0.3716	0.1930	10.7674
	105%	0.0737	-0.1170	-0.3831	-30.6452	0.0237	-0.8115	0.4202	23.4197
	110%	0.1555	0.2671	-0.6464	-46.6699	0.0367	-1.2541	0.6496	36.2148
3M	90%	0	0	0	0	0	0	0	0
	95%	0	0	0	0	0.0018	-0.0597	0.0323	1.8307
	100%	0.0089	-0.0413	-0.0513	-4.3812	0.0172	-0.4395	0.1661	7.9682
	105%	0.0611	0.0606	-0.3082	-22.9771	0.0374	-0.9487	0.3538	16.8452
	110%	0.1335	0.4902	-0.5403	-36.1123	0.0578	-1.4660	0.5470	26.0491
6M	90%	0	0	0	0	0.0004	-0.0122	0.0059	0.3195
	95%	0	0	0	0	0.0064	-0.1288	0.0422	1.8390
	100%	0.0049	0.0155	-0.0225	-1.5587	0.0320	-0.4857	0.1019	2.5508
	105%	0.0364	0.1891	-0.1402	-8.7033	0.0668	-0.9850	0.1908	3.9530
	110%	0.0873	0.5845	-0.2753	-14.7732	0.1030	-1.5152	0.2919	5.9574
9M	90%	0	0	0	0	0.0015	-0.0314	0.0112	0.5207
	95%	0	0	0	0	0.0115	-0.1740	0.0422	1.3489
	100%	0.0032	0.0194	-0.0111	-0.6429	0.0421	-0.4838	0.0750	0.5098
	105%	0.0248	0.1758	-0.0745	-3.8046	0.0839	-0.9151	0.1219	-0.5704
	110%	0.0629	0.5049	-0.1591	-6.7255	0.1285	-1.3909	0.1808	-1.2115
1Y	90%	0	0	0	0	0.0033	-0.0535	0.0152	0.5825
	95%	0	0	0	0	0.0168	-0.2056	0.0401	0.8488
	100%	0.0023	0.0178	-0.0064	-0.3001	0.0504	-0.4773	0.0608	-0.5147
	105%	0.0182	0.1492	-0.0443	-1.7785	0.0960	-0.8481	0.0879	-2.4546
	110%	0.0478	0.4222	-0.1006	-3.1341	0.1455	-1.2679	0.1246	-4.1879
2Y	90%	0	0	0	0	0.0137	-0.1282	0.0205	0.1824
	95%	0	0	0	0	0.0367	-0.2728	0.0320	-0.5060
	100%	0.0013	0.0131	-0.0020	-0.0084	0.0764	-0.4628	0.0382	-2.0878
	105%	0.0089	0.0887	-0.0122	0.0296	0.1271	-0.7015	0.0442	-4.2164
	110%	0.0237	0.2417	-0.0297	0.3413	0.1834	-0.9774	0.0531	-6.5216

Table 5.3.4: GBPUSD 'Up-and-call' Barrier Options and Hedge Ratios with $S < H$, 76 Lattice Points and 5 Regimes (Bolded numbers are compared with the European calls counterparts, indicating the difference of Greeks for options with strikes below the barriers)

	Strike	UOC	UOCA	UOCT	UOC _v	UIC	UICA	UICF	UIC _v
1M	90%	0.1213	-1.6139	-1.2628	-114.3259	0.0724	2.6097	1.2628	125.1223
	95%	0.0542	-0.5522	-0.7333	-62.2116	0.0428	1.5391	0.7420	73.5841
	100%	0.0022	0.0074	-0.0440	-3.2957	0.0136	0.4926	0.2439	24.0453
	105%	0	0	0	0	0.0004	0.0222	0.0186	1.6678
	110%	0	0	0	0	0	0.0007	0.0006	0.0542
2M	90%	0.0888	-1.4774	-0.6869	-68.6901	0.1044	2.4686	0.6872	79.4562
	95%	0.0358	-0.4997	-0.3789	-34.4678	0.0619	1.4582	0.4018	46.6194
	100%	0.0013	-0.0098	-0.0196	-1.6116	0.0210	0.5153	0.1598	17.8414
	105%	0	0	0	0	0.0017	0.0630	0.0370	3.5235
	110%	0	0	0	0	0.0001	0.0045	0.0032	0.2940
3M	90%	0.0709	-1.2805	-0.4480	-48.2358	0.1217	2.2664	0.4490	58.9991
	95%	0.0261	-0.4135	-0.2296	-22.0905	0.0723	1.3410	0.2619	34.6234
	100%	0.0008	-0.0101	-0.0100	-0.8745	0.0261	0.5165	0.1247	15.1637
	105%	0	0	0	0	0.0034	0.0991	0.0456	4.5704
	110%	0	0	0	0	0.0003	0.0115	0.0067	0.6390
6M	90%	0.0419	-0.8351	-0.1813	-22.9515	0.1485	1.7970	0.1872	33.8322
	95%	0.0126	-0.2361	-0.0724	-8.1123	0.0891	1.0815	0.1146	20.5125
	100%	0.0003	-0.0058	-0.0022	-0.2341	0.0373	0.5098	0.0816	11.7874
	105%	0	0	0	0	0.0094	0.1783	0.0506	5.8109
	110%	0	0	0	0	0.0018	0.0435	0.0166	1.7453
9M	90%	0.0284	-0.5857	-0.0980	-13.8660	0.1597	1.5154	0.1093	24.8063
	95%	0.0075	-0.1503	-0.0323	-4.1089	0.0971	0.9374	0.0745	15.8773
	100%	0.0002	-0.0032	-0.0008	-0.0943	0.0448	0.4999	0.0647	10.3808
	105%	0	0	0	0	0.0149	0.2218	0.0475	6.0446
	110%	0	0	0	0	0.0041	0.0751	0.0218	2.4825
1Y	90%	0.0203	-0.4289	-0.0592	-9.1920	0.1657	1.3234	0.0744	20.0520
	95%	0.0049	-0.1021	-0.0170	-2.4098	0.1023	0.8445	0.0571	13.5361
	100%	0.0001	-0.0020	-0.0004	-0.0488	0.0507	0.4905	0.0547	9.5115
	105%	0	0	0	0	0.0199	0.2491	0.0436	6.0443
	110%	0	0	0	0	0.0067	0.1024	0.0241	2.9554
2Y	90%	0.0073	-0.1594	-0.0139	-2.7901	0.1697	0.9281	0.0344	12.6953
	95%	0.0013	-0.0289	-0.0027	-0.5209	0.1101	0.6529	0.0347	9.7376
	100%	0	0	0	0	0.0639	0.4473	0.0363	7.6296
	105%	0	0	0	0	0.0336	0.2841	0.0320	5.5359
	110%	0	0	0	0	0.0162	0.1612	0.0234	3.5424

Table 5.3.5: GBPUSD 'Up-and-put' Barrier Options and Hedge Ratios with $S < H$, 76 Lattice Points and 5 Regimes (Bolded numbers are compared with the Down and In Puts counterparts, as explained in the text)

	Strike	UOP	UOP Δ	UOPT	UOP v	UIP	UIP Δ	UIPT	UIP v
1M	90%	0	0	0	0	0	0	0	0
	95%	0.0001	-0.0089	0.0087	0.5725	0	0	0	0
	100%	0.0153	-0.5199	0.1771	7.9454	0.0004	0.0242	0.0228	2.0090
	105%	0.0802	-1.5979	-0.2997	-40.3019	0.0168	0.6243	0.3183	31.1746
	110%	0.1474	-2.6686	-0.8205	-91.8450	0.0460	1.6735	0.8211	81.1041
2M	90%	0	0	0	0	0	0	0	0
	95%	0.0007	-0.0340	0.0221	1.3291	0	0	0	0
	100%	0.0200	-0.5554	0.0952	1.2754	0.0017	0.0693	0.0450	4.2053
	105%	0.0726	-1.5569	-0.1714	-30.0228	0.0248	0.6284	0.2085	22.7974
	110%	0.1264	-2.5682	-0.4576	-62.9327	0.0657	1.5813	0.4608	52.4777
3M	90%	0	0	0	0	0	0	0	0
	95%	0.0017	-0.0633	0.0296	1.5792	0.0001	0.0037	0.0028	0.2515
	100%	0.0228	-0.5889	0.0594	-1.8292	0.0033	0.1081	0.0554	5.4161
	105%	0.0684	-1.5078	-0.1204	-25.5789	0.0300	0.6197	0.1660	19.4471
	110%	0.1149	-2.4368	-0.3102	-50.2033	0.0764	1.4610	0.3169	40.1400
6M	90%	0.0004	-0.0134	0.0051	0.2484	0	0	0	0
	95%	0.0055	-0.1541	0.0300	0.6277	0.0009	0.0253	0.0122	1.2114
	100%	0.0276	-0.6634	0.0161	-5.9542	0.0093	0.1933	0.0633	6.9463
	105%	0.0617	-1.3973	-0.0656	-20.1800	0.0416	0.6014	0.1162	15.4297
	110%	0.0961	-2.1370	-0.1496	-34.6400	0.0942	1.2062	0.1662	25.8242
9M	90%	0.0013	-0.0374	0.0084	0.2414	0.0002	0.0060	0.0028	0.2793
	95%	0.0090	-0.2294	0.0221	-0.7931	0.0026	0.0554	0.0201	2.1420
	100%	0.0301	-0.7098	0.0016	-7.5703	0.0152	0.2454	0.0623	7.4372
	105%	0.0585	-1.3341	-0.0496	-18.2677	0.0503	0.5948	0.0971	13.8927
	110%	0.0870	-1.9616	-0.1016	-29.0594	0.1044	1.0756	0.1234	21.1224
1Y	90%	0.0026	-0.0684	0.0095	-0.0127	0.0007	0.0149	0.0057	0.5951
	95%	0.0119	-0.2917	0.0148	-2.0275	0.0049	0.0861	0.0253	2.8762
	100%	0.0318	-0.7416	-0.0055	-8.4634	0.0210	0.2821	0.0599	7.6486
	105%	0.0564	-1.2898	-0.0421	-17.2117	0.0578	0.5909	0.0857	12.9785
	110%	0.0811	-1.8399	-0.0791	-26.0087	0.1122	0.9942	0.1031	18.6866
2Y	90%	0.0083	-0.1974	0.0049	-1.7640	0.0054	0.0693	0.0156	1.9465
	95%	0.0196	-0.4554	-0.0011	-5.0210	0.0172	0.1826	0.0331	4.5150
	100%	0.0355	-0.8152	-0.0155	-10.0294	0.0422	0.3655	0.0518	7.9332
	105%	0.0527	-1.2035	-0.0327	-15.5526	0.0833	0.5908	0.0647	11.3658
	110%	0.0700	-1.5920	-0.0498	-21.0789	0.1372	0.8563	0.0732	14.8985

Table 5.4.1: USDBRL European Options and Hedge Ratios with 76 Lattice Points and 5 Regimes (Bolded numbers are compared with the barrier options counterparts in the following tables)

	Strike	Call	Call Δ	Call Γ	Call v	Put	Put Δ	Put Γ	Put v
1M	90%	0.2245	0.9956	0	0	0	0	0	0
	95%	0.1191	0.9926	0.0037	0	0	0	0	0
	100%	0.0278	0.5511	0.1888	0.8999	0.0141	-0.4445	0.1888	0.9650
	105%	0.0053	0.0896	0.0329	0.1574	0.0970	-0.9060	0.0329	0.2226
	110%	0.0018	0.0236	0.0072	0.0341	0.1989	-0.9720	0.0072	0.0993
2M	90%	0.2340	0.9910	0.0003	0	0	0	0	0
	95%	0.1310	0.9654	0.0185	0.0283	0.0006	-0.0259	0.0185	0.0932
	100%	0.0466	0.5859	0.1133	0.5231	0.0199	-0.4054	0.1133	0.5879
	105%	0.0152	0.1902	0.0486	0.2284	0.0921	-0.8011	0.0486	0.2933
	110%	0.0063	0.0687	0.0161	0.0754	0.1869	-0.9226	0.0161	0.1402
3M	90%	0.2427	0.9848	0.0015	0	0.0001	-0.0022	0.0015	0.0077
	95%	0.1424	0.9375	0.0252	0.0634	0.0017	-0.0495	0.0252	0.1280
	100%	0.0629	0.6093	0.0836	0.3743	0.0241	-0.3776	0.0836	0.4389
	105%	0.0266	0.2702	0.0517	0.2387	0.0897	-0.7167	0.0517	0.3033
	110%	0.0130	0.1228	0.0235	0.1087	0.1780	-0.8641	0.0235	0.1733
4M	90%	0.2509	0.9779	0.0026	0	0.0001	-0.0046	0.0026	0.0134
	95%	0.1536	0.9120	0.0278	0.0781	0.0031	-0.0706	0.0278	0.1424
	100%	0.0767	0.6288	0.0682	0.2971	0.0265	-0.3538	0.0682	0.3613
	105%	0.0371	0.3275	0.0509	0.2311	0.0872	-0.6551	0.0509	0.2954
	110%	0.0198	0.1688	0.0277	0.1265	0.1702	-0.8138	0.0277	0.1907
6M	90%	0.2667	0.9593	0.0057	0	0.0007	-0.0146	0.0057	0.0293
	95%	0.1748	0.8787	0.0266	0.0745	0.0059	-0.0952	0.0266	0.1382
	100%	0.1024	0.6546	0.0502	0.2058	0.0306	-0.3193	0.0502	0.2696
	105%	0.0588	0.4136	0.0455	0.1983	0.0842	-0.5603	0.0455	0.2620
	110%	0.0357	0.2536	0.0314	0.1389	0.1581	-0.7203	0.0314	0.2026
1Y	90%	0.3089	0.9082	0.0084	0	0.0035	-0.0402	0.0084	0.0440
	95%	0.2301	0.8294	0.0189	0.0396	0.0131	-0.1191	0.0189	0.1016
	100%	0.1646	0.6976	0.0286	0.0962	0.0360	-0.2508	0.0286	0.1582
	105%	0.1171	0.5488	0.0312	0.1190	0.0769	-0.3996	0.0312	0.1810
	110%	0.0849	0.4212	0.0286	0.1144	0.1331	-0.5273	0.0286	0.1765
2Y	90%	0.3790	0.8288	0.0069	0	0.0146	-0.0717	0.0069	0.0387
	95%	0.3204	0.7770	0.0101	0	0.0292	-0.1235	0.0101	0.0580
	100%	0.2700	0.7138	0.0128	0.0169	0.0519	-0.1867	0.0128	0.0758
	105%	0.2275	0.6469	0.0148	0.0310	0.0825	-0.2535	0.0148	0.0899
	110%	0.1930	0.5821	0.0159	0.0405	0.1212	-0.3183	0.0159	0.0995

Table 5.4.2: USDBRL 'Down-and-call' Barrier Options and Hedge Ratios with $S > H$, 76 Lattice Points and 5 Regimes (Bolded numbers are compared with the European calls and GBPUSD counterparts, indicating the distinct Greeks due to the barrier property, as explained in the text)

	Strike	DOC	DOCA	DOCT	DOC _v	DIC	DICA	DICT	DIC _v
1M	90%	0.2187	1.3563	-0.3296	-1.7224	0.0058	-0.3607	0.3296	1.6573
	95%	0.1178	1.0780	-0.0753	-0.4438	0.0014	-0.0854	0.0791	0.3975
	100%	0.0277	0.5561	0.1833	0.8722	0.0001	-0.0050	0.0055	0.0277
	105%	0.0053	0.0913	0.0311	0.1484	0	0	0	0
	110%	0.0018	0.0244	0.0063	0.0298	0	0	0	0
2M	90%	0.2031	1.7976	-0.3114	-1.6612	0.0308	-0.8066	0.3117	1.5978
	95%	0.1212	1.2294	-0.0919	-0.5362	0.0097	-0.2639	0.1104	0.5645
	100%	0.0453	0.6325	0.0860	0.3851	0.0013	-0.0466	0.0272	0.1380
	105%	0.0147	0.2082	0.0383	0.1763	0.0005	-0.0180	0.0103	0.0521
	110%	0.0060	0.0779	0.0109	0.0491	0.0003	-0.0092	0.0052	0.0263
3M	90%	0.1860	1.8888	-0.1778	-1.0051	0.0567	-0.9041	0.1794	0.9482
	95%	0.1210	1.3020	-0.0621	-0.3932	0.0215	-0.3646	0.0873	0.4566
	100%	0.0580	0.7203	0.0418	0.1600	0.0049	-0.1110	0.0418	0.2143
	105%	0.0245	0.3184	0.0335	0.1450	0.0021	-0.0482	0.0183	0.0937
	110%	0.0118	0.1490	0.0138	0.0584	0.0012	-0.0261	0.0098	0.0503
4M	90%	0.1749	1.8743	-0.1111	-0.6735	0.0761	-0.8963	0.1138	0.6226
	95%	0.1205	1.3343	-0.0438	-0.3046	0.0330	-0.4223	0.0716	0.3827
	100%	0.0669	0.7982	0.0207	0.0502	0.0098	-0.1695	0.0476	0.2468
	105%	0.0326	0.4074	0.0273	0.1089	0.0045	-0.0799	0.0236	0.1222
	110%	0.0173	0.2138	0.0145	0.0576	0.0025	-0.0450	0.0133	0.0688
6M	90%	0.1579	1.7827	-0.0498	-0.3633	0.1089	-0.8234	0.0555	0.3289
	95%	0.1183	1.3525	-0.0233	-0.2040	0.0565	-0.4739	0.0499	0.2784
	100%	0.0787	0.9224	0.0032	-0.0446	0.0237	-0.2677	0.0470	0.2505
	105%	0.0467	0.5626	0.0155	0.0402	0.0122	-0.1490	0.0299	0.1581
	110%	0.0284	0.3447	0.0124	0.0389	0.0073	-0.0911	0.0190	0.1000
1Y	90%	0.1317	1.5780	-0.0113	-0.1592	0.1772	-0.6698	0.0196	0.1412
	95%	0.1110	1.3327	-0.0069	-0.1214	0.1191	-0.5034	0.0258	0.1610
	100%	0.0903	1.0874	-0.0025	-0.0835	0.0743	-0.3898	0.0311	0.1797
	105%	0.0697	0.8438	0.0018	-0.0463	0.0474	-0.2950	0.0294	0.1652
	110%	0.0526	0.6394	0.0041	-0.0214	0.0323	-0.2182	0.0245	0.1359
2Y	90%	0.0977	1.2628	-0.0015	-0.0899	0.2813	-0.4341	0.0083	0.0697
	95%	0.0907	1.1729	-0.0011	-0.0822	0.2297	-0.3959	0.0112	0.0813
	100%	0.0838	1.0830	-0.0007	-0.0745	0.1863	-0.3693	0.0136	0.0914
	105%	0.0768	0.9931	-0.0004	-0.0668	0.1507	-0.3462	0.0152	0.0978
	110%	0.0698	0.9032	0	-0.0591	0.1232	-0.3211	0.0159	0.0997

Table 5.4.3: USDBRL 'Down-and-put' Barrier Options and Hedge Ratios with $S > H$, 76 Lattice Points and 5 Regimes (Bolded numbers are compared with the European puts and GBPUSD counterparts, indicating the distinct Greeks due to the barrier property, as explained in the text)

	Strike	DOP	DOP Δ	DOP Γ	DOP ν	DIP	DIP Δ	DIP Γ	DIP ν
1M	90%	0	0	0	0	0	0	0	0
	95%	0	0	0	0	0	0	0	0
	100%	0.0109	-0.2437	0.0043	0.0374	0.0032	-0.2009	0.1845	0.9277
	105%	0.0894	-0.4302	-0.4021	-1.9650	0.0077	-0.4758	0.4350	2.1876
	110%	0.1867	-0.2189	-0.6811	-3.3621	0.0122	-0.7531	0.6883	3.4614
2M	90%	0	0	0	0	0	0	0	0
	95%	0	0	0	0	0.0006	-0.0259	0.0185	0.0932
	100%	0.0059	-0.0287	-0.0415	-0.2037	0.0140	-0.3768	0.1547	0.7916
	105%	0.0572	0.1153	-0.3086	-1.5375	0.0349	-0.9164	0.3572	1.8308
	110%	0.1305	0.5532	-0.5555	-2.7897	0.0564	-1.4758	0.5716	2.9299
3M	90%	0	0	0	0	0.0001	-0.0022	0.0015	0.0077
	95%	0	0	0	0	0.0017	-0.0495	0.0252	0.1280
	100%	0.0021	0.0050	-0.0118	-0.0588	0.0220	-0.3827	0.0954	0.4977
	105%	0.0336	0.1899	-0.1358	-0.6858	0.0560	-0.9067	0.1876	0.9891
	110%	0.0861	0.6073	-0.2712	-1.3843	0.0919	-1.4714	0.2948	1.5576
4M	90%	0	0	0	0	0.0001	-0.0046	0.0026	0.0134
	95%	0	0	0	0	0.0031	-0.0706	0.0278	0.1424
	100%	0.0007	0.0039	-0.0028	-0.0141	0.0258	-0.3577	0.0710	0.3754
	105%	0.0207	0.1531	-0.0634	-0.3244	0.0665	-0.8081	0.1144	0.6198
	110%	0.0597	0.4995	-0.1436	-0.7446	0.1105	-1.3133	0.1713	0.9353
6M	90%	0	0	0	0	0.0007	-0.0146	0.0057	0.0293
	95%	0	0	0	0	0.0059	-0.0952	0.0266	0.1382
	100%	0	0	0	0	0.0306	-0.3193	0.0502	0.2696
	105%	0.0076	0.0704	-0.0141	-0.0745	0.0766	-0.6307	0.0596	0.3365
	110%	0.0289	0.2826	-0.0437	-0.2351	0.1293	-1.0029	0.0751	0.4377
1Y	90%	0	0	0	0	0.0035	-0.0402	0.0084	0.0440
	95%	0	0	0	0	0.0131	-0.1191	0.0189	0.1016
	100%	0	0	0	0	0.0360	-0.2508	0.0286	0.1582
	105%	0.0002	0.0018	-0.0001	-0.0006	0.0767	-0.4014	0.0313	0.1817
	110%	0.0037	0.0427	-0.0022	-0.0137	0.1293	-0.5700	0.0308	0.1902
2Y	90%	0	0	0	0	0.0146	-0.0717	0.0069	0.0387
	95%	0	0	0	0	0.0292	-0.1235	0.0101	0.0580
	100%	0	0	0	0	0.0519	-0.1867	0.0128	0.0758
	105%	0	0	0	0	0.0825	-0.2535	0.0148	0.0899
	110%	0	0	0	0	0.1212	-0.3183	0.0159	0.0995

Table 5.4.4: USDBRL 'Up-and-call' Barrier Options and Hedge Ratios with $S < H$, 76 Lattice Points and 5 Regimes (Bolded numbers are compared with the European calls and GBPUSD counterparts, indicating the distinct Greeks due to the barrier property, as explained in the text)

	Strike	UOC	UOCA	UOCT	UOC _v	UIC	UICA	UICT	UIC _v
1M	90%	0.1461	-0.8297	-0.9161	-4.4869	0.0784	1.8253	0.9161	4.4218
	95%	0.0685	-0.1579	-0.5573	-2.7521	0.0507	1.1506	0.5610	2.7057
	100%	0.0047	0.0698	-0.0220	-0.1135	0.0231	0.4813	0.2108	1.0134
	105%	0	0	0	0	0.0053	0.0896	0.0329	0.1574
	110%	0	0	0	0	0.0018	0.0236	0.0072	0.0341
2M	90%	0.1089	-0.9362	-0.6053	-2.9392	0.1251	1.9272	0.6056	2.8758
	95%	0.0474	-0.2775	-0.3488	-1.7110	0.0835	1.2429	0.3673	1.7393
	100%	0.0038	0.0022	-0.0339	-0.1681	0.0428	0.5837	0.1471	0.6912
	105%	0	0	0	0	0.0152	0.1902	0.0486	0.2284
	110%	0	0	0	0	0.0063	0.0687	0.0161	0.0754
3M	90%	0.0869	-0.8629	-0.4277	-2.0638	0.1559	1.8477	0.4292	2.0068
	95%	0.0356	-0.2753	-0.2298	-1.1212	0.1068	1.2128	0.2550	1.1846
	100%	0.0033	-0.0155	-0.0258	-0.1270	0.0596	0.6248	0.1094	0.5014
	105%	0	0	0	0	0.0266	0.2702	0.0517	0.2387
	110%	0	0	0	0	0.0130	0.1228	0.0235	0.1087
4M	90%	0.0744	-0.7935	-0.3370	-1.6184	0.1765	1.7714	0.3396	1.5675
	95%	0.0300	-0.2705	-0.1714	-0.8319	0.1236	1.1824	0.1992	0.9100
	100%	0.0034	-0.0245	-0.0229	-0.1118	0.0733	0.6533	0.0911	0.4089
	105%	0	0	0	0	0.0371	0.3275	0.0509	0.2311
	110%	0	0	0	0	0.0198	0.1688	0.0277	0.1265
6M	90%	0.0571	-0.6646	-0.2267	-1.0802	0.2097	1.6239	0.2324	1.0458
	95%	0.0226	-0.2402	-0.1072	-0.5158	0.1522	1.1188	0.1338	0.5902
	100%	0.0034	-0.0340	-0.0181	-0.0874	0.0990	0.6886	0.0682	0.2932
	105%	0	0	0	0	0.0588	0.4136	0.0455	0.1983
	110%	0	0	0	0	0.0357	0.2536	0.0314	0.1389
1Y	90%	0.0353	-0.4665	-0.1135	-0.5322	0.2736	1.3747	0.1219	0.5142
	95%	0.0157	-0.2020	-0.0542	-0.2552	0.2144	1.0313	0.0731	0.2948
	100%	0.0041	-0.0516	-0.0147	-0.0696	0.1605	0.7492	0.0433	0.1658
	105%	0.0004	-0.0045	-0.0013	-0.0061	0.1167	0.5533	0.0325	0.1250
	110%	0	0	0	0	0.0849	0.4212	0.0286	0.1144
2Y	90%	0.0158	-0.2390	-0.0420	-0.1924	0.3631	1.0677	0.0488	0.1721
	95%	0.0083	-0.1247	-0.0223	-0.1026	0.3121	0.9017	0.0324	0.1016
	100%	0.0037	-0.0551	-0.0100	-0.0458	0.2664	0.7688	0.0228	0.0627
	105%	0.0012	-0.0177	-0.0032	-0.0148	0.2263	0.6646	0.0180	0.0458
	110%	0.0002	-0.0032	-0.0006	-0.0026	0.1928	0.5853	0.0164	0.0432

Table 5.4.5: USDBRL 'Up-and-put' Barrier Options and Hedge Ratios with $S < H$, 76 Lattice Points and 5 Regimes (Bolded numbers are compared with the European puts and GBPUSD counterparts, indicating the distinct Greeks due to the barrier property, as explained in the text)

	Strike	UOP	UOP Δ	UOPT	UOP v	UIP	UIP Δ	UIPT	UIP v
1M	90%	0	0	0	0	0	0	0	0
	95%	0	0	0	0	0	0	0	0
	100%	0.0140	-0.4499	0.1839	0.9413	0.0001	0.0054	0.0049	0.0238
	105%	0.0869	-1.1945	-0.1492	-0.6613	0.0101	0.2885	0.1821	0.8839
	110%	0.1646	-1.8692	-0.5043	-2.3774	0.0343	0.8972	0.5115	2.4767
2M	90%	0	0	0	0	0	0	0	0
	95%	0.0006	-0.0261	0.0183	0.0923	0	0	0	0
	100%	0.0191	-0.4309	0.0947	0.4977	0.0008	0.0255	0.0185	0.0902
	105%	0.0773	-1.1176	-0.1099	-0.4716	0.0148	0.3165	0.1585	0.7649
	110%	0.1394	-1.8021	-0.3484	-1.6090	0.0475	0.8795	0.3645	1.7492
3M	90%	0.0001	-0.0022	0.0015	0.0075	0	0	0	0
	95%	0.0016	-0.0509	0.0241	0.1227	0	0	0	0
	100%	0.0222	-0.4274	0.0527	0.2894	0.0019	0.0498	0.0308	0.1495
	105%	0.0717	-1.0482	-0.0967	-0.4110	0.0180	0.3315	0.1485	0.7143
	110%	0.1245	-1.6846	-0.2721	-1.2384	0.0535	0.8205	0.2956	1.4117
4M	90%	0.0001	-0.0047	0.0025	0.0129	0	0	0	0
	95%	0.0030	-0.0749	0.0249	0.1283	0.0001	0.0043	0.0029	0.0141
	100%	0.0236	-0.4220	0.0302	0.1771	0.0030	0.0682	0.0381	0.1842
	105%	0.0674	-0.9906	-0.0902	-0.3823	0.0198	0.3356	0.1411	0.6777
	110%	0.1146	-1.5837	-0.2334	-1.0535	0.0556	0.7700	0.2612	1.2442
6M	90%	0.0006	-0.0157	0.0050	0.0259	0	0	0	0
	95%	0.0053	-0.1086	0.0189	0.1010	0.0006	0.0134	0.0077	0.0372
	100%	0.0253	-0.4198	0.0025	0.0400	0.0053	0.1005	0.0476	0.2296
	105%	0.0610	-0.9031	-0.0850	-0.3620	0.0232	0.3428	0.1304	0.6241
	110%	0.1002	-1.4204	-0.1905	-0.8514	0.0580	0.7001	0.2219	1.0541
1Y	90%	0.0029	-0.0520	0.0030	0.0182	0.0007	0.0118	0.0054	0.0259
	95%	0.0100	-0.1683	-0.0014	0.0043	0.0031	0.0492	0.0203	0.0974
	100%	0.0253	-0.3988	-0.0256	-0.1009	0.0107	0.1480	0.0542	0.2591
	105%	0.0484	-0.7325	-0.0759	-0.3282	0.0285	0.3329	0.1071	0.5092
	110%	0.0749	-1.1088	-0.1383	-0.6130	0.0582	0.5816	0.1669	0.7895
2Y	90%	0.0083	-0.1362	-0.0124	-0.0524	0.0063	0.0645	0.0192	0.0911
	95%	0.0156	-0.2519	-0.0262	-0.1133	0.0136	0.1285	0.0362	0.1713
	100%	0.0257	-0.4122	-0.0473	-0.2073	0.0262	0.2256	0.0601	0.2831
	105%	0.0380	-0.6049	-0.0740	-0.3270	0.0445	0.3513	0.0887	0.4169
	110%	0.0519	-0.8203	-0.1047	-0.4656	0.0693	0.5020	0.1206	0.5650

Chapter 6

Conclusion

In this thesis, we have identified the core sources of uncertainty in the dynamics of FX rates, using implied risk-neutral distributions from OTC option quotes. After a detailed review of the relevant literature, a model that can capture the main features of the smile surface, and is flexible enough to price both European and exotic options, has been developed, calibrated to market quotes and applied to price barrier options for two different currency pairs.

We firstly review various techniques to derive risk-neutral distributions implied by OTC option prices, and select the Malz[65]’s method, which is specifically designed for the FX market, to obtain the implied distributions for two currency pairs. Analysis of these results has helped us to identify three important sources of uncertainty in the FX dynamics: the stochastic exchange rate, the stochastic volatility, and the stochastic skewness. These stochastic elements are all considered in our derivative pricing model. Before going into the pricing model development, we use econometric techniques to explore the explanatory power of the implied higher moments in excess forward returns. An Error Correction Model (ECM) is novelly proposed to help forecasting exchange rates movements, thus providing some econometric evidence for exploiting excess returns with implied higher moments.

Given these sources of uncertainty, we then review several pricing models and analyze their pros and cons. Local volatility models can capture the smile effect and fit well to the market data with tractability. However, such models are

dynamically inconsistent. They cannot produce the stationary smile surface in reality. Stochastic volatility models can fit the market implied volatility smile for the medium maturities quite well, but fail for the short and extremely long maturities[88]. In addition, jumps are a common phenomenon in FX market. This can be captured by Jump diffusion and Variance Gamma models, both of which produce perfectly deterministic smiles. However, smiles produced by jump models tend to flatten out too rapidly, although the short-term skews are closed to those in the market. The disadvantages of individual models lead the literature to a combined approach, which, however, has many issues regarding the appropriateness of the combination and numerical implementation, as well as the problem of failing to produce stochastic skewness with tractability. Finally, the Carr and Wu [25] model, which uses two Lévy processes to model up and down jumps separately, successfully captures both stochastic volatility and stochastic skewness by randomizing the time. Yet it only has semi-closed-form solution for vanilla options, while the extension to exotic options appears to be too challenging and remains untackled.

We therefore adopt the Albanese and Mijatović [4] model, which bypasses the technical difficulties in stochastic calculus and uses spectral theory and functional analysis instead. The model specifies the FX forward rates by a CEV process coupled with Variance Gamma jumps in each local volatility regime, and uses a stochastic volatility process to govern the switch between different regimes. Discretized on a continuous-time lattice, the model, which can obtain stochastic volatility and stochastic skewness simultaneously, is flexible enough to price both European and exotic options. During our implementation, we improve this model by using a more stable methodology to calculate the exponential for the nonnormal matrix, and novelly design a routine to improve the numerical efficiency. The model validation in Black-Scholes' case demonstrates its validity, and the model is then calibrated to two characteristically different currency pairs. The results, including sensible implied volatilities surfaces, implied distribution functions and hedge ratios, show that this model can indeed capture the core features of the implied risk-neutral distribution in the FX market.

In the last part, we innovatively develop the pricing methodology for the FX barrier options within the above mentioned lattice framework. The model valida-

tion in Black-Scholes' case against the closed-form pricing formulae provided by Haug [43] shows only small differences between the model prices and those from the closed-form solutions, demonstrating the validity of our method. Finally, with the calibrated parameters, the model achieves reasonable pricing results for both a developed market currency pair (GBPUSD) and an emerging market currency pair (USDBRL).

In conclusion, our work provides a robust model, which can capture the key sources of uncertainty in FX market, to price FX vanilla and barrier options, as well as to provide hedge ratios for risk management.

Future Research

Although we have covered most of the theoretical and practical issues in developing this robust model, there are still some technical details that should be addressed in the future research.

Firstly, further work should be conducted to validate the proposed modelling framework. For example, the lattice approximation for Markov generator should be further verified, an alternative method for regime switching should be examined, and the adequacy of regimes should be tested.

Secondly, as mentioned in Chapter 4, the calibration method is currently different from the normal optimization scheme. We should further investigate the possibility of designing a conditional optimization scheme, which translates the user's view of the market into the restriction of certain parameters. This has been bypassed now because of the programming difficulty of dealing with such a large number of parameters.

Thirdly, alternative algorithms could be applied to further improve the numerical efficiency.

Last but not least, the extension to the other exotic options, such as Asian options and Look-back options, provides a great opportunity for future research, though we believe that such extension can be well signposted by our work here for barrier options.

Appendix A Derivation of the Implied Pricing Kernel

In risk-neutral pricing, the pricing kernel is actually the discounted PDF. This Appendix shows a brief derivation¹ of the implied pricing kernel from quoted option prices, i.e. $\frac{\partial^2 C(K, \tau)}{\partial K^2} = e^{-r(T-t)} \phi(K) T$.

The price of the European call option can be expressed as follows:

$$C(S_T, K, t, T) = e^{-r(T-t)} \int_K^\infty (S_T - K) \phi(S_T) dS_T \quad (\text{A.1})$$

We can make use of the calculus result:

$$\frac{\partial}{\partial x} \int_0^x f(t, x) dt = f(t, x) + \int_0^x \frac{\partial f(t, x)}{\partial x} dt \quad (\text{A.2})$$

Apply formula (A.2) to (A.1) gives:

$$\begin{aligned} \frac{\partial C(S_T, K, t, T)}{\partial K} &= e^{-r(T-t)} \frac{\partial}{\partial K} \int_K^\infty (S_T - K) \phi(S_T) dS_T \\ &= e^{-r(T-t)} \left[-\frac{\partial}{\partial K} \int_\infty^K (S_T - K) \phi(S_T) dS_T \right] \\ &= e^{-r(T-t)} \left[-(S_T - S_T) \phi(S_T) - \int_\infty^K \frac{\partial [(S_T - K) \phi(S_T)]}{\partial K} dS_T \right] \\ &= e^{-r(T-t)} \int_\infty^K \phi(S_T) dS_T \end{aligned} \quad (\text{A.3})$$

Formula (A.3) shows that the first derivative of the call option price with respect to the exercise price can be expressed in the form of the risk-neutral cumulative distribution function. Further apply the fundamental theorem of calculus:

$$\frac{\partial}{\partial x} \int_0^x f(t) dt = f(x) \quad (\text{A.4})$$

¹Reproduced from Ricardo Rebonato, 2004. Volatility and Correlation, second edition, John Wiley & Sons Ltd.

while differentiating (A.3) again with respect to K , the final result then follows:

$$\frac{\partial^2 C(S_T, K, t, T)}{\partial K^2} = e^{-r(T-t)} \phi(K) \tag{A.5}$$

Appendix B Implied Distribution Examples

Figures below show the examples of certain currency pairs. Data for other samples are available if required.

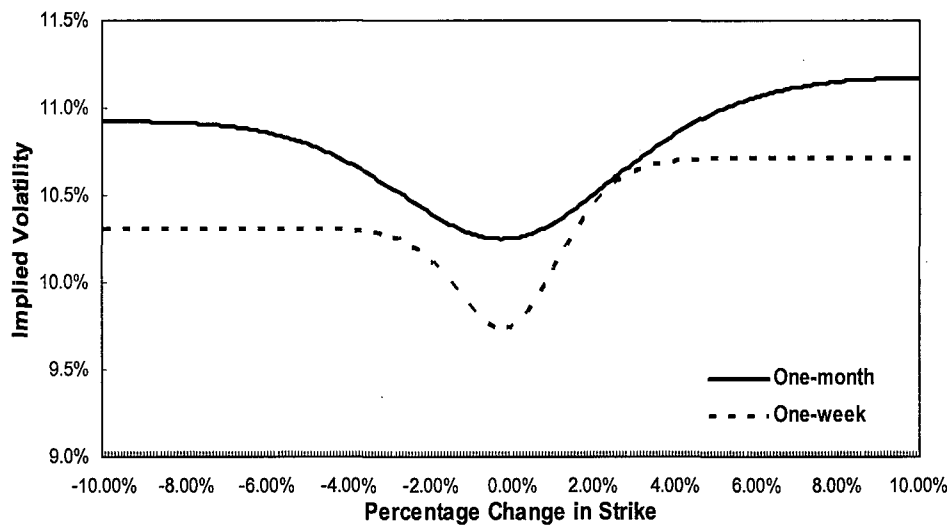


Figure B.1 Implied volatility smile (EURUSD monthly/weekly 23/06/04)

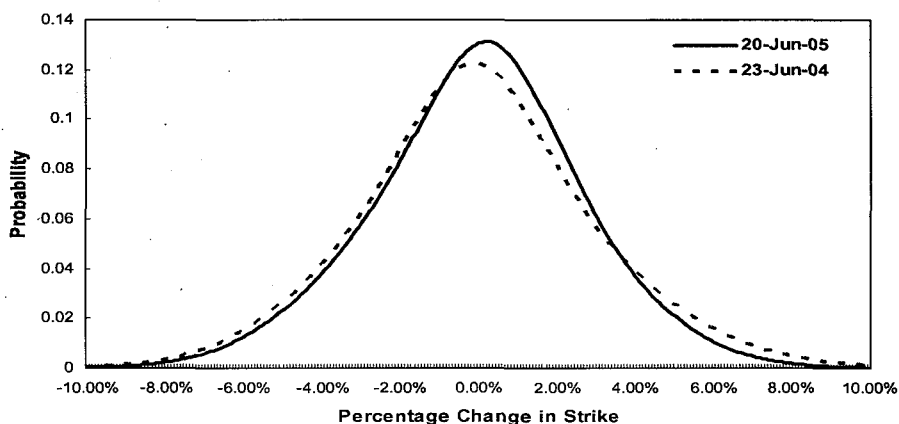


Figure B.2 Option implied PDF (EURUSD monthly)

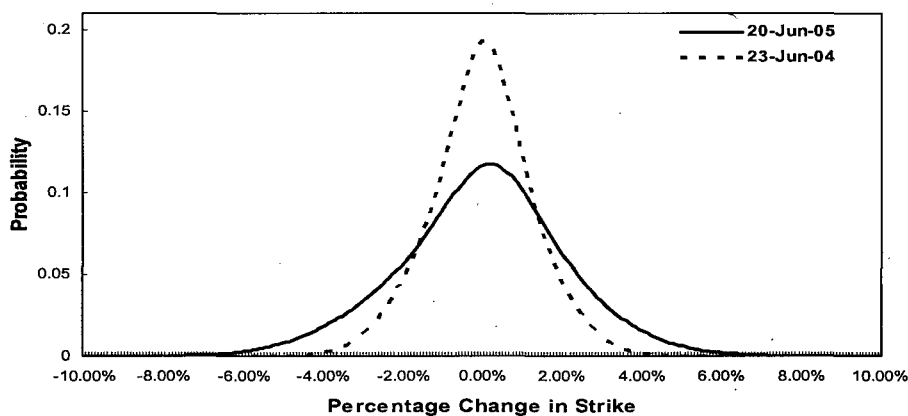


Figure B.3 Option implied PDF (GBPUSD weekly)

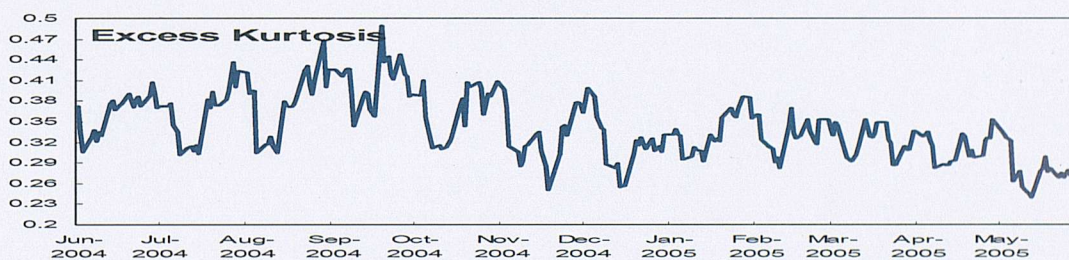
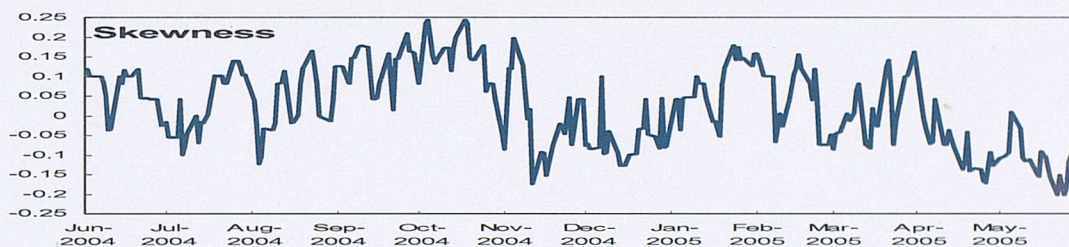
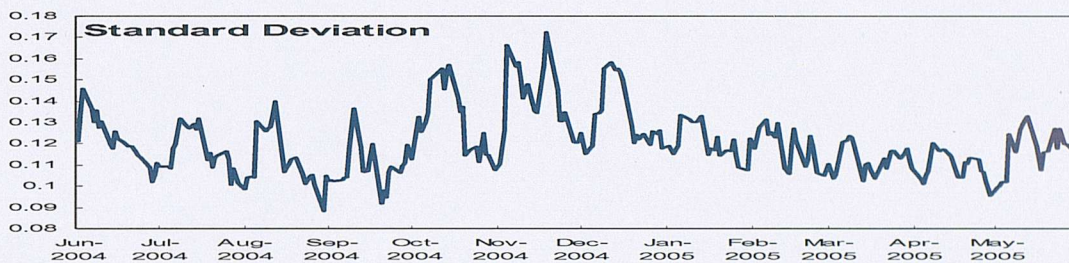
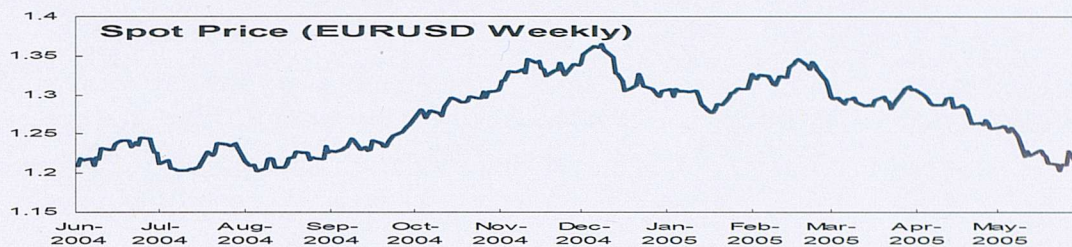


Figure B.4 Spot EURUSD weekly FX rate and the higher moments of implied PDF

Appendix C Proof of Theorems in Chapter 4

Proof. Theorem 4.2.3

The entries of \mathbf{P}_t are probabilities, thus the first 2 conditions are quite straight forward. For part 3, let $\mathbf{1}$ denotes a unit vector in \mathbb{R}^N , for any $x \in \Omega$,

$$(\mathbf{P}_t \mathbf{1})_x = \sum_{y \in \Omega} p(x, 0; y, t) = P \left(\bigcup_{y \in \Omega} \{X_t = y | X_0 = x\} \right) = 1$$

Part 4 can be proved using the Markov property:

$$\begin{aligned} \mathbf{P}_{s+t}(x, y) &= P(X_{s+t} = y | X_0 = x) \\ &= \sum_{z \in \Omega} P(X_{s+t} = y | X_s = z, X_0 = x) P(X_s = z | X_0 = x) \\ &= \sum_{z \in \Omega} P(X_t = y | X_0 = z) P(X_s = z | X_0 = x) \\ &= \sum_{z \in \Omega} p(z, 0; y, t) p(x, 0; z, s) \\ &= (\mathbf{P}_s \mathbf{P}_t)(x, y) \end{aligned}$$

■

Proof. Corollary 4.2.6

$$\text{For 1: } \mathcal{L}(x, y) = \frac{p(x, 0; y, \delta t) - o(\delta t)}{\delta t} \geq 0, \text{ if } x \neq y$$

$$\text{For 2: } \mathcal{L}(x, y) = \frac{p(x, 0; y, \delta t) - o(\delta t) - 1}{\delta t} \leq 0, \text{ if } x = y$$

For statement 3, from the first part of Theorem 4.2.3, we can write

$$\mathcal{L} = \lim_{t \rightarrow 0} \frac{1}{t} (\mathbf{P}_t - \mathbf{I})$$

Let $\mathbf{1}$ and $\mathbf{0}$ denote a vector in \mathbb{R}^N with all its entries equal to 1 and 0 respectively. Theorem 4.2.3 together with finite assumption for Ω will get:

$$\mathcal{L} \mathbf{1} = \lim_{t \rightarrow 0} \frac{1}{t} (\mathbf{P}_t - \mathbf{I}) \mathbf{1} = \lim_{t \rightarrow 0} \frac{1}{t} (\mathbf{P}_t \mathbf{1} - \mathbf{1}) = 0$$

■

Proof. Theorem 4.2.7

For fixed states $x, y \in \Omega$, a fixed time $t \in \mathbb{R}_+$ and a small time interval δt we have:

$$\begin{aligned} p(x, 0; y, t + \delta t) &= \sum_{z \in \Omega} p(x, 0; z, t) p(z, t; y, t + \delta t) \\ &= \sum_{z \in \Omega} p(x, 0; z, t) p(z, 0; y, \delta t) \\ &= p(x, 0; y, t) p(y, 0; y, \delta t) + \sum_{z \in \Omega - \{y\}} p(x, 0; z, t) p(z, 0; y, \delta t) \end{aligned}$$

The first line comes from the Chapman-Kolmogorov equation in Theorem 4.2.3, conditioned on X_t . The second line is obtained by time homogeneity. By Theorem 4.2.5, we can get:

$$\frac{p(x, 0; y, t + \delta t) - p(x, 0; y, t)}{\delta t} = \sum_{z \in \Omega} p(x, 0; z, t) \mathcal{L}(z, y) + \frac{o(\delta t)}{\delta t}$$

Take the limit as $\delta t \rightarrow 0$, the left-hand side of the equation becomes the derivative of the transition probability with respect to time, $p(x, 0; y, t)'$, while the right-hand side limits to the matrix element $(P_t \mathcal{L})(x, y)$. This proves the Kolmogorov's forward equation.

Similarly, conditional on $X_{\delta t}$:

$$\begin{aligned} p(x, 0; y, t) &= \sum_{z \in \Omega} p(x, 0; z, \delta t) p(z, \delta t; y, t) \\ &= \sum_{z \in \Omega} p(x, 0; z, \delta t) p(z, 0; y, t - \delta t) \\ &= p(x, 0; x, \delta t) p(x, 0; y, t - \delta t) + \sum_{z \in \Omega - \{x\}} p(x, 0; z, \delta t) p(z, 0; y, t - \delta t) \end{aligned}$$

Apply Theorem 4.2.5 to $p(x, 0; x, \delta t)$ and $p(x, 0; z, \delta t)$, it yields:

$$\frac{p(x, 0; y, t) - p(x, 0; y, t - \delta t)}{\delta t} = \sum_{z \in \Omega} \mathcal{L}(x, z) p(z, 0; y, t - \delta t) + \frac{o(\delta t)}{\delta t}$$

In the limit we get Kolmogorov's backward equation.

To prove $e^{t\mathcal{L}}$ is the solution, it is just enough to show that it satisfies the forward equation, because $e^{t\mathcal{L}}$ commutes with \mathcal{L} , backward equation will follow from the forward equation.

$$\begin{aligned}\frac{d}{dt}e^{t\mathcal{L}} &= \sum_{n=0}^{\infty} \left[\left(\frac{d}{dt} \frac{t^n}{n!} \right) \mathcal{L}^n \right] \\ &= \sum_{n=0}^{\infty} \left[\left(\frac{t^{n-1}}{(n-1)!} \right) \mathcal{L}^{n-1} \cdot \mathcal{L} \right] \\ &= e^{t\mathcal{L}} \mathcal{L}\end{aligned}$$

Since the first order derivative of an exponential function is uniformly continuous, we can exchange the order of summation and differentiation here. ■

Bibliography

- [1] Aït-Sahalia, Y. and A. Lo. 1995. Nonparametric Estimation of State-Price Densities Implicit in Financial Asset Prices, NBER, working paper, No. 5351.
- [2] Albanese, C. and A. Kuznetsov. 2004. Unifying Volatility Models, *RISK*, March, pp. 94-98.
- [3] Albanese, C., H. Lo, and A. Mijatović. 2006. Spectral Methods for Volatility Derivatives, *Working Paper*, Imperial College London.
- [4] Albanese, C. and A. Mijatović. A Stochastic Volatility Model for Risk-reversals in Foreign Exchange, to appear in *International Journal of Theoretical and Applied Finance*.
- [5] Albanese, C. and A. Mijatović. N.D. Convergence Rates for Diffusion on Continuous-time Lattice, *Working Paper*, Imperial College London.
- [6] Andersen, L. and J. Andreasen. 1999. Jumping Smiles. *RISK*, November, pp. 65-68.
- [7] Andersen, L. B. G. and R. Brotherton-Ratcliffe. 1997. The Equity Option Volatility Smile: An Implicit Finite Difference Approach, *Journal of Computational Finance*, 1, no. 2 (Winter 1997/98), pp. 32-39.
- [8] Andersen, T. and B. Sorensen. 1996. GMM Estimation of a Stochastic Volatility Model: A Monte Carlo Study, *Journal of Business and Economic Statistics*, 14, 326-352.
- [9] Bahra, B. 1997. Implied Risk-Neutral Probability Density Functions from Option Prices: Theory and Application, *Bank of England Working Paper*, 66.
- [10] Barndorff-Nielsen, O. E. and N. Shephard. 2001. Non-Gaussian Ornstein-Uhlenbeck-based Models and Some of Their Uses in Financial Economics (with discussion), *Journal of the Royal Statistical Society, Series B* 63, 167-241.
- [11] Bates, D. S. 1991. The Crash of '87: Was it Expected? The Evidence from Options Markets, *Journal of Finance*, 46, 3, pp. 1009-1044.
- [12] Bates, D. S. 1995. Post-'87 Crash Fears in S&P 500 Futures Options, *working paper*, The Wharton School.
- [13] Bates, D. S. 1996. Jumps and Stochastic Volatility: Exchange Rate Processes Implicit in Deutsche Mark Options. *Review of Financial Studies*, Vol. 9, 69-107.

- [14] Black, F. 1976. The Pricing of Commodity Contracts, *Journal of Financial Economics*, 3(1), pp. 167-179.
- [15] Black, F. and M. Scholes. 1973, May/June. The Pricing of Options and Corporate Liabilities, *Journal of Political Economy*, pp. 637-659.
- [16] Bliss, R. B. and N. Panigirtzoglou. 2000. Testing the Stability of Implied Probability Density Functions, *Bank of England Working Paper*, 114.
- [17] Borak, S. 2004. Lévy Processes, *AQM lecture*, Humboldt-Universität zu Berlin.
- [18] Breeden, D.T. and R.H. Litzenberger. 1978. Prices of State-Contingent Claims Implied in Option Prices, *Journal of Business*, Vol. 51, No. 4, pp. 621-651.
- [19] Breidt, F. J., N. Crato, and P. de Lima. 1998. On the Detection and Estimation of Long Memory in Stochastic Volatility, *Journal of Econometrics*, 83, 325-348.
- [20] Britten-Jones, M. and A. Neuberger. 2000. Option Prices, Implied Prices Processes, and Stochastic Volatility, *Journal of Finance*, 55 (2), 839-866.
- [21] Broadie, M., P., Glasserman and S. G. Kou. 1997. A Continuity Correction for Discrete Barrier Options, *Journal of Mathematical Finance*.
- [22] Campa, J. M., P. H. K. Chang, and R. L. Reider. 1997. Implied Exchange Rate Distributions: Evidence from OTC Option Markets, *NBER Working Paper*, 6179.
- [23] Carr, P. 2003. Option Pricing using Integral Transforms, *Presentation*, New York University Courant Institute.
- [24] Carr, P. and L. Wu. 2004. Time-changed Lévy Processes and Option Pricing, *Journal of Financial Economics*, 71, 113-141.
- [25] Carr, P. and L. Wu. 2005. Stochastic Skew Models for FX Options, *Working Paper*, Columbia University, NY.
- [26] Carr, P. and D. Madan. 1999. Option Pricing Using the Fast Fourier Transform, *Journal of Computational Finance*, 3, 463-520.
- [27] Carr, P., H. Geman, D. Madan and M. Yor. 2001. Stochastic Volatility for Levy Processes, *Mathematical Finance*, July 2003, Vol. 13 No. 3, pp. 345-382.
- [28] Chung, K. L. 1960. *Markov Chains with Stationary Transition Probabilities*, Springer, Berlin.
- [29] Comte, F. and E. Renault. 1998. Long Memory in Continuous-time Stochastic Volatility Models, *Mathematical Finance*, Vol. 8, 291-323.
- [30] Cox, J. C., J. E. Ingersoll, and S. A. Ross. 1985. A Theory of the Term Structure of Interest Rates, *Econometrica*, 53, 385-408.
- [31] Cox, J. C. and S. A. Ross. 1976. The Valuation of Options for Alternative Stochastic Processes, *Journal of Financial Economics*, 3, pp. 145-166.

- [32] Cox, J. C., S. A. Ross, and M. Rubinstein. 1979. Option Pricing: A Simplified Approach, *Journal of Financial Economics*, 7.
- [33] Derman, E. 1999. Regimes of Volatility, *RISK*, April, pp. 55-59.
- [34] Derman, E. and I. Kani. 1994. The Volatility Smile and Its Implied Tree, *Quantitative Strategies Research Notes*, Goldman Sachs, January.
- [35] Derman, E. and I. Kani. 1998. Stochastic Implied Trees: Arbitrage Pricing with Stochastic Term and Strike Structure of Volatility, *International Journal of Theoretical and Applied Finance*, Vol. 1, No.1, 61-110.
- [36] Dupire, B. 1994. Pricing with a smile, *RISK*, February, pp. 18-20.
- [37] Eraker, B., M. Johannes, and N. G. Polson. 2003. The Impact of Jumps in Returns and Volatility. *Journal of Finance*, Vol. 53, 1269-1300.
- [38] Figlewski, S. and B. Gao. 1999. The Adaptive Mesh Model: A New Approach to Efficient Option Pricing, *Journal of Financial Economics*, 53, pp. 313-351.
- [39] Gereben, A. 2002, April. Extracting Market Expectations from Option Prices: an Application to Over-the-Counter New Zealand Dollar Options, *Federal Reserve Bank of New Zealand, Discussion Paper Series*, F31, G13.
- [40] Glasserman, P. and S. G. Kou. 2000. The Term Structure of Simple Forward Rates with Jump Risk, *Working Paper*, Columbia University.
- [41] Grimmett, J. and D. Stirzaker. 2001. *Probability and Random Processes*, 3rd Edition, Oxford University Press.
- [42] Härdle, W. 1991. Smoothing techniques, Springer.
- [43] Haug, E. 1998. *Complete Guide to Option Pricing Formulas*, McGraw Hill.
- [44] Heston, S. L. 1993. A Closed-form Solution for Options with Stochastic Volatility with Applications to Bond and Currency Options, *Review of Financial Studies*, Vol. 6, No.2, pp. 327-343.
- [45] Hoffmann, M. 2002. Rate of Convergence for Parametric Estimation in Stochastic Volatility Models, *Stochastic Processes and Their Application*, 97, 147-170.
- [46] Hull, J. 2003. *Options, Futures, and Other Derivative Securities*, fifth edition. Englewood Cliffs, NJ: Prentice-Hall.
- [47] Hull, J. and A. White. 1987. The Pricing of Options on Assets with Stochastic Volatilities, *Journal of Finance*, Vol. 42, 281-300.
- [48] Jackwerth, J. C. 1996. Implied Binomial Trees: Generalizations and Empirical Tests, *working paper*.
- [49] Jackwerth, J.C. and M. Rubinstein. 1995. Implied Probability Distributions: Empirical Analysis, Haas School of Business, University of California, *Working paper* No. 250.

- [50] Jacquier, E., N. G. Polson, and P. E. Rossi. 1994. Bayesian Analysis of Stochastic Volatility Models, *Journal of Business and Economic Statistics*, 12, 371-417.
- [51] Johnson, H. and D. Shanno. 1987. Option Pricing When the Variance is Changing. *Journal of Financial and Quantitative Analysis*, Vol. 22, 143-151.
- [52] Kamrad, B. and P. Ritchken. 1991. Multinomial Approximating Models for Options with k State Variables, *Management Science*, 3, 1640-1652.
- [53] Julier, S. J. and J. K. Uhlmann. 1997. A New Extension of the Kalman Filter to Nonlinear Systems, In The Proceedings of AeroSense: The 11th International Symposium on Aerospace/Defense Sensing, Simulation and Controls, Multi Sensor Fusion, Tracking and Resource Management II, *SPIE*, 1997.
- [54] Karatzas, I. and S. E. Shreve. 1998. *Brownian Motion and Stochastic Calculus*, Graduate Texts in Mathematics, 2nd Edition, Springer.
- [55] Kim, S., N. Shephard, and S. Chib. 1998. Stochastic Volatility: Likelihood Inference and Comparison with ARCH Models, *Review of Economic Studies*, 65, 361-393.
- [56] Leisen, D. 1999. Valuation of Barrier Options in a Black-Scholes Setup with Jump Risk, *European Finance Review*, 3, 3, 319-342.
- [57] Levitan, S. 2001. Lattice Methods for Barrier Options, *University of Witwatersrand Honours Project*.
- [58] Lipton, A. 2001. *Mathematical Methods for Foreign Exchange*, World Scientific.
- [59] Longstaff, F. 1992. An Empirical Examination of the Risk-Neutral Valuation Model, *working paper*, College of Business, Ohio State University, and the Anderson Graduate School of Management, UCLA.
- [60] Longstaff, F. 1995. Option Pricing and the Martingale Restriction, *Review of Financial Studies*, Vol. 8, No. 4, pp. 1091-1124.
- [61] Lyons, R. K. 1988. Tests of the Foreign Exchange Risk Premium Using the Expected Second Moments Implies by Option Pricing, *Journal of International Money and Finance*, 7, 91-108.
- [62] Madan, D. B., and E. Seneta. 1990. The Variance Gamma (VG) Model for Share Market Returns, *Journal of Business*, 63, 511-524.
- [63] Madan, D. B., and F. Milne. 1991. Option Pricing with V. G. Martingale Components, *Mathematical Finance*, 1(4), 39-55.
- [64] Madan, D. B., P. P. Carr, and E. C. Chang. 1998. The Variance Gamma Process and Option Pricing, *European Finance Review*, 2, 79-105.
- [65] Malz, A. 1995a. Recovering the Probability Distribution of Future Exchange Rates From Option Prices, *mimeo*, Federal Reserve Bank of New York.
- [66] Malz, A. 1995b. Using Option Prices to Estimate Realignment Probabilities in the European Monetary System, *Federal Reserve Bank of New York Staff Reports*, 5.

- [67] Marris, D. 1999. Financial Option Pricing and Skewed Volatility, M.Phil. thesis, Statistical Laboratory, University of Cambridge.
- [68] Melick W. R. and C. P. Thomas. 1997. Recovering an Asset's Implied PDF from Option Prices: An Application to Crude Oil During the Gulf Crisis, *Journal of Financial and Quantitative Finance*, Vol 32, No. 1.
- [69] Melino, R. C. and S. M. Turnbull. 1990. Pricing Foreign Currency Options with Stochastic Volatility, *Journal of Econometrics*, 45, 239-265.
- [70] Merton, R. 1973. Theory of Rational Option Pricing, *Bell Journal of Economics and Management Science*, Vol. 4, No. 1.
- [71] Merton, R. C. 1990. *Continuous-Time Finance*, Oxford: Blackwell.
- [72] Moler, C. and C. VanLoan. 2003. Nineteen Dubious Ways to Compute the Exponential of a Matrix, Twenty-Five Years Later, *SIAM Review*, Vol. 45, No. 1, pp. 3-49.
- [73] Newey, W. K. and K. D. West. 1987. A Simple, Positive Semi-definite, Heteroskedasticity and Autocorrelation Consistent Covariance Matrix, *Econometrica*, 55/3, 703-8.
- [74] Nicolato, E. and E. Venardos. 2003. Option Pricing in Stochastic Volatility Models of the Ornstein-Uhlenbeck Type. *Mathematical Finance*, 13, 445-466.
- [75] Phillips, R. S. 1952. On the Generation of Semigroups of Linear Operators, *Pacific Journal of Mathematics*, 2 (3), 343-369.
- [76] Rebonato, R. 2004. *Volatility and Correlation*, second edition, John Wiley & Sons Ltd.
- [77] Reiner, E. and M. Rubinstein. 1991. Breaking Down the Barriers, *RISK*, 4, 8, pp.28-35.
- [78] Ritchey, R. J. 1990. Call Option Valuation for Discrete Normal Mixtures, *Journal of Financial Research*, Vol. XIII, No. 4, pp. 285-296.
- [79] Rubinstein, M. 1983. Displaced Diffusion Option Pricing, *Journal of Finance*, 38, no.3, 213-217.
- [80] Rubinstein, M. 1994. Implied Binomial Trees, *Journal of Finance*, 69, 3, 771-818.
- [81] Ruiz, E. 1994. Quasi-Maximum Likelihood Estimation of Stochastic Volatility Models, *Journal of Econometrics*, 63, 289-306.
- [82] Schroder, M. 1989. Computing the Constant Elasticity of Variance Option Pricing Formula, *Journal of Finance*, Vol. 44, No.1, 211-219.
- [83] Shimko, D. 1993. Bounds of Probability, *RISK*, Vol.6, No. 4, pp. 33-37.
- [84] Sorensen, M. 2000. Prediction Based Estimating Equations, *The Econometrics Journal*, 3, 123-147.

- [85] Stein, E. M. and J. Stein. 1991. Stock Price Distributions with Stochastic Volatility: an Analytic Approach, *Review of Financial Studies*, 4, 727-752.
- [86] Taylor, S. J. 1982. Financial Returns Modelled by the Product of Two Stochastic Processes - a Study of Daily Sugar Prices 1961-79. In O. D. Anderson (Ed.) *Time Series Analysis: Theory and Practice*, 1, pp. 203-226. Amsterdam: North-Holland.
- [87] Trefethen, L. N. 1997. Pseudospectra of Linear Operators, *SIAM Review*, 39, pp. 383-406.
- [88] Weron, R. 2004. Stochastic Volatility Model of Heston and the Smile, *The Third Nikkei Econophysics Symposium*.
- [89] Wiggins, J. B. 1987. Option Values under Stochastic Volatilities. *Journal of Financial Economics*, Vol. 19, 351-372.
- [90] Wilmott, P. 1998. *Derivatives*. Chichester: John Wiley & Sons.
- [91] Wright, T. G. EigToll Software Package,
<http://web.comlab.ox.ac.uk/projects/pseudospectra/eigtool/>.